# INSTITUTE FOR AEROSPACE STUDIES

UNIVERSITY OF TORONTO

# TURBULENCE MEASUREMENTS RELEVANT TO JET NOISE

by

Wing T. Chu





NOVEMBER 1966

UTIAS REPORT NO. 119

## CORRIGENDA AND ADDENDA

| Page | |
|---|---|
| vi and vii | add "in the moving frame" after the word "frequency" for the notations of $f_t$ and $\omega_t$, |
| 4 | Eq. (2.1.8) - last term - " $\delta\left(t_2 - t + \frac{\lvert \underline{X} - \underline{Y} \rvert}{a_o}\right)$ " should read " $\delta\left(t_2 - t + \frac{\lvert \underline{X} - \underline{Z} \rvert}{a_o}\right)$ " |
| 8 | Eqs. (2.2.8), (2.2.10), and (2.2.12) - " $(\overline{T}_{xx})^2$ " should read " $\overline{T_{xx}^2}$ " |
| 14 | second last line - "...Davies (Ref. 36). This..." should read "...Davies (Ref. 36), this..." |
| 17 | second last paragraph - line 3 - the word"derivations" should read "deviations" |
| 20 | second equation of (7.1) - there should be a " $\int_0^\infty$ " sign between $\frac{\partial^4}{\partial\tau^4}$ and $\frac{se^R(\underline{\eta}, \xi_{m1} + U_c\tau, 0, 0, \tau)}{\overline{u_x^4}}$ |
| 23 | last line - "...90°. The acoustic..." should read "...90°, the acoustic..." |
| Fig. 2 | add $\theta^{-5}$ after "AMPLIFICATION" |
| Appendix B | second paragraph - line 1 - "stationary in time," should read "...statistically stationary", |

Some additional remarks appear necessary regarding the justification in extrapolating our data for the cases of 'shear' noise mentioned on page 18. We have pointed out there that the fourth derivatives at $\tau = 0$ were quite sensitive to the range of data available. The reason being that the fitted curves behaved properly only within the range of data being fitted. They would have maxima and minima outside this range because of the inherent nature a polynomial with a mixture of positive and negative coefficients. Physically speaking the curves in Fig. 29 should not have these sinuosities at large $\tau$ as indicated by the relatively smooth 'self' noise data in Fig. 30. The purpose o the extrapolution, then, is to ensure that the function is of a physically admissible shape in the extrapolation range. The analytical function obtained by least squares to fit the extrapolated data fits the original data points as wel as before, and in addition it now shows a proper behavior at larger values of t argument.

With the 'shear' noise curves so extrapolated, the data were thought to be on a comparable basis with the 'self' noise data; that is, the abscissa scale is long enough to bring the curves (which are integrals of correlations) down by about half. Comparable accuracy of the fourth derivative is then anticipated.

It should be pointed out here that although the absolute magnitude of the fourth derivatives at $\tau = 0$ and their 'half wave-length' were different, the relative magnitudes between the three cases of 'shear' noise and the general shape of the fourth derivative curves remained the same whether we have extrapolated our data or not.

Finally it is to be understood that the significance of the inferred result at $90^{\circ}$ in Fig. 36 depends on the accuracy in obtaining the relative magnitude between the 'shear' and the 'self' noise.

## ACKNOWLEDGEMENT

The author wishes to express his gratitude to Dr. G. N. Patterson, Director, for the opportunity to pursue this investigation at UTIAS.

Special thanks go to Professor H.S. Ribner for suggesting this research, for his valuable guidance and supervision, and for his patient and unflinching optimism. The author is also indebted to Professors B. Etkin and S.J. Townsend for their helpful suggestions.

The value of discussions with fellow students is also acknowledged. In particular the author wishes to thank D.R. Strong who designed the automatic controlling system for the time-delay correlator and N.D. Ellis who helped in building the proto-type.

Thanks are also due to Dr. C.C. Gotlieb, Head of the Institute of Computer Science, University of Toronto, for making time available on the IBM 7094 computer.

The project was supported by the National Research Council of Canada under Grant No. A2003 and the United States Air Force under Grant No. AFOSR 672-66 and earlier grants.

## SUMMARY

Lighthill's equation for aerodynamic noise has been reformulated in terms of its spectral characteristics using the one-dimensional fourier cosine transform. The final formalism is more revealing in that both the Doppler effect of moving eddies and the extent to which retarded time differences can be neglected are explicit in the final equation. Also the convection effect can be distinguished as a combined effect of Doppler shift and amplification.

Experimentally, two-point space-time correlations of both the turbulent velocities and the square of these velocities have been measured in the mixing region ($\eta_1/D = 4$, $\eta_2/D = 0.5$) of a 4 inch model jet (about 142 fps) with constant temperature hot-wire anemometers. These measurements included the ordinary u-component and also the components at $45^\circ$ and $60^\circ$ to the jet axis. Results for the u-component agree well with those of previous investigators.

Using the moving axis transformation of these space-time correlation functions to-gether with the mean velocity measurements, an estimate of the basic directivity, the intensity, and the spectrum of both the 'shear' and the 'self' noise generated by a unit volume of jet turbulence was obtained. The calculations were based on the Proudman form of Lighthill's equation and Ribner's notion of 'shear' and 'self' noise. These results show reasonable quantitative comparison with actual acoustic measurements of other investigators and they are also in qualitative agreement with some of the theoretical predictions made by Ribner.

TABLE OF CONTENTS

## NOTATION

| | |
|---|---|
| $a_o$ | speed of sound |
| C | non-singular convection factor defined by Equation 2.2.11 |
| D | nozzle diameter |
| f | frequency |
| $f_t$ | $= f\theta$ , identified as the turbulence frequency |
| I | noise intensity |
| L, $\mathcal{L}$ | length scales of turbulence given by (6.8) and (6.7) |
| $M_c$ | eddy convection speed/$a_o$ |
| p | instantaneous pressure |
| $p_o$ | ambient pressure |
| $\Delta p$ | acoustic pressure ($\Delta p = p - p_o$) |
| R | two-point space-time correlations |
| $R_m$ | moving-frame two-point space-time correlations (2.1.17) |
| $\mathcal{R}$ | normalized two-point space-time correlations |
| S | effective annular area for noise emitters in the mixing region |
| $T_{ij}$ | Lighthill quadrupole strength ($\rho v_i v_j - \tau_{ij} + (p - a_o^2 \rho_o)\delta_{ij}$) |
| $T_{xx}$ | $= \frac{x_i x_j}{\lvert \underline{X} \rvert^2} T_{ij}$ |
| t | time |
| $\underline{U}$ | local mean velocity |
| $U_c$ | eddy convection velocity |
| $U_j$ | value of U at jet exit |
| $U_x$ | component of U in $\underline{X}$-direction |
| $\underline{u}$ | turbulent velocity |
| $u_x, u_\theta$ | component of $\underline{u}$ in the $\underline{X}$-direction making an angle $\theta$ with the jet axis, u without subscript refers to the ordinary axial component |
| $v_i, v_x$ | instantaneous velocity component ($i = 1,2,3$)($\underline{v} = \underline{U} + \underline{u}$) |

| | |
|---|---|
| $\underline{X}$ | vector position of field point |
| $\underline{Y},\underline{Z}$ | vector positions of source points |
| $\theta$ | angle between field point vector $\underline{X}$ and jet axis |
| $\Theta$ | convection factor $(1 - M_c \cos\theta)$ |
| $\Phi$ | noise spectrum function |
| $\underline{\xi}$ | vector separation in two-point correlation (components $\xi_i$) |
| $\underline{\eta}$ | position vector of center point of separation of probes (components $\eta_i$) |
| $\rho$ | instantaneous local density |
| $\rho_o$ | ambient density |
| $\Delta\rho$ | $= \rho - \rho_o$ |
| $\tau_{ij}$ | viscous stress tensor $\left(\lambda\ \delta_{ij}\ \frac{\partial v_k}{\partial x_k} + \mu\left(\frac{\partial v_i}{\partial x_j} + \frac{\partial v_j}{\partial x_i}\right)\right)$ |
| $\tau,\tau^*$ | differences in emission time for two source points of separation $\underline{\xi}$ (2.1.15) |
| $\tau'$ | arbitrary increment to $\tau$ |
| $\tau_m^*, \tau_m'$ | moving frame values of $\tau$ (2.1.17) |
| $\delta$ | Dirac delta function |
| $\delta_{ij}$ | Kronecker delta |
| $\lambda$ | second coefficient of viscosity |
| $\mu$ | viscosity |
| $\omega$ | radian frequency |
| $\omega_t$ | defined by Eq. 2.2.4 ( $= \omega\Theta$); identified as the turbulence frequency |
| $\omega_f$ | typical radian frequency in the turbulence |
| fps | feet per second |
| Hz | Hertz, new unit in electronics replacing cps |
| rms | root mean square. |
| db | decibel |

# I. INTRODUCTION

A problem in connection with turbulence which is of considerable interest and importance is that of determining the acoustic radiation from the turbulent motion especially from turbulent jets. This 'aerodynamic noise' problem was first formulated successfully by Lighthill (Refs. 1 and 2) using an acoustic analogy. His work stimulated a great number of workers in the field to extend, re-examine and apply the theory. An account of the theory which gives perhaps the broadest coverage of the significant extensions applicable to jet noise is provided in a review article by Ribner (Ref. 3). Comprehensive surveys of experimental results are given in Refs. 4, 5, and 6. Most of these previous experiments deal with the actual acoustic measurements both of model jets and jet engines. There are relatively few measurements of the turbulent flow in model jets that are applicable to noise estimation (Refs. 7, 8, 9, and 10). Even these experiments are of comparatively simple types. Although they have contributed a great deal to the understanding of the turbulent structure of jet flows, they are inadequate for determining the acoustic radiation without relying on major simplifying assumptions to the original theory.

## 1.1 Review of Previous Work

In order to predict the acoustic radiation from known properties of the turbulence, one has to measure or deduce the two-point space-time correlation of the double time derivative of the Reynolds stresses and integrate over the turbulent field. A rigorious evaluation of this kind in three dimensions would be extremely difficult if not impossible. The only circumstance in which the noise emission can be explicitly calculated is for the case of a decaying isotropic turbulent field, considered by Proudman (Ref. 11). But this particular case has no direct application to jet noise estimation. So far, there are two comprehensive developments of approximation to Lighthill's equation that allow the noise emission to be computed in terms of simple properties of a turbulent jet such as turbulence intensities, length scales, moving-frame time scales and mean shear. These are the works of Lilley (Ref. 12) and Ribner (Ref. 13). However, both treatments rely on the postulation of homogeneous and isotropic turbulence and also on the assumption that the space-time correlation function of the Reynolds stresses are separable in space and time.

Lilley's approach is based on an approximation of Lighthill's equation and is applicable only in regions of strong shear. For regions without strong shear he used Proudman's result and labelled the two types of noise the 'shear' and 'self' noise. With Laurence's results (Ref. 7), he is able to show that the noise sources are concentrated in the middle of the mixing layer and that slices of jet within four diameters of the nozzle exit emit the same noise power; beyond that the emission falls off very abruptly. This is in agreement with the theoretical investigation by Ribner (Ref. 14) and a deduction by Dyer (Ref. 15) based on acoustic measurements.

Ribner's calculation (Ref. 13) starts with the Proudman form of Lighthill's equation which is exact. He also treated the total noise as a sum of the'shear' and 'self' noise by splitting the instantaneous velocity into a mean velocity plus a perturbation. But the treatment is coherent in itself. With Laurence's results, he is able to obtain a basic directivity of jet noise

$(1 + \cos^4\theta)$ that agrees better with experimental results than the 'four-leaf-clover' type $(1 + \text{constant} \times \sin^2 2\theta)$ as suggested by Lighthill and Lilley. (See Figure 1 for the definition of $\theta$.) Furthermore, his treatment shows that the 'self' noise spectrum peaks an octave higher than that of the 'shear' noise. With these two spectra, he is able to resolve the paradox concerning the shift of the spectrum with direction of emission.

Other significant contributions to the theory of jet noise are the discoveries of the correct nonsingular convection factor $[(1 - M_c \cos\theta)^2 + \alpha^2 M_c^2]^{-5/2}$ by Ribner (Ref. 16) and Williams (Ref. 17) and of the power laws ($f^2$ and $f^{-2}$) for the total noise spectrum by Powell (Ref.18).

## 1.2 Present Investigation

The present investigation took a more direct approach to estimating the characteristics of the noise emission from a unit volume of turbulence in the mixing region of a jet with very few generalizations and assumptions. Instead of using the original Lighthill's equation, the Proudman form was used as the basis of the present work. This approach involves much simpler experimental procedure because of the fact that the noise intensity in a certain direction is determined by the velocity component at that direction. For directions making angles smaller than $70^\circ$ to the jet axis, the velocity components can be measured accurately with inclined hot-wires. Using the original Lighthill's equation and the response of inclined hot-wires, Williams (Ref. 19) arrived at the same conclusion.

Following Ribner's notion of 'shear' and 'self' noise, two-point space-time correlations of both the turbulent velocities and the square of these velocities were measured in the mixing region of a 4 inch low-speed model jet (about 142 fps) for three directions $\theta = 0^\circ$, $45^\circ$, and $60^\circ$. Previous experiments were concentrated on the u-components only. Using the moving axis transformations of these space-time correlation functions to-gether with the mean velocity measurements, an attempt was made to estimate in a direct fashion the basic directivity, the intensity, and also the spectrum of both the 'shear' and the 'self' noise generated by a unit volume of jet turbulence. With existing knowledge about the distribution of noise sources in a jet, a quantitative comparison between the present work and other workers' acoustic measurements of the overall jet noise was possible. The agreement was reasonably good.

# II. THEORY

Since different ideas have been drawn from a number of sources to arrive at a convenient formalism for the present experimental investigation, it is advisable to give a brief coherent treatment of the theory here. Furthermore, during the course of this work, the author came across a simpler way of expressing the spectral aspect of the acoustic radiation problem. Although it is mathematically less elegant than some of the previous work, it embodies most of the main features of this 'aerodynamic noise' problem in simpler fashion. This is given in greater detail in Section 2.2.

## 2.1 Intensity Analysis of the Acoustic Field

In this section, a brief derivation of the acoustic 'far field' pressure generated by a finite region of turbulent flow is given using tensor notation with the summation convention. Starting from the Navier-Stokes equation

$$\rho \frac{\partial v_i}{\partial t} + \rho v_j \frac{\partial v_i}{\partial x_j} = - \frac{\partial p}{\partial x_i} + \frac{\partial \tau_{ij}}{\partial x_j} \qquad (2.1.1)$$

and the equation of continuity,

$$\frac{\partial \rho}{\partial t} + \frac{\partial}{\partial x_i} (\rho v_i) = 0 \qquad (2.1.2)$$

for an arbitrary continuous fluid without sources, sinks, or external forces, Lighthill (Ref. 1) has obtained the following expression

$$\frac{\partial^2 \rho}{\partial t^2} - a_o^2 \frac{\partial^2 \rho}{\partial x_i^2} = \frac{\partial^2}{\partial x_i \partial x_j} (T_{ij}) \qquad (2.1.3)$$

where

$$T_{ij} = \rho v_i v_j - \tau_{ij} + (p - a_o^2 \rho) \delta_{ij} \qquad (2.1.4)$$

Now, if the small effects of heat-conduction and viscosity are neglected in a medium without flow where $v_i, v_j$ are the velocities associated with acoustic waves only, the right-hand side of Eq. 2.1.3 is negligible and we have the classical wave equation for a stationary acoustic medium without sound sources. On the other hand, a medium with flow is equivalent to a stationary medium containing a spatial distribution of virtual sound sources whose strength per unit volume is given by $\partial^2 T_{ij} / \partial x_i \partial x_j$ . In other words an aerodynamic flow provides a forcing term for generating an acoustic field. Because of reasons connected with the double differentiation, Lighthill calls $T_{ij}$ the quadrupole strength per unit volume.

Let a volume element in the source field be $d^3\underline{Y}$ at point $\underline{Y}$. Then the solution for the density field at point $\underline{X}$ and time t in an unbounded medium is given by the Kirchhoff retarded potential solution (Ref. 20),

$$\Delta\rho (\underline{X},t) = \frac{1}{4\pi |\underline{X}-\underline{Y}| a_o^2} \iiint_{\infty} \frac{\partial^2 T_{ij}(\underline{Y})}{\partial y_i \partial y_j} \delta \left( t' - t + \frac{|\underline{X}-\underline{Y}|}{a_o} \right) dt' d^3\underline{Y} \qquad (2.1.5)$$

where the function $\delta(t')$ is the Dirac delta function. In other words, the quantity $\partial^2 T_{ij} / \partial y_i \partial y_j$ has to be evaluated at the retarded time $t - |\underline{X}-\underline{Y}| / a_o$. In the acoustic 'far field' where the distance $|\underline{X}|$ is large compared with a typical wave length and the dimensions of the flow region, the solution can be rwritten as (e.g., Refs. 21 and 22).

$$\Delta\rho (\underline{X},t) \simeq \frac{x_i x_j}{4\pi a_o^4 |\underline{X}|^3} \iiint_{\infty} \frac{\partial^2 T_{ij}(\underline{Y})}{\partial t^2} \delta \left( t' - t + \frac{|\underline{X}-\underline{Y}|}{a_o} \right) dt' d^3\underline{Y} \qquad (2.1.6)$$

Since it is customary to talk about acoustic pressure in the 'far field', we will rewrite the above equation in terms of pressure using the isentropic relationship,

$$\Delta p(\underline{X},t) \simeq \frac{x_i x_j}{4\pi a_o^2 |\underline{X}|^3} \iint_{\infty} \frac{\partial^2 T_{ij}(\underline{Y})}{\partial t^2} \delta\left(t' - t + \frac{|\underline{X}-\underline{Y}|}{a_o}\right) dt' \, d^3\underline{Y} \qquad (2.1.7)$$

The mean square pressure is then given by (Ref. 1),

$$\overline{\Delta p^2}(\underline{X},t) \simeq \frac{x_i x_j x_k x_\ell}{16\pi^2 a_o^4 |\underline{X}|^6} \iint_{\infty} \overline{\frac{\partial^2 T_{ij}(\underline{Y})}{\partial t_1^2} \delta\left(t_1 - t + \frac{|\underline{X}-\underline{Y}|}{a_o}\right) dt_1 d^3\underline{Y}}$$

$$\times \iint_{\infty} \overline{\frac{\partial^2 T_{k\ell}(Z)}{\partial t_2^2} \delta\left(t_2 - t + \frac{|\underline{X}-\underline{Y}|}{a_o}\right) dt_2 \, d^3\underline{Z}} \qquad (2.1.8)$$

where overbar denotes time average. For a statistically stationary turbulent motion, Eq. 2.1.8 can be written as (Refs. 16, 17, and 23),

$$\overline{\Delta p^2}\,(\underline{X}) \simeq \frac{x_i x_j x_k x_\ell}{16\pi^2 a_o^4 |\underline{X}|^6} \iiint_{\infty} \left[ \frac{\partial^4}{\partial \tau^4} \overline{T_{ij}(\underline{Y}) T_{k\ell}(\underline{Z},\tau)} \right] \delta(\tau - \tau^*) d\tau d^3\underline{Y} d^3\underline{Z}$$

where
$$\tau = t_2 - t_1$$
$$\tau^* = \frac{|\underline{X}-\underline{Y}|}{a_o} - \frac{|\underline{X}-\underline{Z}|}{a_o} \qquad (2.1.9)$$

Equation 2.1.9 can be generalized to give the pressure autocorrelation function by introducing an arbitrary time delay $\tau'$, i.e.,

$$\overline{\Delta p(\underline{X}) \Delta p(\underline{X},\tau')} \simeq \frac{x_i x_j x_k x_\ell}{16\pi^2 a_o^4 |\underline{X}|^6} \iiint_{\infty} \left[ \frac{\partial^4}{\partial \tau^4} \overline{T_{ij}(\underline{Y}) \, T_{k\ell}(Z,\tau)} \right] \delta[\tau - (\tau^* + \tau')]$$

$$d\tau d^3\underline{Y} \, d^3\underline{Z} \qquad (2.1.10)$$

A considerable simplification results on expressing the tensor contraction in the Proudman form (Ref. 11),

$$x_i x_j T_{ij} = |\underline{X}|^2 \, T_{xx} \qquad (2.1.11)$$

where $T_{xx}$ is the value taken on by $T_{11}$ when the 1-axis is aligned with the vector $\underline{X}$. Then we have,

$$\overline{\Delta p(\underline{X}) \Delta p(\underline{X},\tau')} \simeq \frac{1}{16\pi^2 a_o^4 |\underline{X}|^2} \iiint_{\infty} \left[ \frac{\partial^4}{\partial \tau^4} \overline{T_{xx}(\underline{Y}) T_{xx}(\underline{Z},\tau')} \right] \delta\,[\tau - (\tau^* + \tau')d\tau$$

$$d^3\underline{Y} d^3\underline{Z} \qquad (2.1.12)$$

Following Ref. 16, we introduce the following new variables for experimental convenience, see Fig. 1,

$$\underline{\eta} = \tfrac{1}{2}(\underline{Y} + \underline{Z})$$
$$\underline{\xi} = \underline{Y} - \underline{Z} \qquad (2.1.13)$$

The corresponding pressure autocorrelation function reads,

$$\overline{\Delta p(\underline{X})\Delta p(\underline{X},\tau')} \simeq \frac{1}{16\pi^2 a_o^4 |\underline{X}|^2} \iiint_{\infty} \left[\frac{\partial^4}{\partial\tau^4} R(\underline{\eta},\underline{\xi},\tau)\right]\delta\left[\tau - (\tau^* + \tau')\right] d\tau \, d^3\underline{\xi} d^3\underline{\eta}$$

where

$$R(\underline{\eta},\underline{\xi},\tau) = \overline{T_{xx}(\underline{\eta} + \underline{\xi}/2,\tau)T_{xx}(\underline{\eta} - \underline{\xi}/2)} \qquad (2.1.14)$$

and the difference in emission times given approximately by (Refs. 23 and 24),

$$\tau^* \simeq \frac{\underline{\xi} \cdot \underline{X}}{a_o |\underline{X}|} \qquad (2.1.15)$$

For reasons fully explained in his papers (Refs. 2 and 25), Lighthill suggests the use of a moving frame in analysing the turbulent field when the eddies are moving at non-negligible velocities. This is not a requirement - as pointed out by Ribner in Ref. 3 - if the differences in retarded time are maintained. However, for experimental convenience in neglecting the retarded time differences, the moving frame approach was chosen herein. Referring to a co-ordinate system moving with a uniform eddy convection velocity $U_c$, the pressure autocorrelation function takes on the following form (see Ref. 17 for detailed transformation),

$$\overline{\Delta p(\underline{X})\Delta p(\underline{X},\tau')} \simeq \frac{1}{16\pi^2 a_o^4 |\underline{X}|^2 \theta^5} \iiint_{\infty} \left[\frac{\partial^4}{\partial\tau^4} R_m(\underline{\eta},\underline{\xi}_m,\tau)\right]\delta\left[\tau - (\tau_m^* + \tau_m')\right] d\tau \, d^3\underline{\xi}_m d^3\underline{\eta} \qquad (2.1.16)$$

where

$$\underline{\xi}_m = \underline{\xi} - \underline{U}_c \tau$$

is the equivalent separation vector defined by the transformation allowing the moving frame correlation function to be defined in terms of the fixed frame correlation function and the time delay in terms of $\underline{\xi}_m$, i.e.,

$$R_m(\underline{\eta}, \underline{\xi}_m, \tau) = R(\underline{\eta},\underline{\xi},\tau)$$

$$\tau_m^* + \tau_m' = \frac{\underline{\xi}_m \cdot \underline{X}}{a_o |\underline{X}|(1 - M_c \cos\theta)} + \frac{\tau'}{(1 - M_c \cos\theta)}$$

and

$$\theta = (1 - M_c \cos\theta) \qquad (2.1.17)$$

The acoustic intensity can then be obtained from the following relation,

$$I(\underline{X}) = \frac{\overline{\Delta p^2(\underline{X})}}{\rho_o a_o} \tag{2.1.18}$$

## 2.2 Spectral Analysis of the Acoustic Field

Although a bit more information regarding the power spectral density can be extracted from the four-dimensional Fourier analysis as used by Kraichman (Ref. 26), Mawardi (Ref. 27), Lilley (Ref. 12), and Williams (Ref. 17), we have found that the essential features can more easily be obtained by the one-dimensional Fourier cosine transform technique. According to the well known Wiener-Khinchin relations for stochastic processes, the power spectral density of the acoustic pressure field is given by the Fourier cosine transform of its autocorrelation, i.e.,

$$\Phi(\underline{X},\omega) = \frac{2}{\pi}\int_0^\infty \overline{\Delta p(\underline{X})\Delta p(\underline{X},\tau')}\cos\omega\tau' d\tau'$$

$$= \frac{1}{\pi}\int_{-\infty}^{\infty} \overline{\Delta p(\underline{X})\Delta p(\underline{X},\tau')}\cos\omega\tau' d\tau' \tag{2.2.1}$$

Substituting (2.1.16) in (2.2.1),

$$\Phi(\underline{X},\omega) = \frac{1}{16\pi^3 a_o^4 |\underline{X}|^2\theta^5}\int_{-\infty}^{\infty}\cos\omega\tau' d\tau' \iiint_{-\infty}^{\infty}\left[\frac{\partial^4}{\partial\tau^4} R_m(\underline{\eta},\underline{\xi}_m,\tau)\right]\delta\left[\tau-(\tau_m^* + \tau')\right] d\tau d^3\underline{\xi}_m d^3\underline{\eta} \tag{2.2.2}$$

Changing the order of integration,

$$\Phi(\underline{X},\omega) = \frac{1}{16\pi^3 a_o^4 |\underline{X}|^2\theta^4}\int_{-\infty}^{\infty} d^3\underline{\eta}\int_{-\infty}^{\infty} d^3\underline{\xi}_m\int_{-\infty}^{\infty}\frac{\partial^4}{\partial\tau^4} R_m(\underline{\eta},\underline{\xi}_m,\tau)d\tau$$

$$\times\int_{-\infty}^{\infty}\delta\left[(\tau-\tau_m^*) - \frac{\tau'}{\theta}\right]\cos\omega\theta\,\frac{\tau'}{\theta}\,d\left(\frac{\tau'}{\theta}\right)$$

$$= \frac{1}{16\pi^3 a_o^4 |\underline{X}|^2\theta^4}\int_{-\infty}^{\infty} d^3\underline{\eta}\int_{-\infty}^{\infty} d^3\underline{\xi}_m\int_{-\infty}^{\infty}\frac{\partial^4}{\partial\tau^4} R_m(\underline{\eta},\underline{\xi}_m,\tau)\cos[\omega\theta(\tau-\tau_m^*)]d\tau \tag{2.2.3}$$

Now defining

$$\omega_t = \omega\,\theta \tag{2.2.4}$$

and expanding the cosine term, we have

$$\cos\omega_t(\tau-\tau_m^*) = \cos\omega_t\tau\cos\omega_t\tau_m^* + \sin\omega_t\tau\sin\omega_t\tau_m^* \tag{2.2.5}$$

Experimental evidence (Ref. 28 and 29) indicates that $R_m(\underline{\eta},\underline{\xi}_m\tau)$ is an even function in $\tau$, so the sine term will integrate to zero. Therefore

$$\Phi(\underline{X},\omega) = \frac{1}{16\pi^3 a_o^4 |\underline{X}|^2 \theta^4} \int_\infty d^3\underline{\eta} \int_\infty d^3\underline{\xi}_m \cos \omega_t \tau_m^* \int_\infty \frac{\partial^4}{\partial\tau^4} R_m(\underline{\eta}, \underline{\xi}_m, \tau)$$

$$\times \cos \omega_t \tau \, d\tau \qquad (2.2.6)$$

Since $R_m(\underline{\eta},\underline{\xi}_m,\tau)$ is even,

$$\frac{\partial R_m}{\partial\tau} = \frac{\partial^3 R_m}{\partial\tau^3} = 0 \quad \text{at } \tau = 0$$

If, in addition,

$$R_m = \frac{\partial^n R_m}{\partial\tau^n} = 0 \quad \text{at } \tau = \infty \quad \text{for } n = 1,2,3$$

then according to the theory of Fourier transforms (Ref. 30) we have

$$\Phi(\underline{X},\omega) = \frac{1}{16\pi^3 a_o^4 |\underline{X}|^2} \frac{\omega_t^4}{\theta^4} \int_\infty d^3\underline{\eta} \int_\infty d^3\underline{\xi}_m \cos\omega_t \tau_m^* \int_\infty R_m(\underline{\eta},\underline{\xi}_m,\tau) \cos\omega_t \tau d\tau$$

$$= \frac{\omega^4}{16\pi^3 a_o^4 |\underline{X}|^2} \int_\infty d^3\underline{\eta} \int_\infty d^3\underline{\xi}_m \cos\omega\theta\tau_m^* \int_\infty R_m(\underline{\eta},\underline{\xi}_m,\tau) \cos\omega\theta\tau \, d\tau \qquad (2.2.7)$$

Several interesting observations can be made of the above equation. Firstly, we can identify $\omega_t$ as the frequency in the turbulence; the corresponding radiated frequency $\omega$ is then the Doppler-shifted frequency (i.e., $\omega = \omega_t/\theta$). This is a logical result which one could have obtained on physical grounds. Secondly, Lighthill's criterion for neglecting retarded time shows up automatically in the $\cos\omega\theta\,\tau_m^*$ term. According to Lighthill, retarded time can be neglected if $\omega\ell/a_o$ is small so that the eddy size $\ell$ is small compared with the wave-length of the sound it generates. If this condition is met in our case, then for $\xi_m \leq \ell$ the term $\cos\omega\theta\tau_m^*$ can be approximated as unity. Thirdly, if retarded time is neglected, Lighthill's convection factor $(1 - M_c\cos\theta)^{-5}$, which accounts for the main effect of convection at limited speeds is exhibited as a vertical shift $(1 - M_c\cos\theta)^{-4}$ plus a Doppler shift $(1 - M_c\cos\theta)^{-1}$ in the power spectrum and is illustrated in Fig. 2. This concept is a low-speed version of a similar idea presented in Ref. 3. Fourthly, although the Lighthill's convection factor is not applicable for high-speed convection because of its singularity where $1 - M_c\cos\theta = 0$, the following example will show that Eq. 2.2.7 is still valid for high speed if retarded time is not neglected. In fact this moving frame integral with proper account of retarded time possesses a zero that exactly cancels the $(1 - M_c\cos\theta)^{-5}$ singularity and replaces it by a nonsingular convection factor (c.f. also Refs. 16 and 17).

The correlation function chosen for the present example is the equivalent nonconvective form of the one used by Ribner (Refs. 16 and 24)

for a homogeneous and isotropic turbulent flow, i.e.,

$$R_m(\underline{\eta},\underline{\xi}_m,\tau) = (\overline{T}_{xx})^2 e^{-\left[\frac{\pi}{L^2}(\xi_{m_1}^2 + \xi_{m_2}^2 + \xi_{m_3}^2) + \omega_f^2 \tau^2\right]} \tag{2.2.8}$$

where L and $\omega_f$ refer to a typical length scale and frequency respectively. Because of the assumption of isotropy, it suffices to consider $\underline{X}$ to be in the 1-2 plane. The exact integral can then be evaluated directly with the proper retarded time given by

$$\tau_m^* = \frac{\xi_{m_1} \cos\theta + \xi_{m_2} \sin\theta}{a_o(1 - M_c \cos\theta)} \tag{2.2.9}$$

Substituting (2.2.8) and (2.2.9) in (2.2.7), we obtain for the spectrum of noise from a unit volume of turbulence,

$$\frac{\partial^3 \Phi(\underline{X},\omega)}{\partial^3 \underline{\eta}} = \frac{(\overline{T}_{xx})^2 L^3 \omega^4}{16\pi^{5/2} a_o^4 |\underline{X}|^2 \omega_f} e^{-\frac{\omega^2 C^2}{4\omega_f^2}} \tag{2.2.10}$$

where

$$C = \left[(1 - M_c \cos\theta)^2 + \frac{\omega_f^2 L^2}{\pi a_o^2}\right]^{\frac{1}{2}} \tag{2.2.11}$$

The mean square pressure is obtained by integrating Eq. 2.2.10 with respect to frequency,

$$\frac{\partial^3 \overline{\Delta p^2}(\underline{X})}{\partial^3 \underline{\eta}} = \int_0^\infty \frac{\partial^3}{\partial^3 \underline{\eta}} \Phi(\underline{X}, \omega)\, d\omega \tag{2.2.12}$$

$$= \frac{3}{4} \frac{(\overline{T}_{xx})^2 \omega_f^4 L^3}{\pi^2 a_o^4 |\underline{X}|^2 C^5}$$

This result is the same as that obtained by Ribner (c.f. Eq. 7.9 in Ref. 3) using a fixed frame formalism with a convective correlation function.

The above example shows that when the convection Mach number is supersonic the mean square pressure has a finite peak at $\cos\theta = 1/M_c$ instead of an infinite one, provided proper retarded time has been considered - a fact first recognized by Ribner (Ref. 24).

## 2.3 'Shear Noise' and 'Self Noise'

For large Reynolds number and moderate Mach number, $T_{ij}$ can be approximated by $\rho_o v_i v_j$ (Ref. 1), then

$$T_{xx} \cong \rho_o v_x^2 \tag{2.3.1}$$

where $v_x$ is the instantaneous velocity component along the vector $\underline{X}$ from the

origin to the observer. Writing the instantaneous velocity $\underline{v}$ as the sum of a mean velocity plus a perturbation, we have,

$$v_x = U_x + u_x \tag{2.3.2}$$

and thus

$$R(\underline{\eta},\underline{\xi},\tau) = \rho_o^2 \left[\overline{u_x^2 u_x'^2} + 4U_x U_x' \overline{u_x u_x'} + \text{other terms}\right] \tag{2.3.3}$$

where unprimed quantities refer to the point $Q = \underline{\eta} + \underline{\xi}/2$ at time $t + \tau$ and the primed quantities refer to the point $Q' = \underline{\eta} - \underline{\xi}/2$ at time $t$ (see Fig. 1). The 'other terms' are either time independent and differentiate out or they are negligible compared with the first two terms. Ribner (Ref. 3) labels the first term 'self noise' and the second term 'shear noise'.

Using a simplified model of isotropic turbulence superposed on a mean flow and a joint Gaussian probability density for $u_x$ and $u_x'$, he obtains the following relation,*

$$\frac{\text{shear-noise}}{\text{self-noise}} \sim \frac{\cos^4\theta + \cos^2\theta}{2} \tag{2.3.4}$$

He is also able to obtain separate spectra for the 'shear' and 'self' noise peaking an octave apart.

We are going to follow his notion of 'shear' and 'self' noise and try to measure both the covariance of the velocity squared as well as that of the velocity itself. Thus we shall replace his conceptual model by measurements in a real turbulent jet.

## III. EXPERIMENTAL APPARATUS

### 3.1 4 Inch Low-Speed Model Jet

A detailed description of the 4 inch model jet has already been given in Ref. 28. Basically, it consisted of a screened diffuser, a settling chamber and a 12:1 contraction ending in a 4 inch diameter jet. It was powered by a one horsepower centrifugal blower giving a velocity of approximately 142 fps. The intake of the blower was connected to a large wooden chamber whose opening was covered with three layers of ordinary furnace filter to provide a dust free air flow (Fig. 3).

### 3.2 Hot-Wire Probes Traversing Gear

This has also been reported in Ref. 28. Essentially, it provided identical movement in opposite directions with respect to a common point for the two probes. In addition, it had three degrees of freedom for this common point (Fig. 3).

---

* Unpublished work; this is a correction of the ratio $\cos^4\theta$ obtained in Refs. 3 and 13.

3.3 Hot-Wire Probes and Anemometer

The hot-wire probes were conventionally built from hypodermic tubing with sewing needles as supporting prongs. The wire itself was 0.000132 (nominal diameter) tungsten wire copper plated at the ends to leave a sensing element in the middle of about 1/32 of an inch. A close-up picture of the probes is shown in Fig. 4.

The hot-wire anemometer used was the Hubbard Model II HR Type 3A dual channel constant temperature anemometer. It has a built-in linearizing circuit and the frequency response of the combination is flat up to ten kHz . As was found in Ref. 31, we could obtain linearity in our speed range only with an overheating ratio of 0.3 to 0.4. The output circuit was slightly modified to give a smooth d-c voltage reading for the mean speed. The d-c voltages were measured with two Simpson multimeters which had been calibrated against a 0.01% digital voltmeter.

3.4 Time-Delay Correlator

The existing UTIAS time-delay correlator as reported in Ref. 32 consists of essentially a two-track tape recorder, an analog multiplier, and an active R-C integrator. The adjustable time delay is obtained by a special staggered play-back heads assembly (Fig. 5). In order to meet the required accuracy and performance for the present investigation, the unit has been modified and improved. The integrator circuit was replaced by a better performance (0.2% accuracy) active R-C integrator and the output was read with a four-figures reading digital voltmeter. An automatic controlling circuit has been incorporated into the system. This special circuit controlled the operating switches of the tape recorder, the starting and timing of the integrator and the displaying of the result on the digital voltmeter in a proper sequence. See Fig. 3 for the general set up. The frequency response of the whole system was essentially flat from 30 to 10,000 Hz (Fig. 6). Its performance is illustrated in Fig. 7 showing accurate correlations of sine waves of three different frequencies.

## IV. EXPERIMENTAL PROCEDURE

The main work of the present investigation involved longitudinal two-point space-time correlations of not only the turbulent velocities but also the square of these velocities. The measurements included the ordinary u-component and components at $45^{\circ}$ and $60^{\circ}$ to the jet axis. Space correlations of these velocity components were also obtained along the two transverse axes to give the lateral length scales. In addition, the mean velocity of these components were also measured.

4.1 Calibration of Hot-Wires

All wires were calibrated in the laminar core of the jet near the exit using a pitot-static probe. The calibration was done at the beginning of every period of testing and a two-point check was performed at the end to ensure that there had been no appreciable change in the calibration. Since the individual probe constants cancel out in forming the nondimensional correlation, no attempt was made to match the probe characteristics. A typical calibration curve is shown in Fig. 8.

## 4.2 Determination of Hot-Wire Position

All our measurements were taken about the location $\eta_1/D = 4$ and $\eta_2/D = 0.5$ as a center. The traversing mechanism enabled the two hot-wire probes to be moved at equal distances from this point along three orthogonal axes. This center point of investigation was located by means of two telescopes: one placed downstream and the other across the jet. Since it was fairly difficult to relocate the probe after a wire failure during a run, that particular test was repeated using a new wire. However, such failure did not occur very often.

## 4.3 Determination of Hot-Wire Inclination

For measurements of the $45^\circ$ and $60^\circ$ components a dynamic determination of the wire inclination was used rather than a static geometrical one. The wires were first placed in the laminar core of the jet. They were then rotated to one proper inclination as indicated by the mean velocity measurements which were computed from the usual sine-law response of inclined wires. (A discussion of the sensitivity of inclined wires is given in Appendix A.) The wires were then transferred to the location of investigation. Our special traversing mechanism enabled such a transfer without changing the inclination of the wires to the jet axis.

## 4.4 Method of Measurements

For each separation of the two hot-wire probes in the flow, the electrical signals that were related to the turbulent velocity components were recorded simultaneously on the two tracks of the tape recorder. The d-c readings that were proportional to the mean velocities were recorded separately. When correlating the square of turbulent velocities the signals were first squared by means of a dual-channel Philbrick Analog Multiplier before they were taped. At the initial position of zero separation the true rms values of the a-c signals were measured with a Flow Corporation Random Signal Meter. The product of the two wires' readings served to give the mean square values of the turbulent velocities at the center point. After readings at maximum separation were taken, the two probes were returned to their initial positions and a check was performed on both the a-c and d-c readings. The deviation was usually less than 5%. Block diagrams of the recording and data processing system are shown in Figs. 9 and 10.

In order to detect any changes in sensitivity of the recording tape and possible electronic drift, a fixed intensity 1,000 Hz sine wave was recorded at fixed intervals during the run to serve as reference points. Such possible changes were later corrected by assuming a linear variation between the reference points in the data processing.

When the two recorded signals were played back, a finite time delay $\tau$ was inserted between them by means of the adjustable staggered playback heads. Then the signals were amplified, multiplied, and averaged by means of an active R-C integrator whose integration time is 10 seconds. The results were normalized with respect to the mean square value at the center point. This process was repeated for a sequence of values of $\tau$ .

## V. EXPERIMENTAL RESULTS

The main objective of the present investigation has been to estimate the intensity, the spectrum, and the basic directivity of the noise generated by a unit volume of turbulence from the two-point space-time correlation measurements of turbulent velocities. However, we feel it is worth reporting here first some of the characteristics of jet turbulence, particularly the 45° and 60° components which have not been measured before. Whenever possible, the present results are compared with those of other workers.

### 5.1 Mean Velocity Measurements

The variation of the mean velocity across the jet has previously been measured with a single hot-wire by the present author and reported in Ref. 33. A similarity parameter has been rediscovered which enabled the mean velocity profiles of jets up to low supersonic speed to be plotted on one single universal curve.

### 5.2 Turbulence Intensity

A complete survey of the turbulent intensities across the jet has not been carried out herein. But parts of the turbulent intensity profiles around $\eta_2/D = 0.5$ were obtained from recorded data of two-point space-time correlations. They are shown in Fig. 11(a). Note that the intensity of the 45° component was higher than that of the ordinary u-component, and that of the 60° component was lower. Other workers (Ref. 9) have shown that the intensity of the 90° (or v) component was lower than that of the u-component, which seems consistent. Figure 11(b) shows a favourable comparison between the present result and that of Laurence (Ref. 7) for the nondimensional quantity $\sqrt{\overline{u^2}}/(\sqrt{\overline{u^2}})_{max}$ at the same downstream location.

### 5.3 Space Correlations and Length Scales

The signals from two hot-wire probes separated by a distance $\xi$ can be correlated to define a region over which the velocities at the two points are strongly related. These results can then be used to define an integral length scale or typical 'eddy' size. For conveniences in later computational work, the space correlation coefficient is defined as follows,

$$\mathcal{R}(\eta,\xi,\theta) = \frac{\overline{u_\theta(\eta + \xi/2)\, u'_\theta(\eta - \xi/2)}}{\overline{u^2_\theta(\eta)}} \qquad (5.3.1)$$

where $u_\theta$ is the turbulent velocity component making an angle $\theta$ with the jet axis and the overbar denotes an average over a period of time sufficiently long to obtain a stationary value.

The integral length scale is defined as

$$L_{u\theta}(\eta) = \int_0^\infty \mathcal{R}(\eta,\xi,\theta)\, d\xi \qquad (5.3.2)$$

or alternatively as

$$L^*_{u\theta}(\eta) = \int_0^{\xi^*} \mathcal{R}(\eta,\xi,\theta)\, d\xi \qquad (5.3.3)$$

depending on experimental convenience (see later), where $\underline{\xi}^*$ is the maximum separation at which $\mathcal{R}(\underline{\eta},\underline{\xi},\theta)$ goes to zero. Similar definitions are used for the correlations of the square of the velocities.

The nine quantities $\mathcal{R}(\underline{\eta},\underline{\xi},\theta)$ are shown in Fig. 12 for correlations of both the turbulent velocities and the square of these velocities. The general forms of the u-component correlations in the three orthogonal axes were in close agreement with those of Ref. 9. The decrease in magnitude of the negative correlation with increasing $\theta$ in the circumferential traverse was also compatible with results of Ref. 9 which showed a non-negative correlation for the component at $\theta = 90^o$.

In computing the integral length scales, Eq. 5.3.2 was used for the radial and circumferential cases whereas Eq. 5.3.3 was used for the axial case. In this connection, the negative correlation in the axial traverse was most likely a spurious effect due to inadequate low-frequency cut-off of the tape recorder in the time-delay correlator. A detailed discussion of the effect of low-frequency cut-off is given in Appendix B. Estimates based on the finding in Appendix B indicated that our transverse length scales might be lower by about 10% and that the longitudinal scales might be off by as much as 20%. The different length scales nondimensionalized by the jet diameter are given below.

for correlation of $u_\theta$

| | $(\xi_1, 0, 0)^*$ | $(0, \xi_2, 0)$ | $(0, 0, \xi_3)$ |
|---|---|---|---|
| $L_{u_{0^o}}/D$ | 0.191 | 0.138 | 0.023 |
| $L_{u_{45^o}}/D$ | 0.168 | 0.187 | 0.025 |
| $L_{u_{60^o}}/D$ | 0.144 | 0.223 | 0.048 |

for correlation of $u_\theta^2$

| | $(\xi_1, 0, 0)^*$ | $(0, \xi_2, 0)$ | $(0, 0, \xi_3)$ |
|---|---|---|---|
| $L_{u^2{}_{0^o}}/D$ | 0.102 | 0.057 | 0.050 |
| $L_{u^2{}_{45^o}}/D$ | 0.080 | 0.059 | 0.041 |
| $L_{u^2{}_{60^o}}/D$ | 0.070 | 0.061 | 0.044 |

The small length scale associated with the correlation of $u_\theta$ along the $\xi_3$ axis (third column of first table) arises from the large negative loops in Fig.12. This does not imply that the eddies are physically very short in the $\xi_3$ direction.

## 5.4 Two-Point Space-Time Correlation

If the signal from the upstream probe is delayed a time $\tau$ before being correlated with the other, the two-point space-time (or cross) correlation will be obtained

$$\mathcal{R}(\underline{\eta},\underline{\xi},\theta,\tau) = \frac{\overline{u_\theta(\underline{\eta}+\underline{\xi}/2,\tau)\, u'_\theta(\underline{\eta}-\underline{\xi}/2)}}{\overline{u^2_\theta(\underline{\eta})}} \qquad (5.4.1)$$

A similar definition is used for correlations of the square of velocities. Results for the three components in the axial traverse are shown in Figs. 13 - 18. The convective nature of the turbulent field is revealed by the 'yawing' of the correlation 'ridge' of the typical three dimensional plot in Fig. 19 (e.g., Ref. 16).

The correlation coefficients for different probe separations did not rise to unity with optimum time delay as shown in previous figures. This fact showed that the turbulence 'pattern' was not a 'frozen pattern'. According to Ref. 29 the envelope of these cross-correlation curves is the autocorrelation of the fluctuation which would be seen by an observer moving with the turbulence. The Fourier cosine transform of this evenlope will give the spectral density of the turbulence relative to axes moving with the flow. Figure 20 shows a comparison between the fixed frame and the moving frame spectra of the axial turbulent velocity. The fixed frame spectrum was obtained as usual with a Murhead wave analyser. The moving frame spectrum was obtained from the moving frame autocorrelation using Filon's numerical method (Ref. 34). The computation was done with the IBM 7094 computer at the Institite of Computer Science in the University of Toronto. It is seen that the fixed frame spectrum contains more of the high frequencies due to the convection of a spatial pattern passing the fixed hot-wire probe.

Richards and Williams (Ref. 35) considered this moving frame turbulence spectrum and speculated that the radiated sound spectrum could roughly be deduced from it by the addition of twelve db per octave. This is equivalent to multiplying the moving frame spectrum by $\omega^4$. However, the very strong amplification of the high frequencies makes accurate estimation very unlikely. Also the assumption that the simple u-velocity spectrum will represent the spectrum of the more complex $T_{ij}$ is a great over-simplification. Therefore, there is no escape from using a more elaborate approach as given in Section VII here.

## 5.5 Convection Velocity

For a frozen pattern as found in turbulence behind grids the turbulent convection velocity is equal to the mean flow velocity. In the case of turbulent shear flow the shear stresses distort the convected pattern as it travels downstream. As a result there is no unique convection velocity. However, from the view point of aerodynamic noise generation, a good criterion for the definition of convection velocity is that the time scale of the fluctuating turbulent stress should be a maximum in a reference frame moving with this velocity. Thus a meaningful definition of the convection velocity is the ratio $\xi_1/\tau$ at the point where $\partial/\partial\xi_1\ \mathcal{R}(\underline{\eta},\xi_1,\tau) = 0$ . As has been pointed out by Williams (Ref. 29) and Fisher and Davies (Ref. 36). This corresponds to the convection velocity defined by the time delay for which

the curve of $\mathcal{R}(\underline{\eta}, \underline{\xi}, \tau)$ versus $\tau$ coincides with the envelope of all such curves. From Figs. 13 - 18, the following values for convection velocity were obtained;

| Cases: | $u_o$ | $u_{45^o}$ | $u_{60^o}$ | $u_o^2$ | $u_{45^o}^2$ | $u_{60^o}^2$ |
|---|---|---|---|---|---|---|
| $\frac{U_c}{U_j}$ : | 0.58 | 0.61 | 0.61 | 0.62 | 0.63 | 0.66 |

Within experimental error, it seemed that the different velocity components travelled with the same convection velocity. This was in agreement with results of Ref. 9 for the axial and radial components. Also the approximate magnitude was in agreement with results of Refs. 8 and 9 at the same cross stream location.

## VI. ESTIMATION OF NOISE INTENSITY AND BASIC DIRECTIVITY

In our case of a low velocity jet, the differences in retarded time within a correlation volume could be neglected because the 'eddy' size was small compared with the typical wavelength of sound it generated. A posteriori check showed that the ratio was about 0.01. Neglecting retarded time, we can interchange the integration and differentiation processes, and Eq. 2.1.16 then becomes

$$\overline{\Delta p(\underline{X})\Delta p(\underline{X},\tau')} \simeq \frac{1}{16\pi^2 a_o^4 |\underline{X}|^2 C^5} \int_\infty d^3\underline{\eta} \int_\infty \left[ \frac{\partial^4}{\partial\tau^4} \int_\infty R_m (\underline{\eta},\underline{\xi}_m,\tau) d^3\underline{\xi}_m \right] \times \delta(\tau-\tau_m')d\tau \qquad (6.1)$$

Note that the Lighthill's convection factor $\Theta^{-5}$ has been replaced by the non-singular factor $C^{-5}$. This may be justified as follows. We have seen in material leading to Eq. 2.2.12 that when retarded time is included the final convection factor is of the cited form $C^{-5}$. Therefore the replacement of $\Theta^{-5}$ by $C^{-5}$ here should constitute a first approximation to a correction for the neglect of retarded time. The intensity of noise generated from unit volume of turbulence follows from Eq. 2.1.18 as

$$\frac{\partial^3 I(\underline{X})}{\partial^3 \underline{\eta}} \simeq \frac{1}{16\pi^2 \rho_o a_o^5 |\underline{X}|^2 C^5} \int_\infty \left[ \frac{\partial^4}{\partial\tau^4} \int_\infty R_m (\underline{\eta},\underline{\xi}_m,\tau) d^3\underline{\xi}_m \right] \delta(\tau) d\tau \qquad (6.2)$$

In the present co-ordinate system there was convection only in the axial (or 1) direction, therefore, from Eq. 2.1.17,

$$R_m(\underline{\eta}, \xi_{m_1}, \xi_{m_2}, \xi_{m_3}, \tau) = R(\underline{\eta}, \xi_{m_1} + U_c\tau, \xi_2, \xi_3, \tau) \qquad (6.3)$$

Note that even for the simple case of estimating $R_m(\underline{\eta},0,\xi_{m_2},0,\tau)$ one of the probes has to be displaced not only in the 2-direction but also in the 1-direction by an amount of $U_c\tau$. The fact that the convection velocity varies across the jet (Ref. 8 and 9) adds more complication to the investigation. Thus to hold the amount of labour within reasonable bounds we were

forced to use the simplifying assumption that the four-dimensional space-time correlation function was separable in space in the two transverse axes while keeping the nonseparable nature in space and time in the axial direction, i.e.,

$$R(\underline{\eta},\xi_{m_1} + U_c\tau,\xi_2,\xi_3,\tau) = R_1(\underline{\eta},\xi_{m_1} + U_c\tau,\tau)\, R_2(\underline{\eta},\xi_2)\, R_3(\underline{\eta},\xi_3) \qquad (6.4)$$

Note that the present assumption is less restrictive than the usual one of a completely separable function in space and time (Refs. 3, 12, and 17). With this assumption, it can be shown that

$$R(\underline{\eta},\xi_{m_1} + U_c\tau,\xi_2,\xi_3,\tau) = \frac{R(\underline{\eta},\xi_{m_1} + U_c\tau,\, 0,0,\tau)R(\underline{\eta},0,\xi_2,0,0)R(\underline{\eta},0,0,\xi_3,0)}{[R(\underline{\eta},0,0,0,0)]^2} \qquad (6.5)$$

The intensity per unit volume becomes,

$$\frac{\partial^3 I(\underline{X})}{\partial^3 \underline{\eta}} \simeq \frac{R(\underline{\eta},0,0,0,0)}{2\pi^2 \rho_o a_o^5 |\underline{X}|^2 c^5} \int_0^\infty \frac{R(\underline{\eta},0,0,\xi_3,0)}{R(\underline{\eta},0,0,0,0)}\, d\xi_3 \int_0^\infty \frac{R(\underline{\eta},0,\xi_2,0,0)}{R(\underline{\eta},0,0,0,0)}\, d\xi_2$$

$$\times \int_{-\infty}^{\infty} \delta(\tau)d\tau \left[ \frac{\partial^4}{\partial\tau^4} \int_0^\infty \frac{R(\underline{\eta},\xi_{m_1} + U_c\tau,\, 0,0,\tau)}{R(\underline{\eta},0,0,0,0)}\, d\xi_{m_1} \right] \qquad (6.6)$$

Using results of Section 2.3, we have for the 'shear'noise:

$$\left(\frac{\partial^3 I(\underline{X})}{\partial^3 \underline{\eta}}\right)_{\text{shear}} \simeq \frac{2\rho_o U_x^2(\underline{\eta})\overline{u_x^2}(\underline{\eta})}{\pi^2 a_o^5 |\underline{X}|^2 c^5}\, \mathcal{L}_3 \mathcal{L}_2 \int_{-\infty}^{\infty} \delta(\tau)d\tau \left[ \frac{\partial^4}{\partial\tau^4} \int_0^\infty \frac{{}_{sh}R(\underline{\eta},\xi_{m_1}+U_c\tau,0,0,\tau)}{U_x^2(\underline{\eta})\, \overline{u_x^2}(\underline{\eta})}\, d\xi_{m_1} \right]$$

where

$$\mathcal{L}_3 = \int_0^\infty \frac{U_x U_x'\, \overline{u_x u_x'}\, (\underline{\eta},0,0,\xi_3,0)}{U_x^2(\underline{\eta})\, \overline{u_x^2}(\underline{\eta})}\, d\xi_3 \qquad \text{etc.}$$

and

$${}_{sh}R(\underline{\eta},\xi_1,0,0,\tau) = U_x U_x'\, \overline{u_x u_x'}(\underline{\eta},\xi_1,0,0,\tau) \qquad (6.7)$$

and for the 'self' noise:

$$\left(\frac{\partial^3 I(\underline{X})}{\partial^3 \underline{\eta}}\right)_{\text{self}} \simeq \frac{\overline{u_x^4}(\underline{\eta})\rho_o}{2\pi^2 a_o^5 |\underline{X}|^2 c^5}\, L_3 L_2 \int_{-\infty}^{\infty} \delta(\tau)d\tau \left[ \frac{\partial^4}{\partial\tau^4} \int_0^\infty \frac{{}_{se}R\,(\underline{\eta},\xi_{m_1} + U_c\tau,0,0,\tau)}{\overline{u_x^4}(\underline{\eta})}\, d\xi_{m_1} \right.$$

where

$$L_3 = \int_0^\infty \frac{\overline{u_x^2 u_x'^2}\ (\underline{\eta},0,0,\xi_3,0)}{\overline{u_x^4}(\underline{\eta})}\, d\xi_3 \qquad \text{etc}$$

and

$${}_{se}R(\underline{\eta},\xi_1,0,0,\tau) = \overline{u_x^2 u_x'^2}\ (\underline{\eta},\xi_1,0,0,\tau) \qquad (6.8)$$

Knowing the convection velocity, $R(\eta,\xi_{m_1}+U_c\tau,0,0\tau)$ can be obtained from $R(\eta,\xi_1,0,0,\tau)$.

In obtaining $R(\eta,\xi_1,0,0,\tau)$ for the 'shear' noise, the mean velocities were first corrected for the effect of turbulence using the following equation (Ref. 37),

$$U_{corr.} \simeq U_{exp.} - \tfrac{1}{2}\frac{\overline{u^2}}{U_{exp.}} \tag{6.9}$$

Figures 21 - 26 show plots of $\dfrac{U_x U'_x\,\overline{u_x u'_x}(\eta,\xi,0)}{U_x^2(\eta)\overline{u}_x^2(\eta)}$

for the three components in the two transverse axes together with the respective areas under these curves. This quantity in the axial direction will be the same as the correlation function defined in Sec. 5.4 because of the uniformity of the mean velocities within our correlation separations. Figures 27 and 28 show the typical forms of $R(\eta,\xi_{m_1}+U_c\tau,0,0,\tau)$ as derived from the fixed frame correlation for both the 'shear' and 'self'noise. As has been pointed out earlier, the negative correlation at large separation was most likely due to the inadequate low frequency response of the instrument. Results from Appendix B suggest that to a first approximation, the correction term due to low-frequency cut-off when transformed to the moving frame is independent of time delay. This conclusion is manifested by the collapsing of the families of curves onto a single curve at large separation shown in Figs. 27 and 28. The integrated areas of $R(\eta,\xi_{m_1}+U_c\tau,0,0,\tau)$ versus $\xi_{m_1}$ as a function of $\tau$ are shown in Figs. 29(a) and 30(a). The problem now is to determine the fourth derivative of these final curves with respect to $\tau$.

## 6.1 Extraction of Higher Order Derivative

Since the whole problem hinges on the extraction of the fourth derivative of some experimental curves, a sophisticated method is required. In Ref. 38, several methods have been tried to obtain the second derivative of experimental data. It was concluded there that the traditional technique of fitting (by least square) a high degree polynomial to the data was still the best method. For the present purpose a more elaborate IBM 7094 computer program was written whereby the data points could be fitted by a polynomial of any degree. Only even power terms in the polynomial were used because we were dealing theoretically with an even function.

It was impossible to estimate in any simple ways the probable error in the final experimental data points, so the criterion of best fit could only be furnished by the sum of the standard derivations (Ref. 39). The number of terms in the polynomial were increased one at a time until the sum of the standard deviations was approaching a minimum. It turned out that the fourth derivative at the origin was also approaching approximately an asymptotic value.

This approach was first tested out with a Gaussian function. This function was sampled at approximately the same intervals as our experimental data. In order to introduce some arbitrary error the magnitudes of these sampled points were rounded off at two decimal places. Figure 31 shows that the comparison between the theoretical fourth derivative and that obtained from the best polynomial fit is very good up to a fair range of $\tau$.

Since we do not have the complete four' derivative curve from the polynomial approximation, it is necessary to investigate the range of the fourth derivative curve required to give a proper Fourier cosine transform for estimating the spectrum. It turned out that when the fourth derivative curve resembled a damped oscillation, the first half wave-length would suffice to give a fairly good estimate of both the peak and the general shape of its Fourier cosine transform. This is illustrated in Fig. 32, still using the Gaussian function. The fourth derivative of the approximating polynomial was fitted with an analytical function $(Ae^{-B\tau^2}\cos C\tau)$ whose Fourier cosine transform was then compared with the theoretical result.

When this technique was applied to actual experimental results, two other types of function were tried in addition to the straight polynomial. They were

(1) $$e^{-(a_0 + a_2\tau^2 + \ldots + a_n\tau^n)}$$

(2) $$\frac{1}{a_0 + a_2\tau^2 + \ldots + a_n\tau^n}$$

These were obtained by fitting an even degree polynomial, still in the least square sense, to the logarithm and the reciprocal of the experimental data respectively. A comparison of the typical results for the three types of fitting is given in Figs. 33 and 34. Note the consistant behaviour of the fourth derivative at the origin as a function of the degree in the fitting polynomial for the three cases. It must be pointed out here that even if the magnitude of the fourth derivative at the origin changes by a factor of two, the resulting noise intensity will change by only three db. This is not considered to be a serious error in acoustic measurements. The exponential function with a polynomial exponent was chosen for consistency because it gave the damped oscillatory shape of the fourth derivative for all cases considered (Figs. 29(b), and 30(b)). The straight polynomial fit was rejected because the fourth derivative obtained from it resembled a pure cosine function. The Fourier cosine transform of it would be a delta function implying that a pure tone was generated by the unit volume of turbulence considered. Physically this is less plausible than the peaky spectra obtained from the other two functions.

Although the least square curve fitting method seems to be the most promising and consistent way of dealing with our data, it should be pointed out that the results so obtained are quite sensitive to the range of data available. When we first applied this method to our data, we found that at zero degree to the jet axis, the 'shear' noise intensity was about twenty-two times higher than that of the 'self' noise and that the peak frequency of the 'self' noise was only 1.3 times that of the 'shear' noise. These results are incompatible with measured jet noise.

Upon carefully re-examining the data, we observed that because of the limited abscissa scale we had only about 25% variation in magnitude of our correlation for the 'shear' noise cases as compared to the 45% variation for the 'self' noise cases (Figs. 29(a), and 30(a)). In order to obtain a fair comparison between the two types of noise, the 'shear' noise

data should be extrapolated to give approximately the same percentage variation in magnitude as those of the 'self' noise. Exponential functions of the type $e^{-(a\tau)^n}$ were used in the extrapolation by replotting the logarithm of the tail end data of Fig. 29(a) on a log log scale (Fig. 35). Extrapolated values of the three 'shear' noise cases were shown as black dots in Fig. 29(a).

From results of Section VI, the length scales obtained in Sec. 5.3, and the fourth derivative of the moving-frame longitudinal space-time correlation at zero time delay obtained here, an estimate of the noise intensity generated by a unit volume of turbulence could be obtained through Eqs. 6.6 and 6.7. A listing of the coefficients in the polynomial exponent of the exponential functions used in the least square curve fitting is shown in Appendix C. The corresponding curves are shown in Figs. 29(a) and 30(a).

The final results are given in the following table in the non-dimensional form.

| | $\frac{\partial^3}{\partial^3 \underline{\eta}} \left( \frac{I(\underline{x}) \pi^2 a_o^5 \lvert \underline{x} \rvert^2 c^5 D}{\rho_o U^8} \right)_{shear}$ | $\frac{\partial^3}{\partial^3 \underline{\eta}} \left( \frac{I(\underline{x}) \pi^2 a_o^5 \lvert \underline{x} \rvert^2 c^5 D}{\rho_o U^8} \right)_{self}$ |
|---|---|---|
| $0^\circ$ case | $11.48 \times 10^{-5}$ | $4.36 \times 10^{-5}$ |
| $45^\circ$ | $9.36 \times 10^{-5}$ | $1.63 \times 10^{-5}$ |
| $60^\circ$ | $6.63 \times 10^{-5}$ | $3.77 \times 10^{-5}$ |

Note that the results given here are for noise generated from a unit volume of turbulence to an observer in the far field located in the plane of the jet axis and the center of our unit volume. Therefore one cannot really infer the emission in direction $\theta$ from a slice of jet without results from different unit volumes around the jet at the same axial and radial location. However the differences are not expected to be large. A more detailed discussion of this aspect is given in Appendix D.

One way to check the consistency of our approach in extracting the fourth derivative is by means of the peak frequencies obtained in a later section. Since the radiated intensity is proportional to $(f_{peak})^4$ approximately, other things being equal, the ratio of the fourth derivative at zero time delay for the 'self' and 'shear' noise normalized correlation functions should roughly equal to the ratio of their peak frequencies raised to the fourth power. The results showed that they were approximately equal, being 56 and 42 respectively.

Within the limitation of our simplifying assumptions, the present investigation indicated that at zero degrees to the jet axis the 'shear' noise was about 2.6 times higher than the 'self' noise generated by a unit volume of turbulence in the mixing region. Had we followed other investigators (Refs. 12, 13, and 17) in assuming complete separability for the four-dimensional space-time correlation function and approximating the moving-frame autocorrelation function by $e^{-\omega_f |\tau|}$ we could have obtained approximately equal magnitude for the 'shear' and 'self' noise as suggested in

Ref. 13. However, a ratio of 1.7 was obtained if a Gaussian function was used instead of the exponential function. In view of the compatibility test of the last paragraph, our present results might not be too far from reality.

The basic directivity for the 'shear' noise, as inferred from the present experiment in three directions, varied about like $|\cos\theta|$ ($|\cos\theta|^{0.7}$ to be more exact) over the range from $0^\circ$ to $60^\circ$ from the jet axis. Since $U_x U_x' = 0$ at $90^\circ$ it seems reasonable to extrapolate the $|\cos\theta|$ variation up to $90^\circ$. This directivity resembled better Ribner's $(\cos^4\theta+\cos^2\theta)/2$ pattern* than the four-leaf clover $\sin^2\theta\cos^2\theta$ suggested by Lighthill (Ref. 2) and Lilley (Ref. 12). For the case of 'self' noise, a minimum value was obtained at $45^\circ$. This was considered as more likely an experimental error than a true physical situation. Results for $0^\circ$ and $60^\circ$ suggested on the other hand that the 'self' noise had a more or less omnidirectional pattern. This was in agreement with Refs. 3 and 13.

The overall basic directivity would roughly be given by $(1 + 2.6|\cos\theta|)$. This result is plotted in Fig. 36 where the convection factor $C^{-5}$ has been incorporated. Note that the basic directivity pattern shows no valley along the jet axis. The observed valley or dimple in all acoustic measurements of jet noise is, in fact, due to refraction. This is well substantiated by recent work done at UTIAS (Ref. 40). The effect of refraction qualitatively sketched in as the dashed curve in Fig. 36.

## VII. ESTIMATION OF NOISE SPECTRUM

Following the assumptions made in Sec. VI, Eq. 2.2.6 for the spectrum function can be written as in the following,

for the 'shear' noise:

$$\left[\frac{\partial^3\Phi(\underline{X},f)}{\partial^3\underline{\eta}}\right]_{shear} \simeq \frac{8\rho_o U_x^2(\underline{\eta})\overline{u_x^2}(\underline{\eta})}{\pi^2 a_o^5 |\underline{X}|^2 C^5} L_3 L_2 \int_0^\infty \left[\frac{\partial^4}{\partial\tau^4}\int_0^\infty \frac{sh R(\underline{\eta},\xi_{m_1}+U_c\tau,0,0,\tau)}{U_x^2(\underline{\eta})\overline{u_x^2}(\underline{\eta})}\, d\xi_{m_1}\right] \times \cos 2\pi f_t\tau\, d\tau \qquad (7.1)$$

and for the 'self' noise:

$$\left[\frac{\partial^3\Phi(\underline{X},f)}{\partial^3\underline{\eta}}\right]_{self} \simeq \frac{2\rho_o \overline{u_x^4}(\underline{\eta})}{\pi^2 a_o^5 |\underline{X}|^2 C^5} L_3 L_2 \int_0^\infty \left[\frac{\partial^4}{\partial\tau^4} \frac{se R(\underline{\eta},\xi_{m_1}+U_c\tau,0,0,\tau)}{\overline{u_x^4}}\, d\xi_{m_1}\right] \times \cos 2\pi f_t\tau\, d\tau$$

where $f_t = f(1 - M_c\cos\theta)$

and $\partial^3\Phi(\underline{X},f)/\partial^3\underline{\eta}$ refers to the noise spectrum from unit volume of turbulence. The problem here is to determine the Fourier cosine transform of

---

* Unpublished work; corrected from $\cos^4\theta$ pattern obtained in Refs. 3 and 13.

the fourth derivative curves obtained in the last section. Following the example with the Gaussian function, an analytical function ($A \operatorname{sech} B\tau \cos\omega_0\tau$) was first fitted to the fourth derivative curve and an analytical spectrum function could then be obtained. In addition, a numerical Fourier cosine transform was performed on the fourth derivative curve up to the third zero crossing, assuming zero value thereafter. Filon's method was used. Figure 37 shows the approximating curves and Fig. 38 shows the corresponding spectrum functions for the axial direction case. The occurrence of negative values in the spectrum function in the second method was due to truncation of the fourth derivative curve at a finite $\tau$ as illustrated in Appendix E. Thus it was felt that the spectrum function given by the analytical case was the most probable one, with the uncertainty given by the shaded area in Fig. 38. The results indicated that the 'self' noise had a peak frequency which was about 2.5 times that of the 'shear' noise. This was even higher than the factor 2 inferred by Ribner (Ref. 13) from the squaring of the turbulent velocities for the 'self' noise. However, the general shape of the spectrum function was in agreement with his function

$$\omega^4 e^{-2\frac{\omega^2}{\omega_p^2}}$$

where $\omega_p$ is the peak frequency.

The spectra of the noise intensity at $45^\circ$ and $60^\circ$ to the jet axis would have very nearly the same peak and shape as for the $0^\circ$ case judging from the fourth derivative curves. These will not be presented.

## VIII. COMPARISON WITH ACOUSTIC MEASUREMENTS

Before the quantitative comparisons are presented, one should be aware of the limitations and extra assumptions involved. Firstly, we have to infer emission for a slice of jet from volume element measurements taken in a plane containing the observer and the jet axis. Secondly, we have to rely on existing knowledge about the distribution of noise sources in a jet based on theoretical models. Thirdly, extrapolation of higher speed jet data was used because of the unavailability of acoustic measurements at our low speed range.

### 8.1 Dominant Frequency

There have been conflicting reports (Refs. 6, 41, 42, 43, 44, and 45) as to the dependence of the peak frequency in the noise spectrum on jet velocity. Lee's results (Ref. 43) were chosen for comparison because they were in the relatively low speed range. Figure 39 is a replot of his results taken at $25^\circ$ from the jet axis and they suggested that the peak frequency varied like $U^{0.58}$. The variation would be even smaller if Doppler shift had been accounted for. Using the results (Refs. 46 and 47) that the peak frequency was inversely proportional to the jet diameter, a peak frequency of about 330 Hz was estimated for the present 4 inch jet from Lee's results.

Now the noise spectrum for the whole jet can be considered as being made up of spectra from different slices of the jet. In the mixing region, the spectrum of noise from a slice of jet will have approximately

the same peak as that from a unit volume at the region of maximum shear because the chief noise-emitting eddies are confined in a small volume at this region (Ref. 12). Results of Ref. 15 suggested that the peak frequency of the over-all noise spectrum was generated by a slice located at about 5 diameters downstream. Similarity consideration (Ref. 18) implied that frequency was inversely proportional to axial distance in the mixing region. From all these considerations, the peak frequency of the noise generated by a unit volume of turbulence at the position of the present investigation was estimated to be about 410 Hz. The present experimental result gave a value of approximately 340 Hz which was 1.2 times lower. This is the value of the 'shear' noise spectrum at zero degree since the 'shear' noise spectrum dominates at that direction. In view of the discrepancies of different data and all the uncertainties in estimating the slice peak frequency, the comparison is considered quite satisfactory.

## 8.2 Reverse Doppler Shift Paradox

Assuming that the relative separation between the 'shear' and 'self' noise spectra was the same for different slices of the jet in forming the total spectra, our results would predict qualitatively one observed 'paradox' in acoustic measurements of jet noise. References 6, 43, and 44 reported that the noise spectrum at small angle to the flow peaked at lower frequency than that at right angles. This is just the reverse of the expectation from a single spectrum subjected to Doppler shift at small emission angles. But, considering the whole spectrum as made up from a 'shear' and a 'self' noise spectrum, our results indicated that at small angles, the 'shear' noise spectrum dominated because of the relatively low magnitude of the 'self' noise. However, as the angle increased, the 'shear' noise was diminishing as $|\cos\theta|$. At right angles to the flow, the contribution would be from the 'self' noise only which peaked at a higher frequency than the 'shear' noise as found experimentally here.

## 8.3 Acoustic Power

Finally, an estimate of the total acoustic power generated by the present 4 inch jet was made. Based on existing knowledge about the noise sources distribution in a jet, an equivalent volume of turbulence responsible for the noise emission was obtained whereby the total noise power could be obtained by multiplying this volume by the noise power from our volume element. A detailed calculation is shown in Appendix F. The result is plotted as a single point in Fig. 40 along with a replot of Fig. 7 of Ref. 6. Our noise prediction inferred from the turbulence measurements is seen to be about an order of magnitude higher than the extrapolation of the curves of measured noise obtained by others. This prediction of overall jet noise, however, is itself a tenuous extrapolation of data applying to a single volume element. It involves a number of assumptions of considerable uncertainty, and it should not be surprising that the different error sources might accumulate to give the observed discrepancy.

## IX. CONCLUSION

The aerodynamic noise problem first solved by Lighthill has been reformulated in terms of its spectral characteristics using the one-dimensional Fourier cosine transform. The final formalism was just as revealing as other workers' results using the four-dimensional Fourier Transform. The Doppler effect of moving eddies resulted automatically from the mathematics and the convection effect could be distinguished as a combination of Doppler shift and amplification. The extent to which differences in retarded time could be neglected was explicit in this formulation; the importance of retaining the differences in retarded time at high speed was demonstrated following Ribner's work.

The main objective of the present investigation was to estimate from turbulence measurements the characteristics (i.e., intensity, directivity, and spectral density) of the noise generated by a unit volume of turbulence in the mixing region of a model jet. To accomplish this, two-point space-time correlations of both the turbulent velocities and the square of these velocities have been obtained. These measurements included the ordinary u-component and also the components at $45^{\circ}$ and $60^{\circ}$ to the jet axis.

The measured quantities approximate the actual integrand in the Proudman form of Lighthill's integral connecting turbulence and the noise it radiates; they go well beyond the measurements reported elsewhere which rely on analogies to simulate the integrand. The requirement to delineate a three-dimensional integral has necessitated a great volume of measurements. Moreover the requirement of a fourth derivative operation on the experimental curves has put a premium on precision of measurement and data processing.

Where comparable measurements exist comparisons have been made. Both the intensity of the u-component and the eddy convection velocity agreed well with those measured elsewhere. Additionally, comparable space-time correlations are qualitatively similar to those of other workers.

Results from the quantitative estimate of the noise characteristics suggested that the basic directivity of the noise generated by a unit volume of turbulence varied about like $(1 + 2.6|\cos\theta|)$. The absence of a valley along the jet axis agreed with Ribner's finding based on a theoretical model; it disagreed with the 'four-leaf clover' pattern suggested by Lighthill and Lilley. The observed dimple in experimental jet noise patterns along the jet axis is due to another effect, namely, refraction. At small angles to the jet axis the 'shear' noise intensity was found to be more than twice that of the 'self' noise; at right angles the 'self' noise was inferred to be the main contributor. The 'self' noise spectrum peaked at a higher frequency than the 'shear' noise as expected from theory. Also the peak frequency of the present unit volume spectrum agreed well with extrapolated value from acoustic measurements of other investigators. However, the estimated total acoustic power was about an order of magnitude higher than the extrapolated value from acoustic measurements based on the $U^8$ law.

In addition, the present investigation had demonstrated the usefulness of considering the 'shear' and 'self' noise separately somewhat in the manner suggested by Ribner. Looking at the relative importance of these two types of noise at different angles to the jet axis, one can predict at least qualitatively between $40^{\circ}$ to $90^{\circ}$. The acoustic 'paradox' that the

overall noise spectrum peaks at higher frequencies for larger angles from the jet axis. This is contrary to the deduction from the Doppler shift of a single spectrum, considering the eddies as moving sources.

Finally, it is thought that, compared with earlier work, the present investigation has taken a much closer step to a quantitative connection between measurements of turbulence and measurements of jet noise.

## REFERENCES


1. Lighthill, M.J. — On Sound Generated Aerodynamically.I - General Theory, Proc. Roy. Soc. A,211, 564-587 (1952).

2. Lighthill, M.J. — On Sound Generated Aerodyanmically. II - Turbulence as a Source of Sound . Proc. Roy. Soc. A, 222, 1-32 (1954).

3. Ribner, H.S. — The Generation of Sound by Turbulent Jets. Advances in Applied Mechanics, Vol. VIII, Acad. Press. (N.Y. and London, 1964).

4. Fowell, L.R. Korbacher, G.K. — Review of Aerodyanmic Noise. Univ. of Toronto, Inst. of Aerophysics, UTIA Review No. 8 (1955).

5. von Gierke, H.E. — Aircraft Noise Sources, in "Handbook of Noise Control" (C.M. Harris, Ed.) pp. 33-30to 33-65. McGraw-Hill, New York (1957).

6. Howes, W. L. — Similarity of Far Noise Fields of Jets. NASA TR R-52 (1960).

7. Laurence, J.C. — Intensity, Scale, and Spectra of Turbulence in Mixing Region of Free Subsonic Jet. NACA Rep. 1292 (1956).

8. Davies, P.O.A.L. Barratt, M.J. Fisher, M.J. — Turbulence in the Mixing Region of a Round Jet. ARC 23, 728-N200-FM3181 (1962).

9. Bradshaw, B.A. Ferriss, D.H. Johnson, R.F. — Turbulence in the Noise-Producing Region of a Circular Jet. NPL Aero. Rept. 1054 (1963).

10. Kolpin, M.A. — Velocity Correlation Measurements in the Mixing Region of a Jet. Mass. Inst. of Tech., Aeroelastic and Struct. Res. Lab., ASRL TR 1008 (1963).

11. Proudman, I. — The Generation of Noise by Isotropic Turbulence. Proc. Roy. Soc. A,214, 119-132 (1952).

12.. Lilley, G.M. — Onthe Noise from Air Jets. ARC 20, 376-N40-FM 2724 (1958).

13. Ribner, H.S. — On Spectra and Directivity of Jet Noise. J. Acoust. Soc. Amer. 35, 614-616 (1963).

14. Ribner, H.S. — On the Strength Distribution of Noise Sources, along a Jet. Univ. of Toronto, Inst. of Aerophysics, UTIA Rep. 51 (AFOSR TN 58-359, AD 154 264) (1958); abridged in J. Acoust. Soc. Amer. 30, 876 (1958).

15. Dyer, I. — Distribution of Sound Sources in a Jet Stream. J. Acoust. Soc. Amer. 31, 1016-1021 (1959).

16. Ribner, H.S. — Aerodynamic Sound from Fluid Dilatations - A Theory of the Sound from Jets and Other Flows. Univ. of Toronto, Inst. of Aerophysics, UTIA Rep. 86 (AFOSR TN 3430) (1962).

17. Williams, J.E.Ff. — The Noise from Turbulence Convected at High Speed. Phil. Trans. Roy. Soc. London, Series A. 255, 469-503 (1963).

18. Powell, A. — Similarity Considerations of Noise Production from Turbulent Jets, Both Static and Moving. Douglas Aircraft Co., Rep. SM-23246 (1958); abridged in J. Acoust. Soc. Amer. Vol. 31, pp. 812-813 (1959).

19. Williams, J.E.Ff. — Measuring Turbulence with a View to Estimating the Noise Field. ARC 20, 381-N42-FM2726(1958).

20. Lass, H. — Vector and Tensor Analysis. McGraw-Hill, New York (1950).

21. Franz, G.J. — The Near-Sound Field of Turbulence. David Taylor Model Basin (Washington, D.C.). DTMB Rep. 982 (1959).

22. Ribner, H.S. — A Theory of the Sound from Jets and Other Flows in Terms of Simple Sources. Univ. of Toronto, Inst. of Aerophysics, UTIA Rep. 67 (AFOSR TN 60-950) (1960).

23. Meecham, W.C. Ford, G.W. — Acoustic Radiation from Isotropic Turbulence. J. of Acoust. Soc. of Amer., 30, 4, 318 (1958).

24. Ribner, H.S. — New Theory of Jet-Noise Generation, Directivity, and Spectra. J. Acoust. Soc. Amer. 31, 245-246 (1959).

25. Lighthill, M.J. — The Bakerian Lecture, 1961. Sound Generated Aerodynamically. Proc. Roy. Soc. A, 267, 147-182 (1962).

26. Kraichnan, R.H. — The Scattering of Sound in a Turbulent Medium. J. Acoust. Soc. Amer. 25, 1096-1104 (1953).

27. Mawardi, O.K. — On the Spectrum of Noise from Turbulence. J. Acoust. Soc. Amer. 27, 442-445 (1955).

28. Chu, W.T. — Hot-Wire Investigation of Jet Turbulence. Univ. of Toronto, UTIA M.A.Sc. Thesis (1962).

29. Williams, J.E.Ff. — On Convected Turbulence and Its Relation to Near Field Pressure. Univ. of Southampton, USAA Report No. 109 (1960).

30. Sneddon, I.N. — Fourier Transform, McGraw-Hill, New York (1951).

31. Wilson, L.N. — An Experimental Investigation of the Noise erated by the Turbulent Flow Around a Rotat Cylinder. Univ. of Toronto, Institute of A physics, UTIA Report No. 57 (AFOSR TN-59-48 AD 215 780) (1959).

32. el Baroudi, M.Y. — Turbulence - Induced Panel Vibration. Univ of Toronto, Institute for Aerospace Studies UTIAS Report 98 (AFOSR 64-0883) (1964).

33. Chu, W.T. — Velocity Profile in the Half-Jet Mixing Reg of Turbulent Jets. AIAA Journal Vol. 3, Nc p. 789 (1965).

34. Filon, L.N.G. — On a Quadrature Formula for Trigonometric Integrals. Proc. Roy. Soc. Edin., XLIX, 38- (1928-29).

35. Richards, E.J.
Williams, J.E.Ff. — Some Recent Developments in Jet Noise Rese Univ. of Southampton, USAA Report 118 (195

36. Fisher, M.J.
Davies, P.O.A.L. — Correlation Measurements in a Non-Frozen P of Turbulence. J. of Fluid Mech. Part 1, 97-116 (1964).

37. Hinze, J.O. — Turbulence. McGraw-Hill, New York (1959).

38. Surry, J. — Experimental Investigation of the Characte tics of Flow About Curved Circular Cylinde Univ. of Toronto, Institute for Aerospace Studies, UTIAS Tech. Note No. 89 (1965).

39. Birge, R.T. — Lease-Squares Fitting of Data by Means of Polynomials. Review of Modern Physics, Vol No. 4 (1947).

40. Atvars, J.
Schubert, L.K.O.
Ribner, H.S. — Refraction of Sound from a Point Source Pl in an Air Jet. J. Acoust. Soc. Amer. Vol. 168-170 (1965).

41. Fitzpatrick, H.M.
Lee, Robert — Measurements of Noise Radiated by Subsonic Jets. David Taylor Model Basin, Washingtor D.C., DTMB Report 835 (1952).

42. Westley, R.
Lilley, G.M. — An Investigation of the Noise Field From Small Jet and Methods for Its Reduction. College of Aeronaut. (Cranfield) Rep. 53

43. Lee, R. — Free Field Measurements of Sound Radiated Subsonic Air Jets. David Taylor Model Ba Washington, D.C., DTMB Rep. 868 (1953).

44. Gerrard, J.H. — An Investigation of the Noise Produced by a Subsonic Air Jet. J. Aero. Sci. 23, 855-866 (1956)

45. Mollo-Christensen,E. Narasimha, R. — Sound Emission from Jets at High Subsonic Velocities. J. Fluid Mech. 8, 49-60, (1960).

46. Tyler, J.M. Perry, E.C. — Jet Noise. Preprint No. 287 Society of Automotive Engineers (1954).

47. Mollo-Christensen,E. Kolpin, M.A. Martuccelli, J.R. — Experiments on Jet Flows and Jet Noise Far-Field Spectra and Directivity Patterns. J. Fluid Mech. 18, 285-301 (1964).

48. Schubauer, G.B. Klebanoff, P.S. — Theory and Application of Hot-Wire Instruments in the Investigation of Turbulent Boundary Layer. NACA Adv. Conf. Rep. No. 5K27, War-time Report W-86 (1946).

49. Weske, J.R. — Measurement of the Arithmetic Mean Velocity of a Pulsating Flow of High Velocity by the Hot-Wire Method. NACA TN 990 (1946).

50. Newman, B.G. Leary, B.G. — The Measurement of the Reynolds Stresses in a Circular Pipe as Means of Testing a Hot Wire Anemometer. Aero. Res. Lab. Rep. A72, Dept. of Supply, Australia (1950).

51. Sandborn, V.A. Laurence, J.C. — Heat Loss From Yawed Hot-Wires at Subsonic Mach Numbers. NACA TN 3563 (1955).

52. Webster, C.A.G. — A Note on the Sensitivity to Yaw of a Hot-Wire Anemometer. J. of Fluid Mech. 13, 307-312 (1962).

53. Champagne, F.H. — Turbulence Measurements with Inclined Hot-Wires. Boeing Scientific Research Laboratories Document D1-82-0491 (1965).

54. Wooldridge, C.E. Willmarth, W.W. — Measurements of the Correlation Between the Fluctuating Velocities and Fluctuating Wall Pressure in a Thick Turbulent Boundary Layer. Univ. of Michigan Report 02920-2-T, (1962).

55. Bull, M.K. Wilby, J.F. Blackman, D.R. — Wall Pressure Fluctuations in Boundary Layer Flow and Response of Simple Structures to Random Pressure Fields. Univ. of Southampton, A.A.S.U. Report No. 243 (1963).

56. Favre, A. Gaviglio,J. Dumas, R. — Corrélations dans le temps et l'espace, avec filtre de bande, en aval d'une grille de turbulence. La Recherche Aéronautique, No. 40, Paris, France, pp. 7-14 (1954).

57. Chu, W.T.
Nayer, B.M.
Siddon, T.E.
Properties of the Turbulence in the Transition Region of a Round Jet. UTIAS Report to be published.

58. Waterhouse, R.V.
Berendt, R.D.
Reverberation Chamber Study of the Sound Power Output of Subsonic Air Jets. J. Acoust. Soc. Amer., Vol. 30, No. 2, pp. 114-121 (1958).

59. Callaghan, E.E.
Coles, W.D.
Far Noise Field of Air Jets and Jet Engines. NACA Rep. 1329, 1957 (Supersedes NACA TN's 3590 and 3591.)

60. Rollin, V.G.
Effect of Jet Temperature on Jet-Noise Generation. NACA TN 4217 (1958).

61. Eldred, K.
Noise Measurements of Four Rohr Aircraft Model Jet Nozzles. Rep. No. 238-11-1, Paul S. Veneklasen & Assoc., Los Angeles (Calif.) (1958)

62. Clark, W.E., et al
Noise Produced by Aircraft During Ground Run-up Operations. TR 56-60, WADC, (1957).

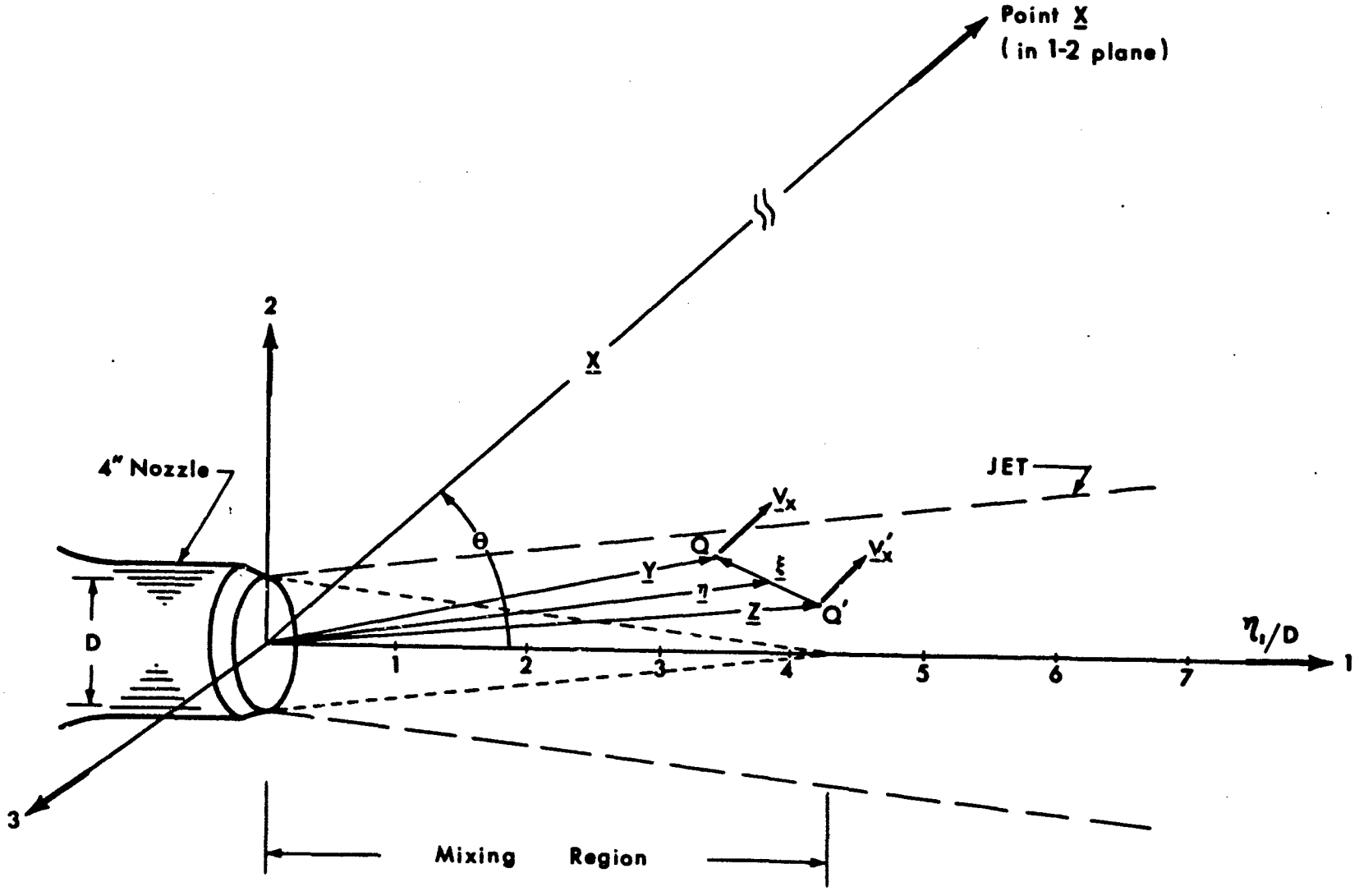


FIG. 1 CO-ORDINATE SYSTEM

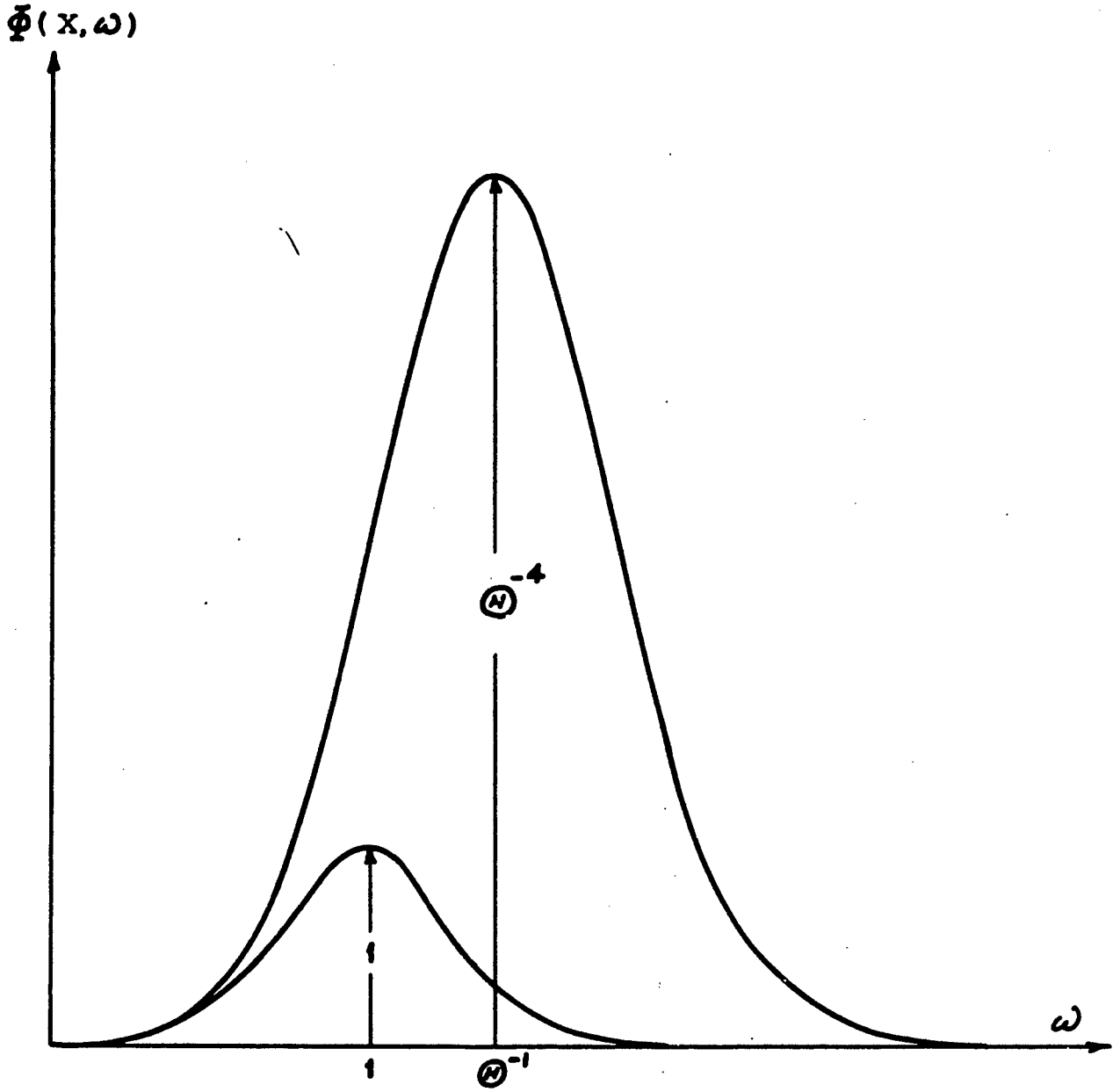


FIG. 2 NOISE SPECTRUM RADIATED BY UNIT VOLUME OF JET TURBULENCE: CONVECTIVE PEAK AMPLIFICATION AND 'DOPPLER' SHIFT ARE GIVEN BY FACTORS $\omega^{-4}$ AND $\omega^{-1}$ RESPECTIVELY, TO GIVE POWER AMPLIFICATION (ADOPTED FROM REF. 3)

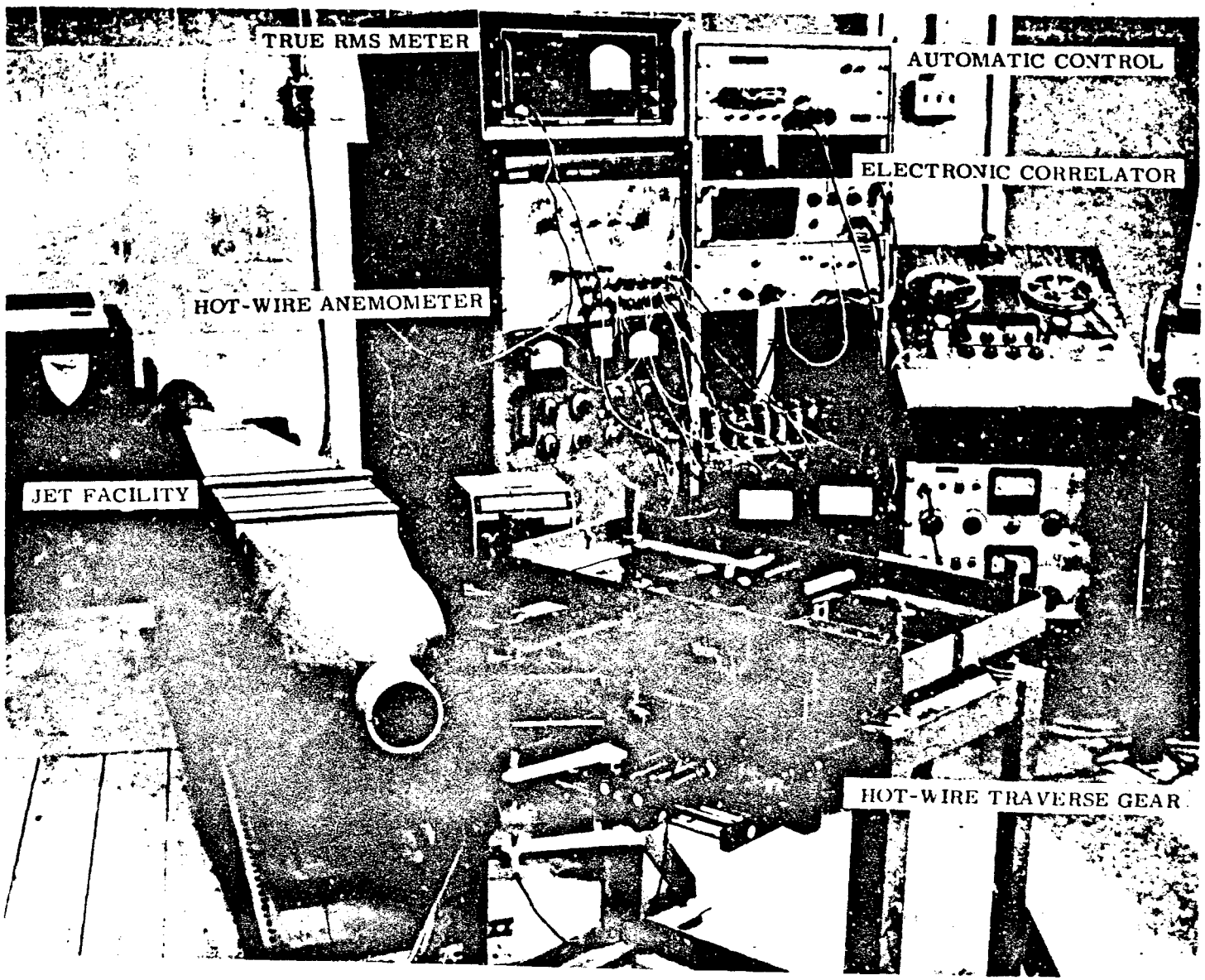
TRUE RMS METER
AUTOMATIC CONTROL
ELECTRONIC CORRELATOR
HOT-WIRE ANEMOMETER
JET FACILITY
HOT-WIRE TRAVERSE GEAR

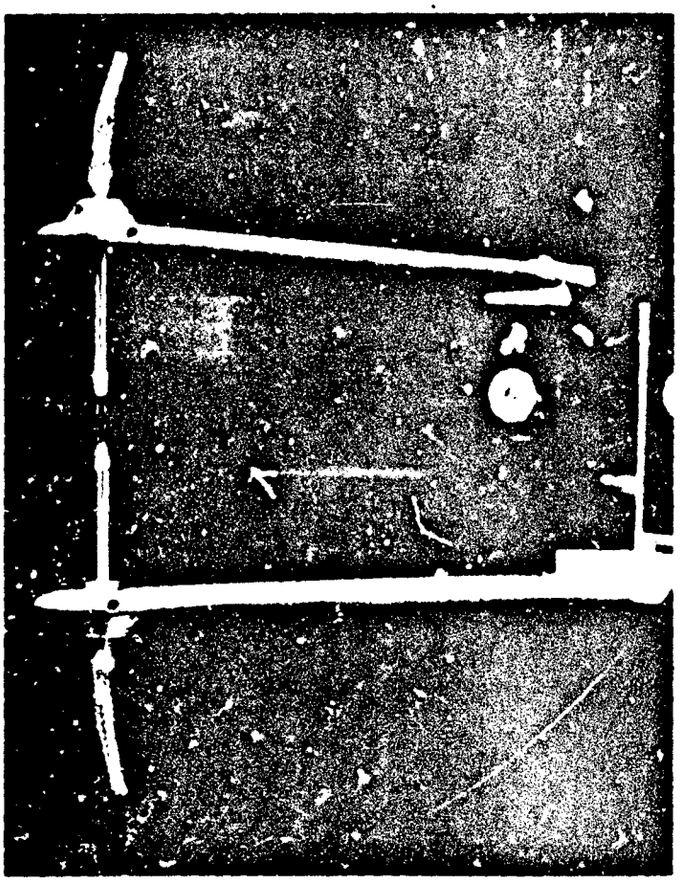

FIG. 4 CLOSE-UP OF HOT-WIRE PROBES

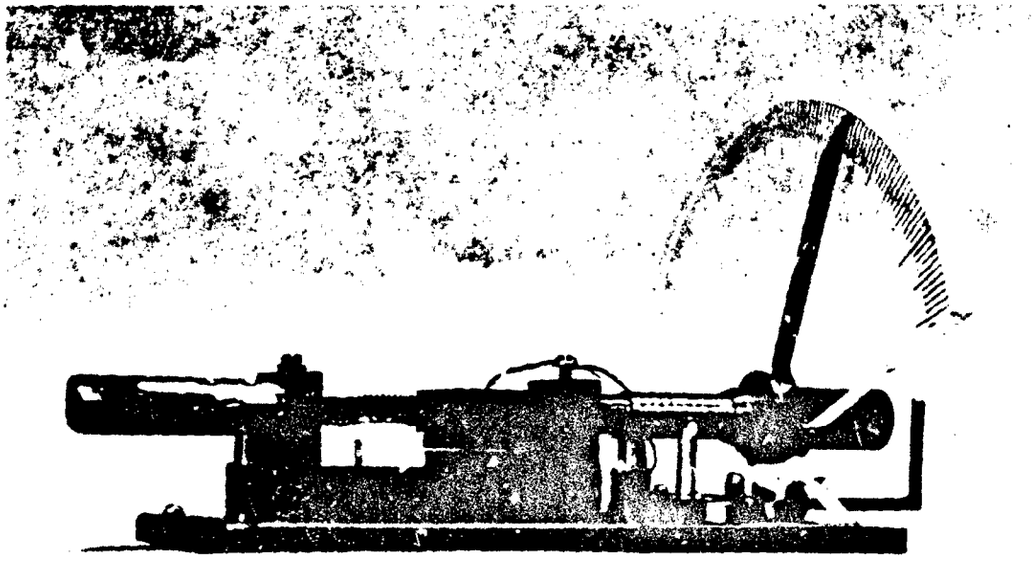

FIG. 5 STAGGERED-HEAD TAPE RECORDER PLAYBACK ASSEMBLY FOR INTRODUCING TIME DELAY

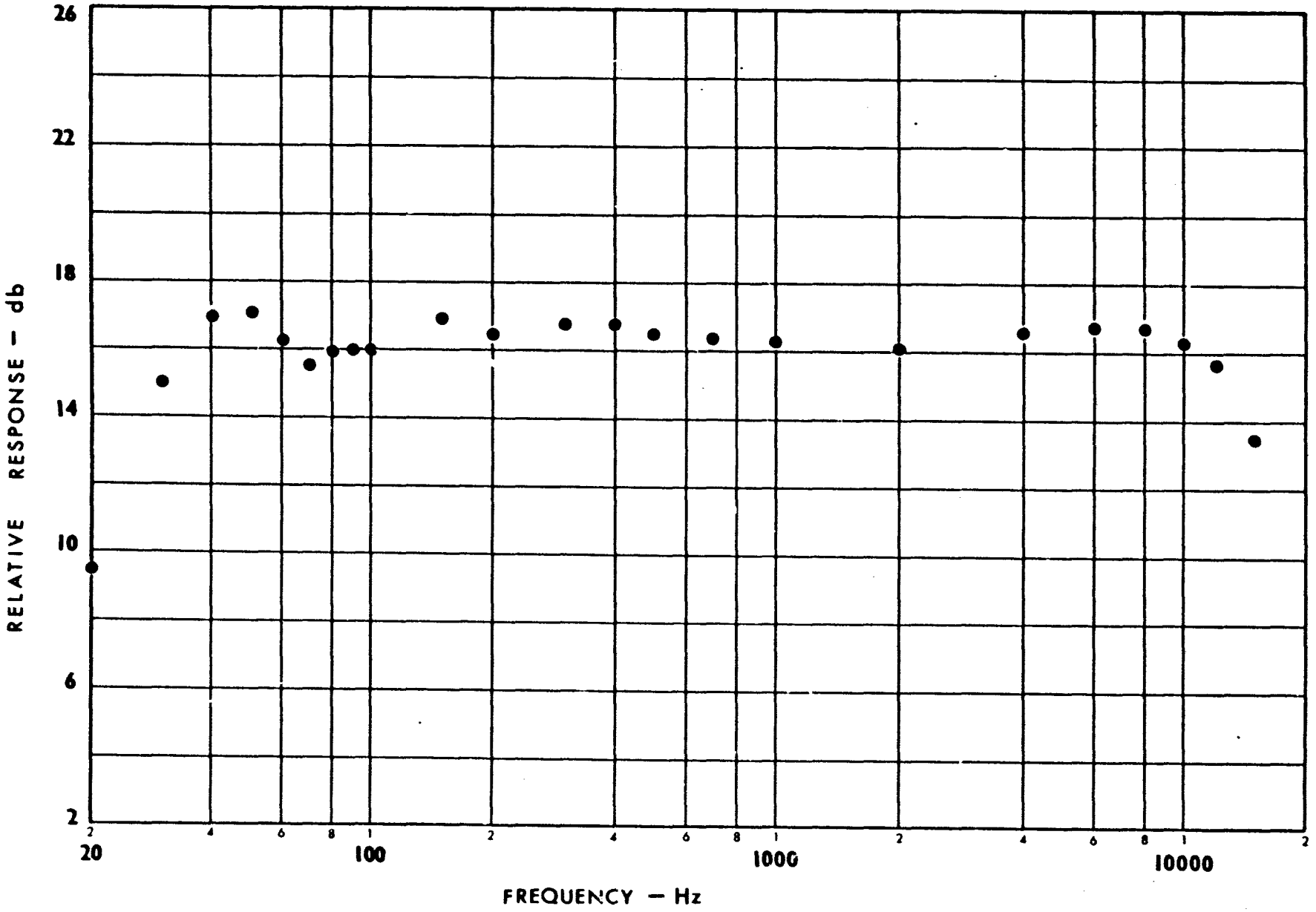


FIG. 6 FREQUENCY RESPONSE OF ELECTRONIC CORRELATOR

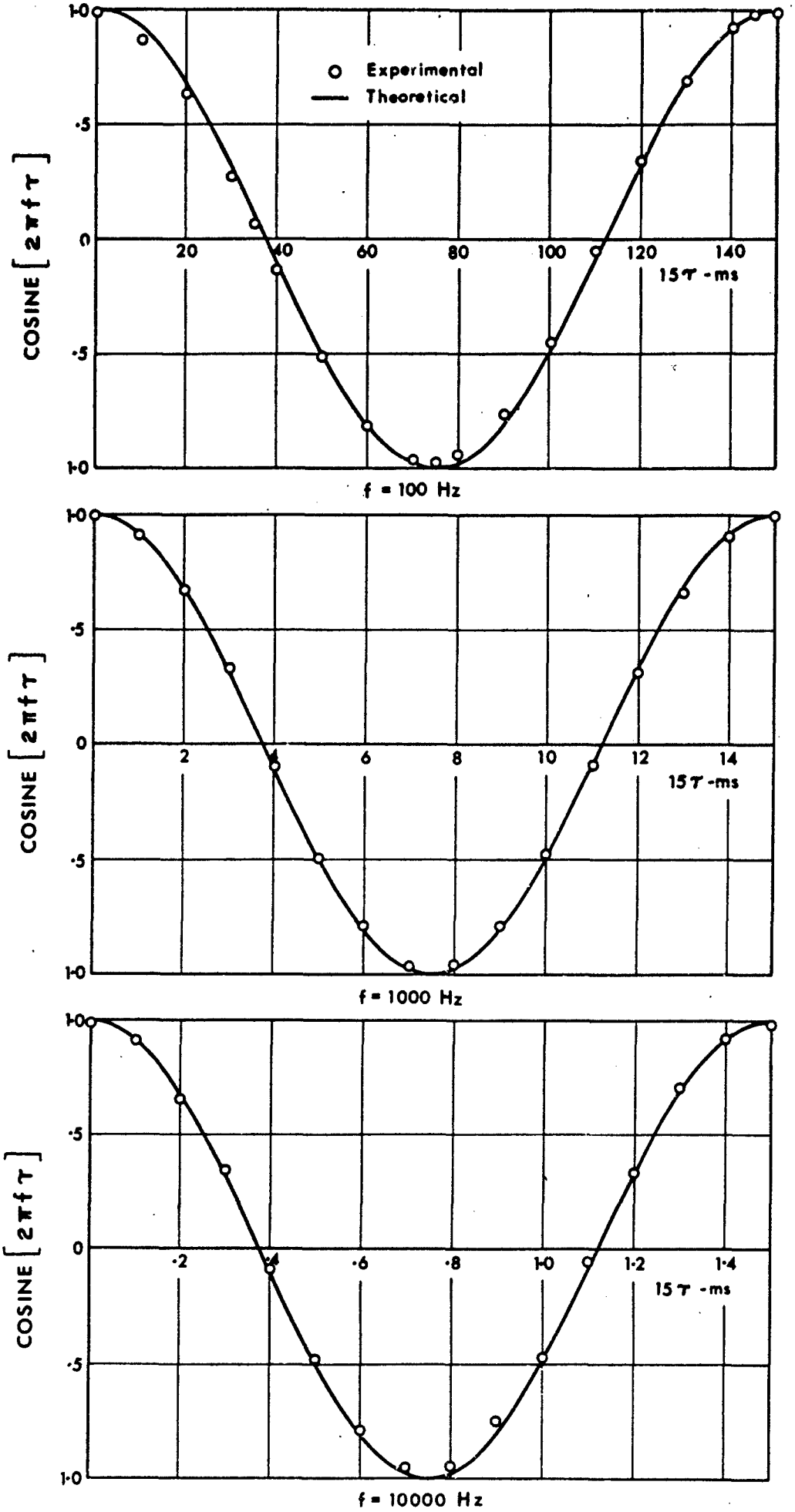


FIG. 7 AUTOCORRELATION OF SINE WAVES (CARRIED

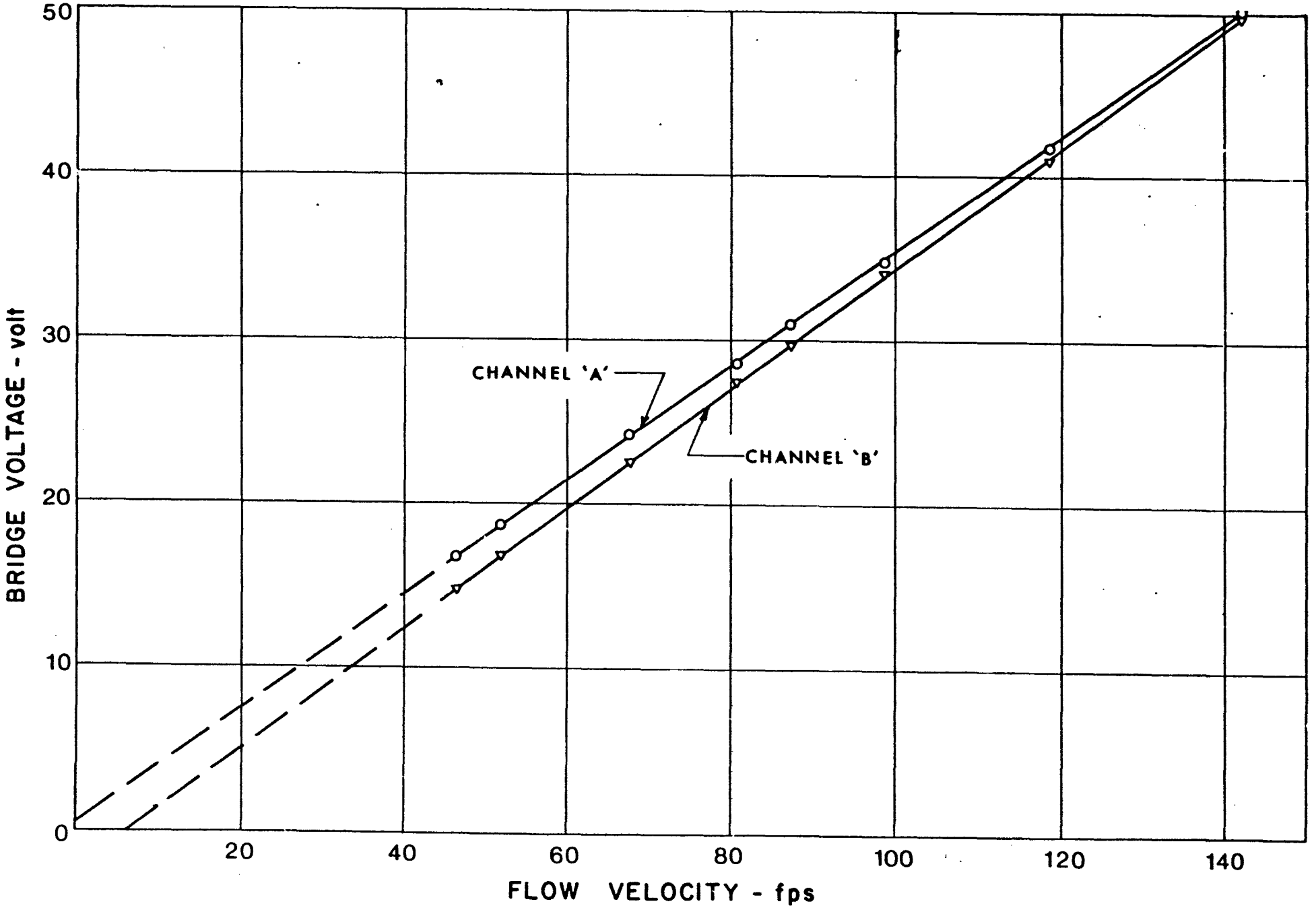


FIG. 8 TYPICAL CALIBRATION CURVES OF HOT-WIRE ANEMOMETERS

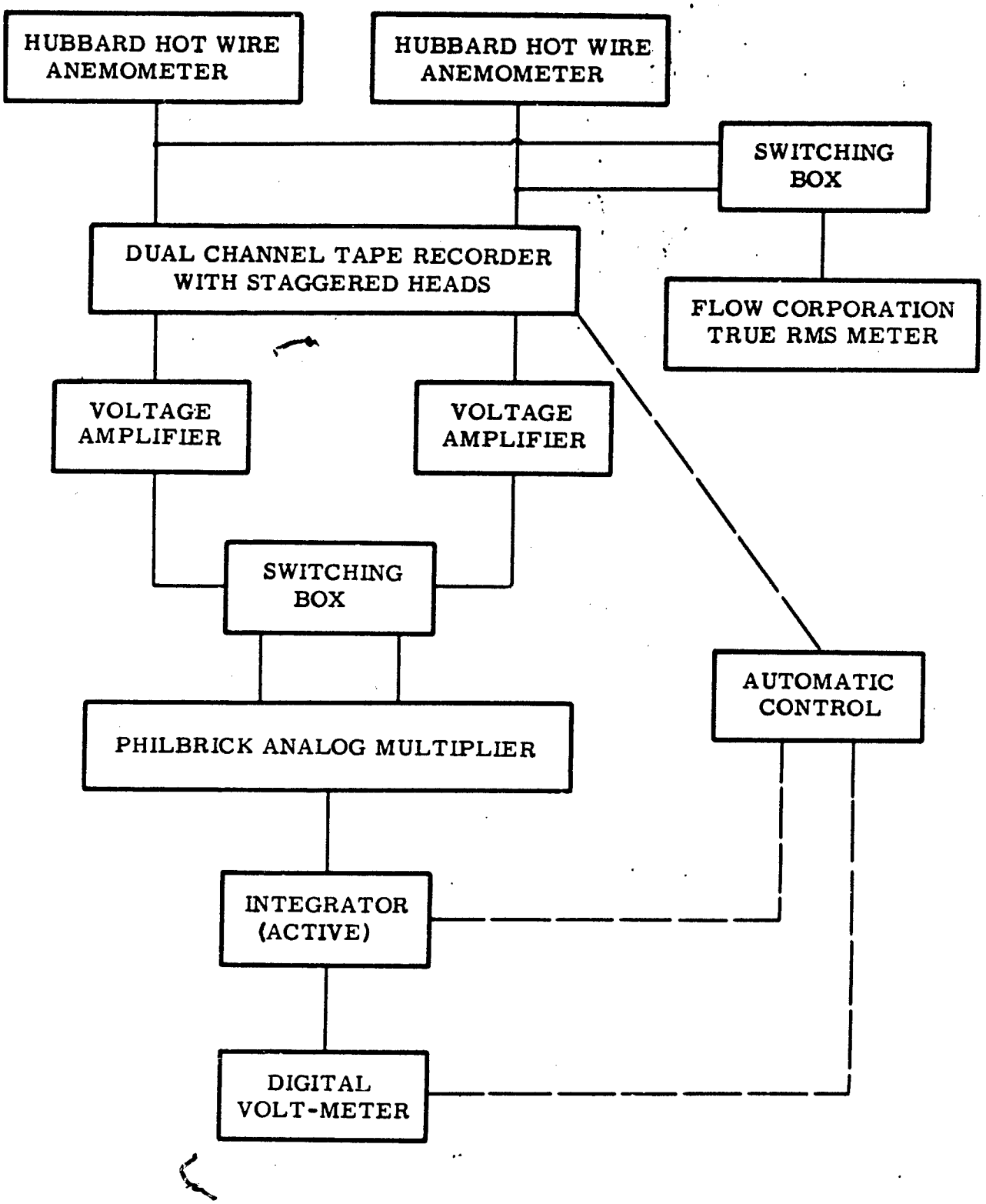


FIG. 9 BLOCK DIAGRAM OF THE VELOCITY CORRELATION MEASUREMENT SYSTEM

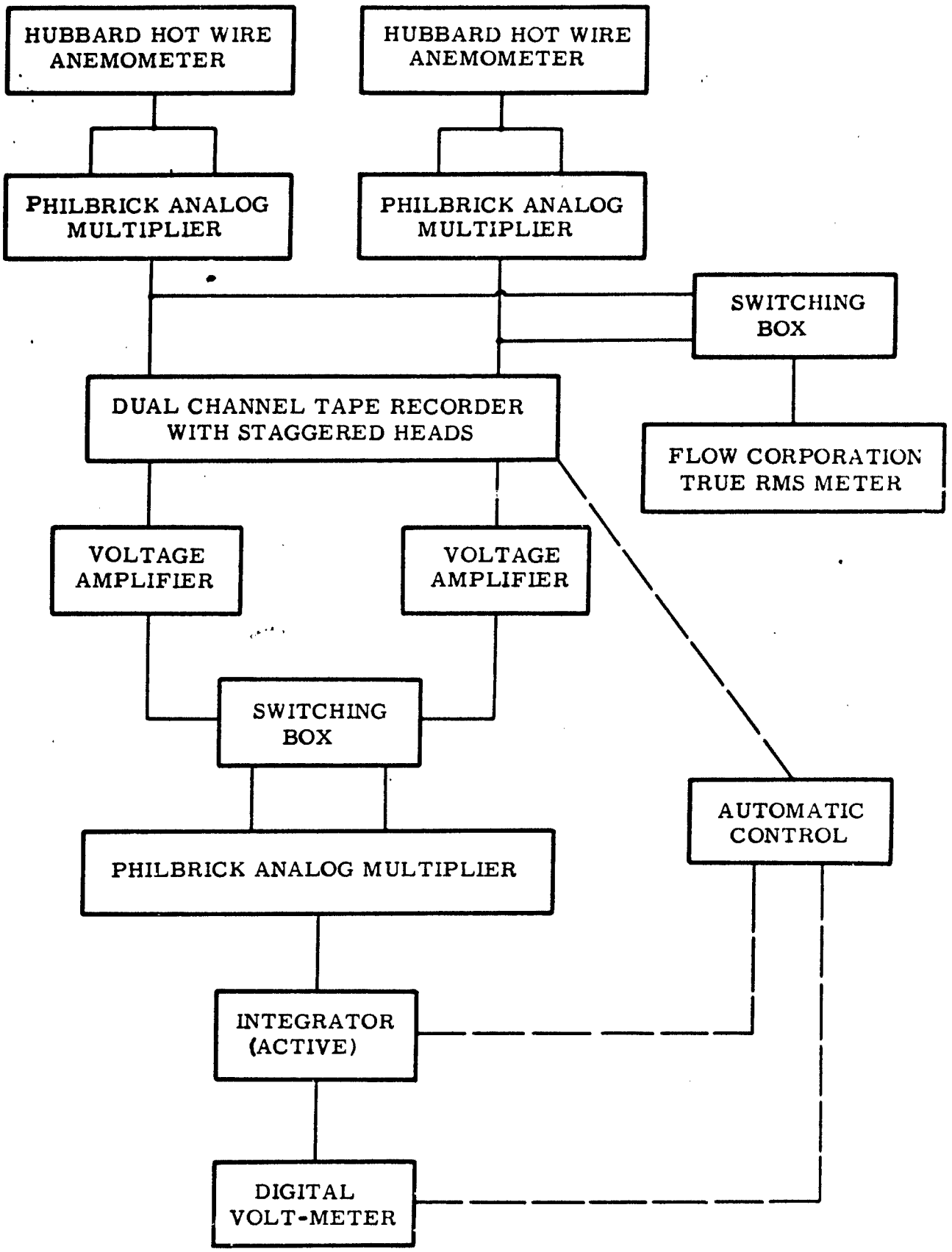


FIG. 10 BLOCK DIAGRAM OF THE VELOCITY SQUARED CORRELATION MEASUREMENT SYSTEM

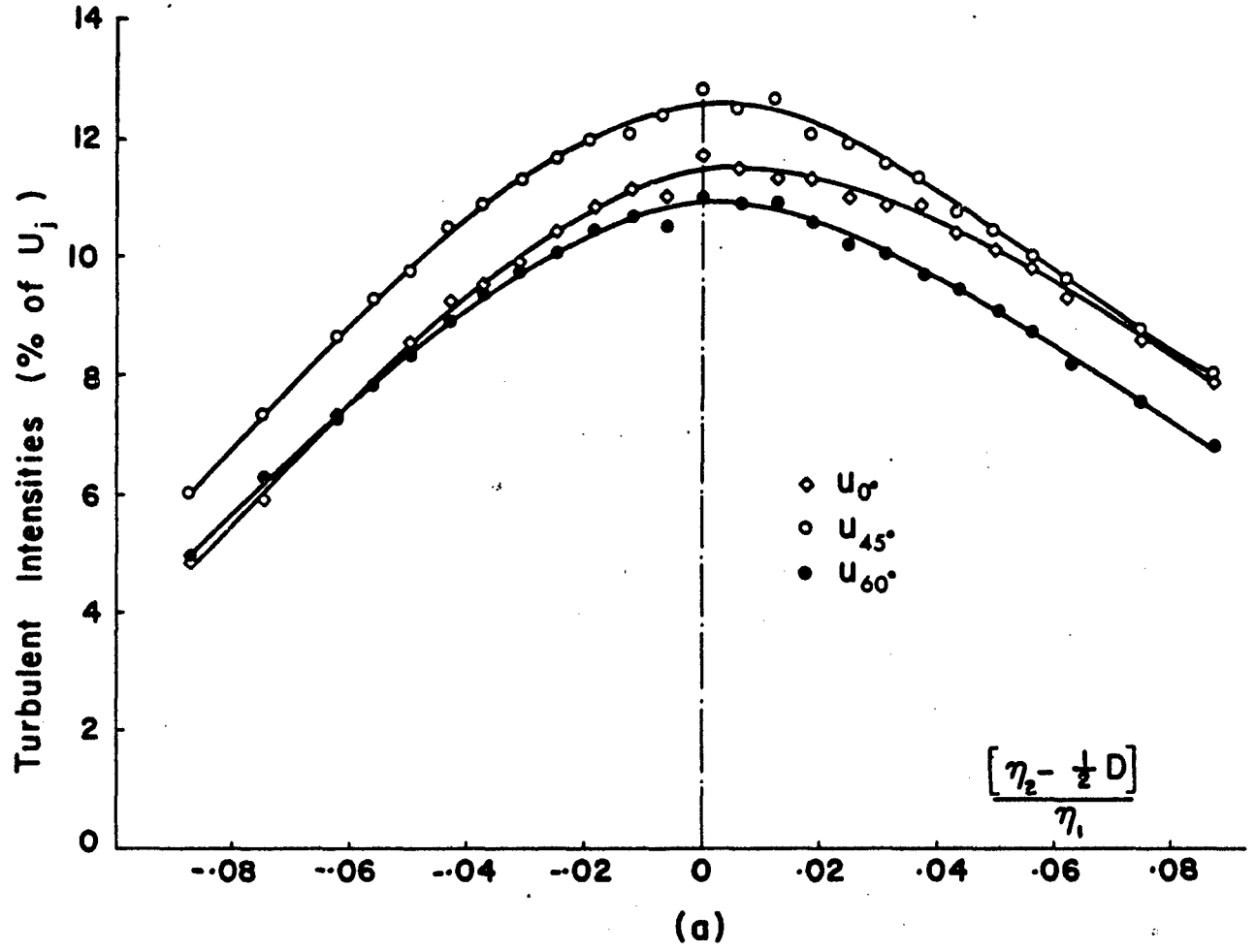


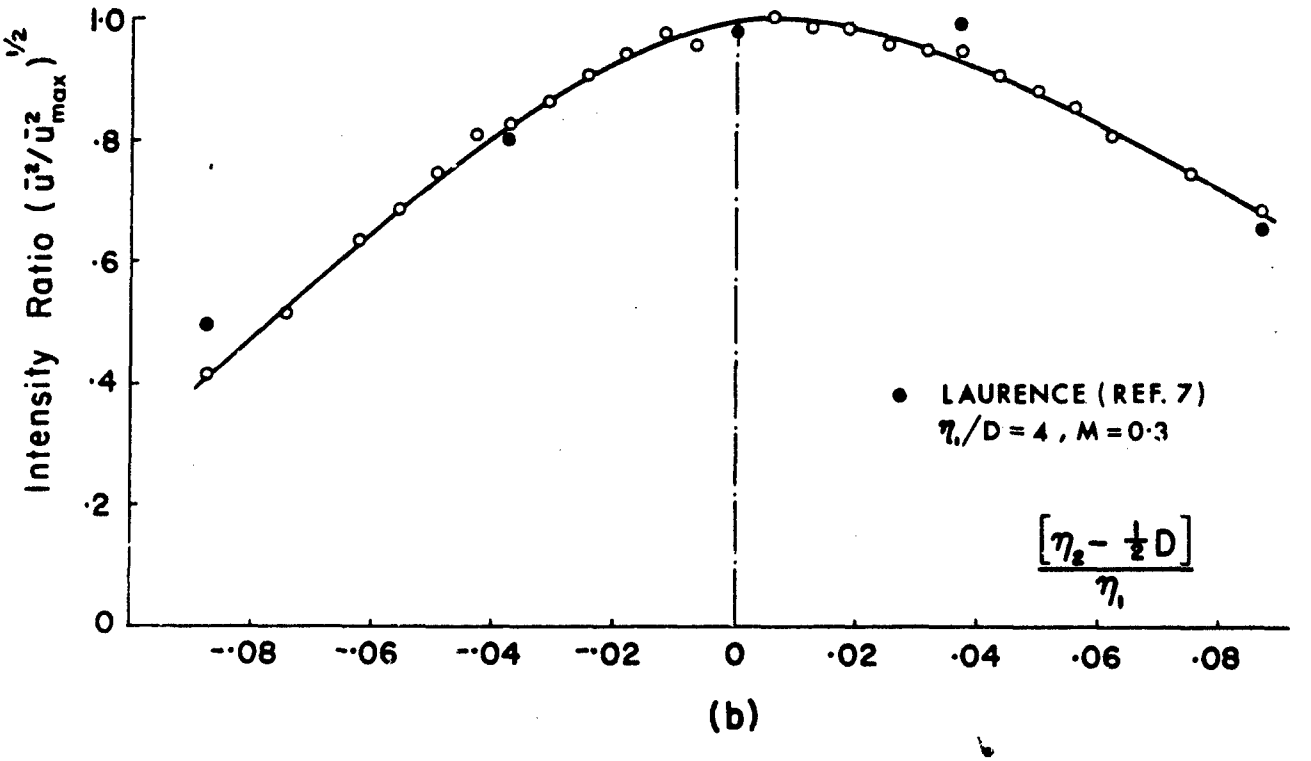


FIG. 11 (a) RADIAL DISTRIBUTION OF TURBULENT INTENSITIES; $\eta_1/D=4$, $U_j/a_o=0.13$

(b) COMPARISON OF THE AXIAL COMPONENT DISTRIBUTION WITH RESULTS OF REF. 7

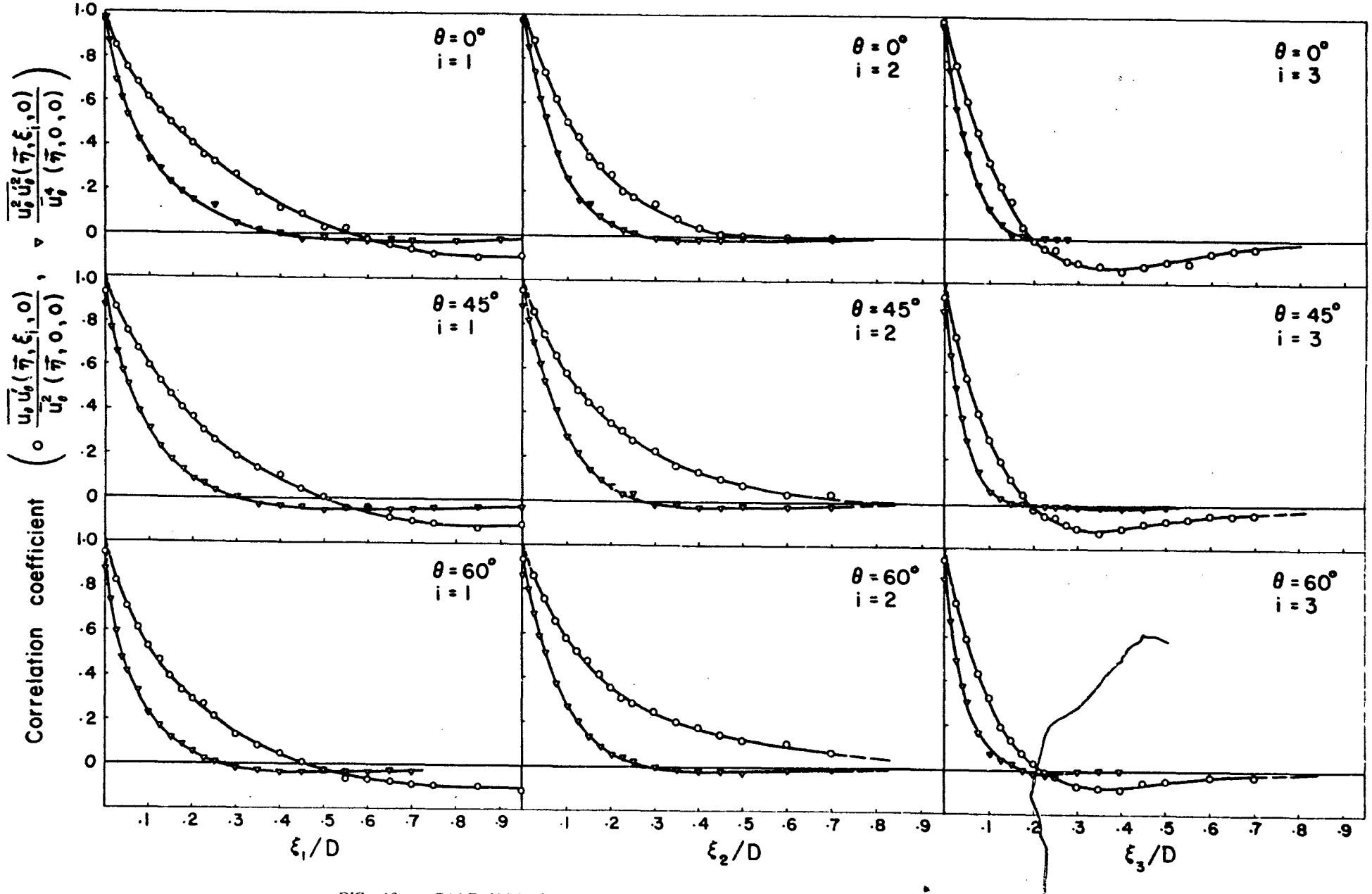


FIG. 12 SPACE CORRELATIONS OF BOTH THE VELOCITY AND THE VELOCITY SQUARED IN THREE ORTHOGONAL AXES; $\bar{\eta}/D=4$, $U_j/a_o=0.13$

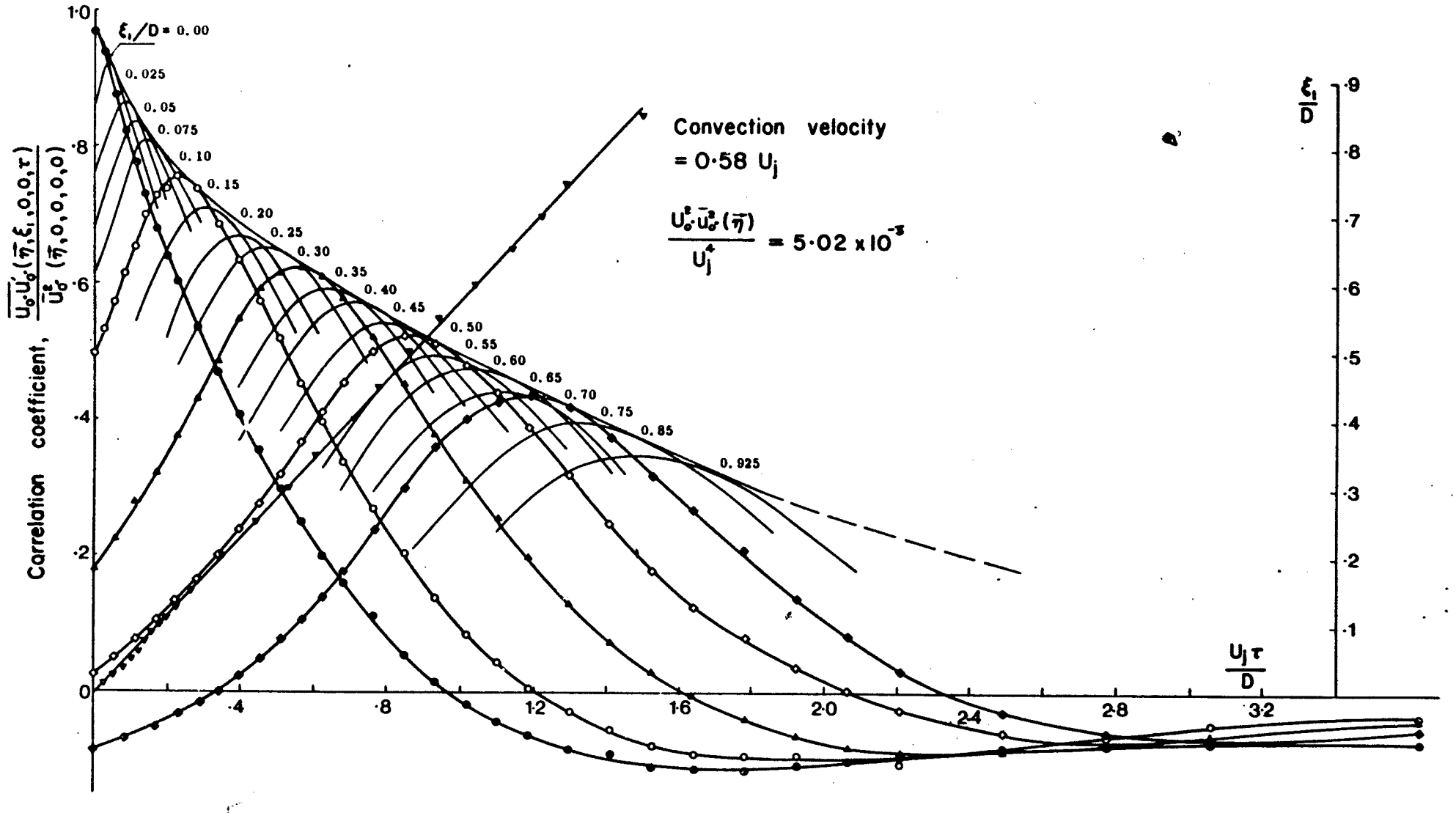


FIG. 13 LONGITUDINAL SPACE-TIME CORRELATION OF $u_{o\sigma}$; $\bar{r}_1/D=4$, $\bar{r}_2/D=0.5$, $U_j/a_o=0.13$

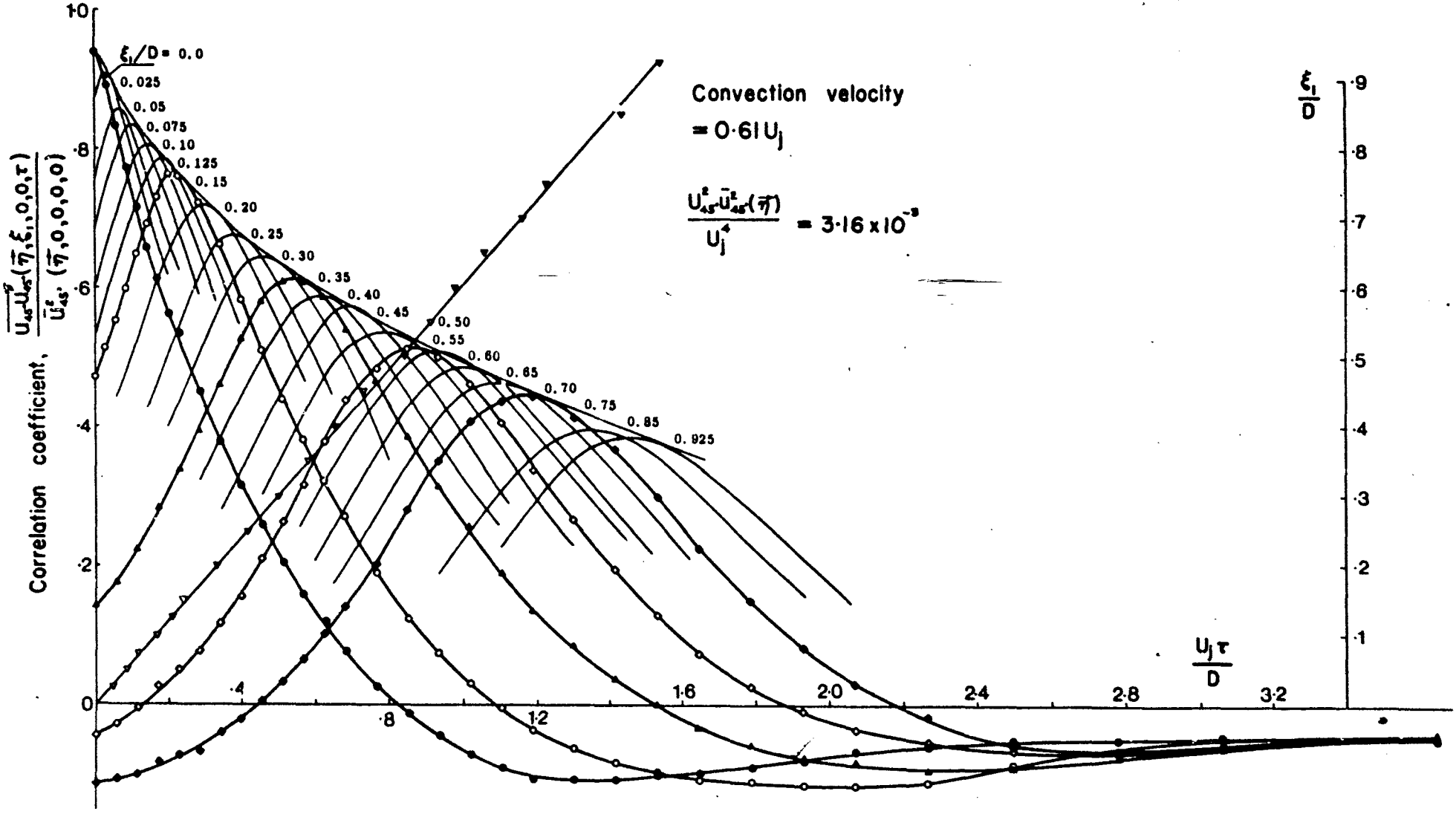


FIG. 14 LONGITUDINAL SPACE-TIME CORRELATION OF $u_{45°}$; $\vec{\eta}/D$=4, $\eta_3/D$=0.5, $U_j/a_o$=0.13

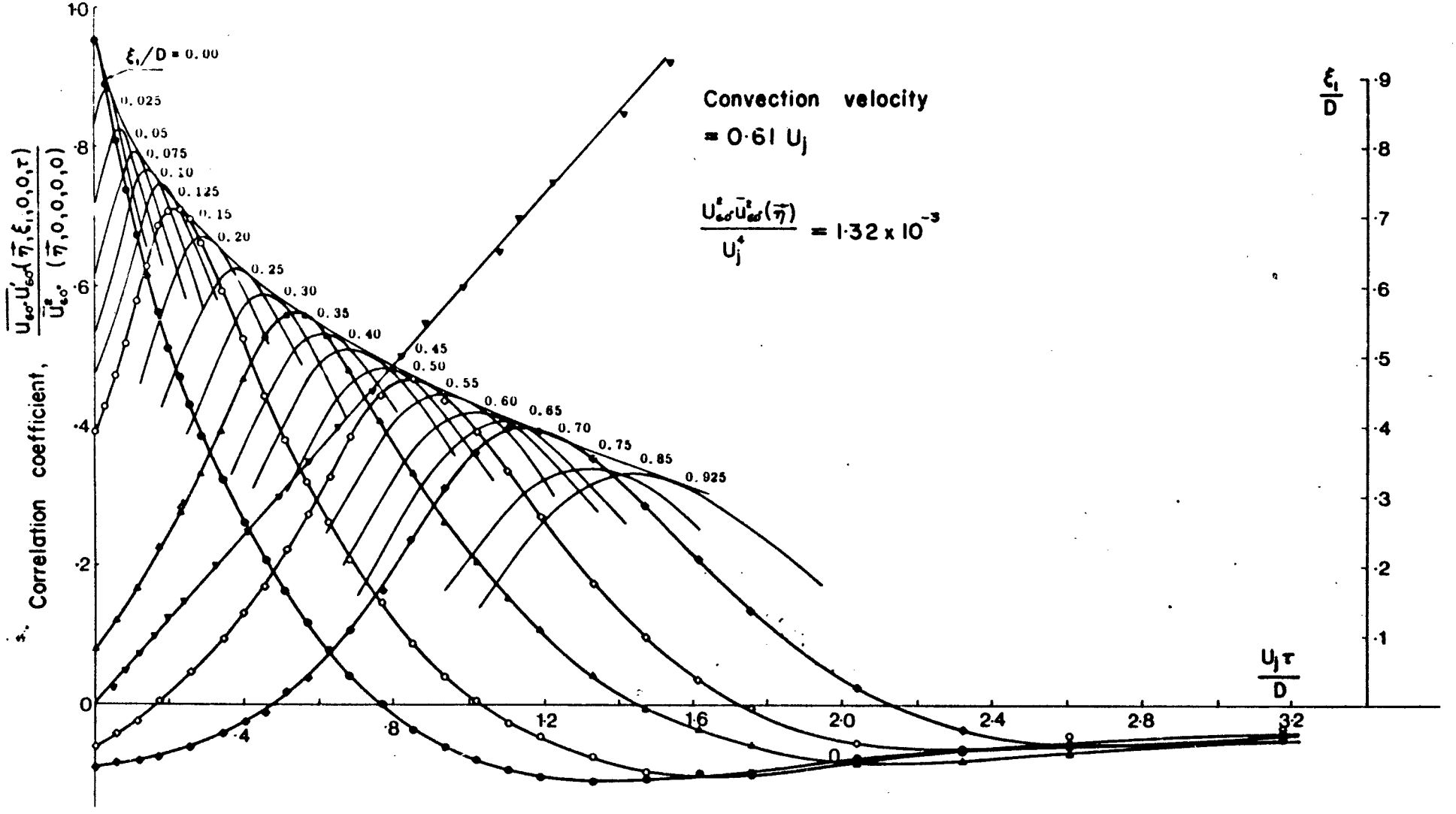


FIG. 15 LONGITUDINAL SPACE-TIME CORRELATION OF $u_{60}$ ; $\eta_1/D$=4, $\eta_2/D$=0.5, $U_j/a_0$=0.13

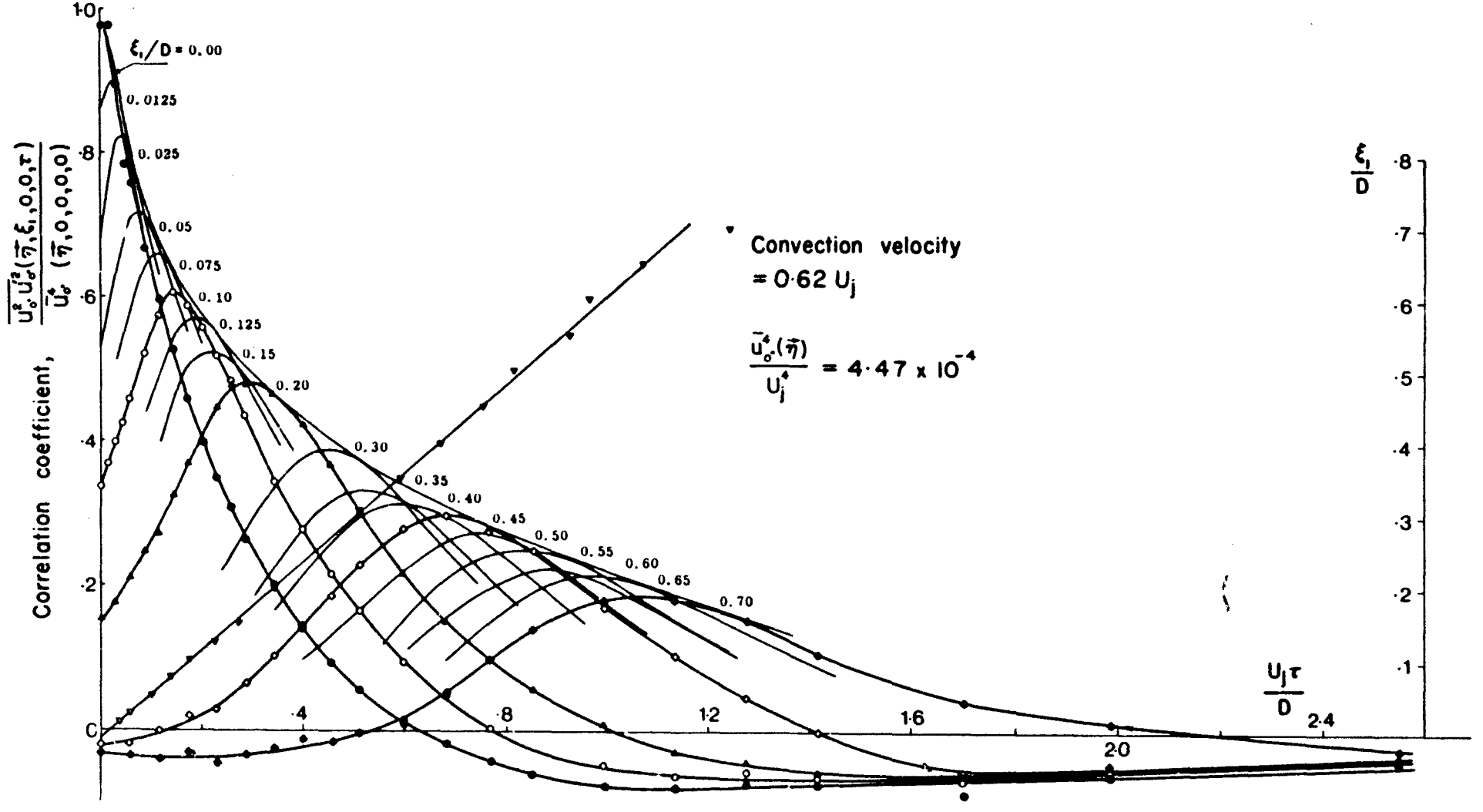


FIG. 16 LONGITUDINAL SPACE-TIME CORRELATION OF $u_{rr}^2$, $\eta/D=4$, $\eta_2/D=0.5$, $U_j/a_o=0.13$

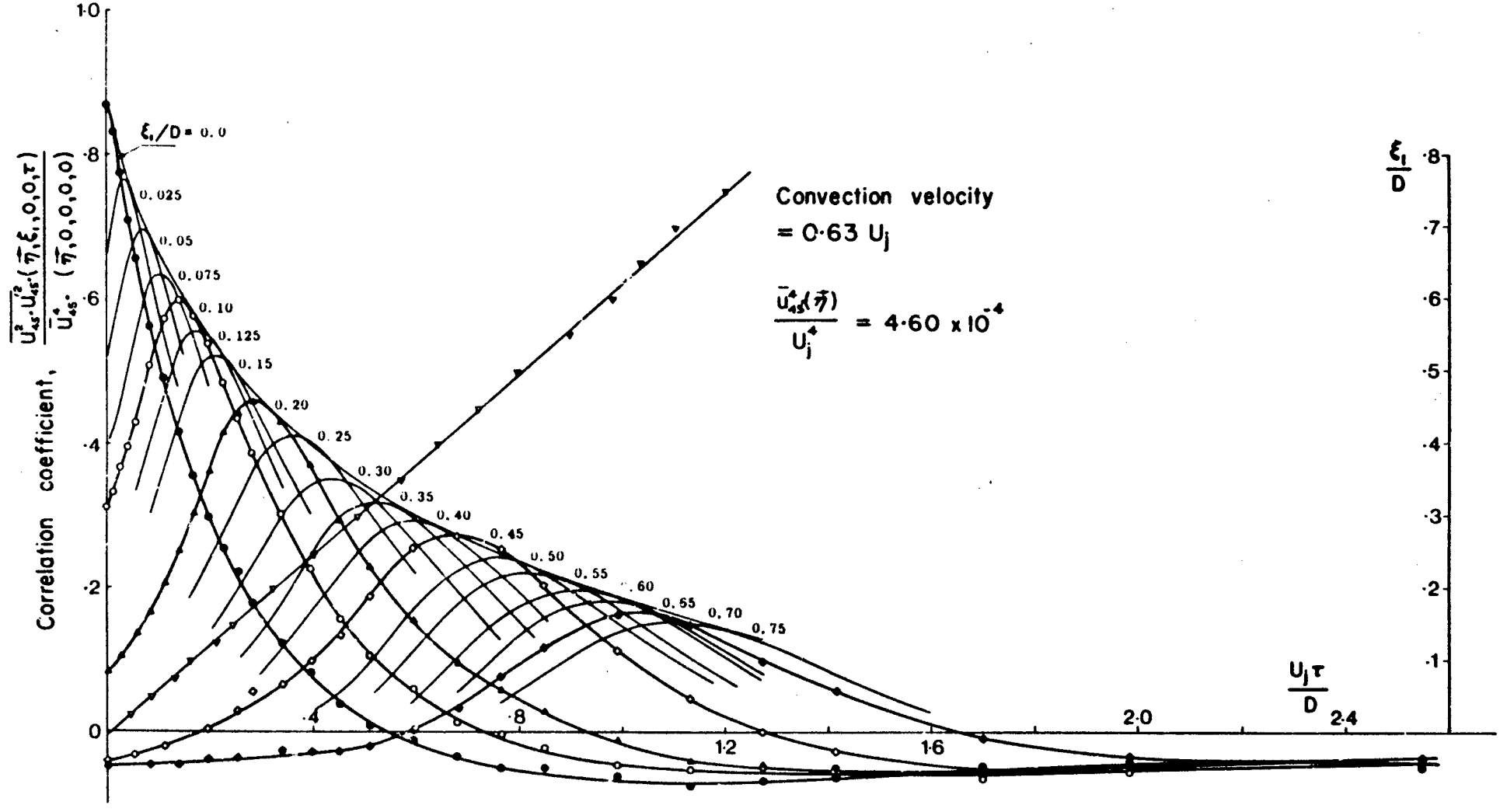


FIG. 17 LONGITUDINAL SPACE-TIME CORRELATION OF $u_{45°}^2$; $\eta/D=4$, $\eta_z/D=0.5$, $U_j/a_o=0.13$

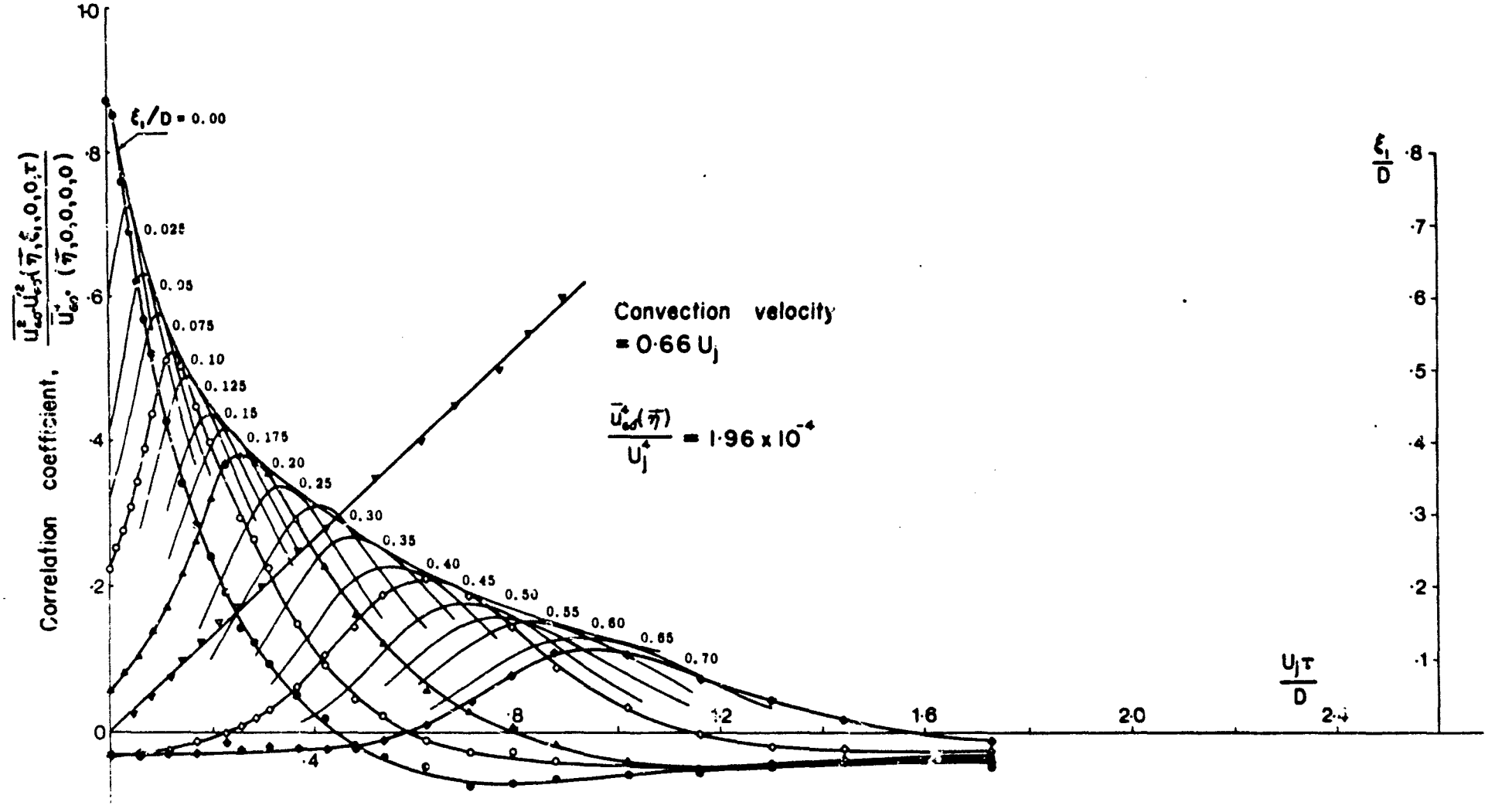


FIG. 18 LONGITUDINAL SPACE-TIME CORRELATION OF $u^2_{60^\circ}$; $\bar{\eta}/D=4$, $\bar{\eta}_2/D=0.5$, $U_j/a_o=0.13$

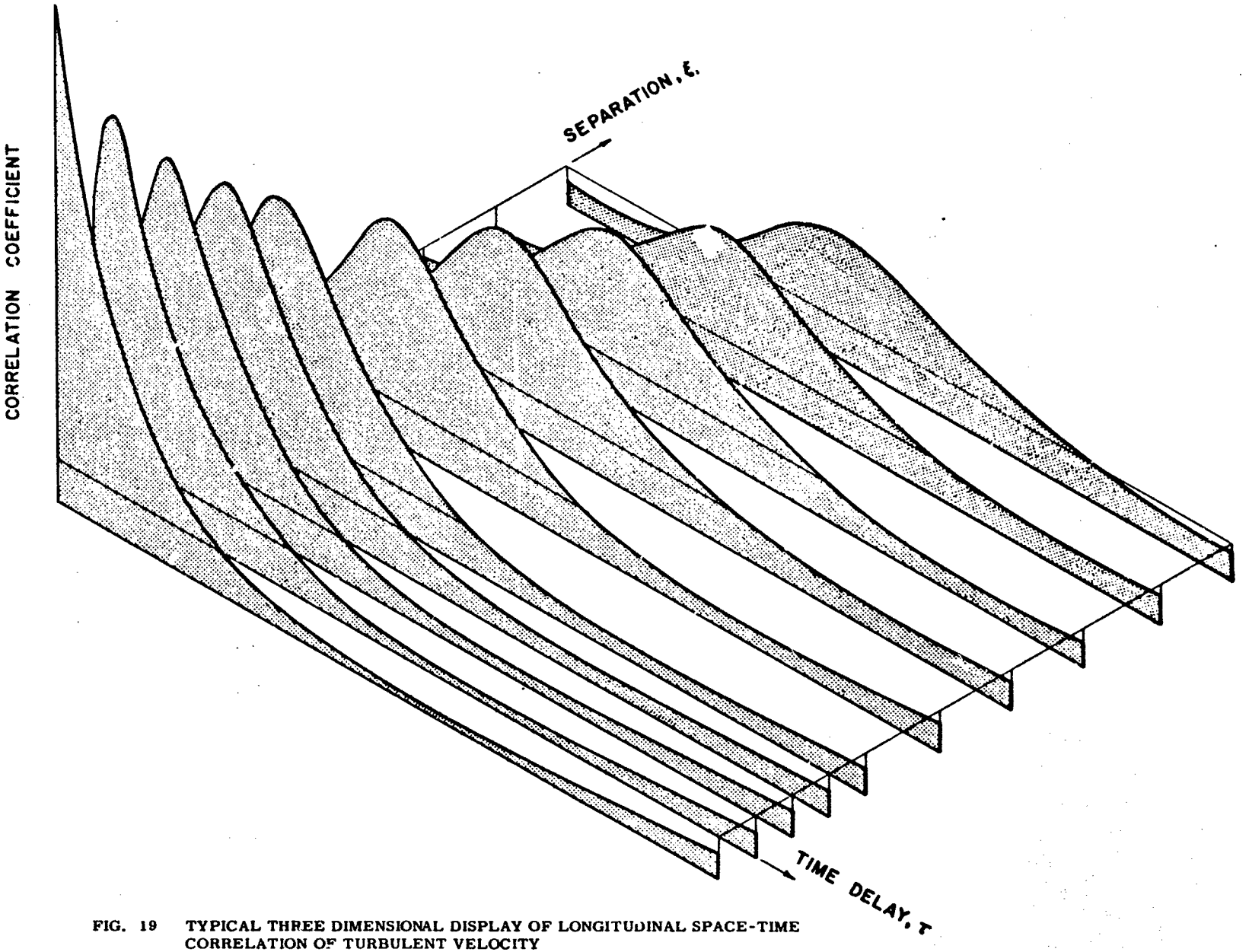


FIG. 19 TYPICAL THREE DIMENSIONAL DISPLAY OF LONGITUDINAL SPACE-TIME CORRELATION OF TURBULENT VELOCITY

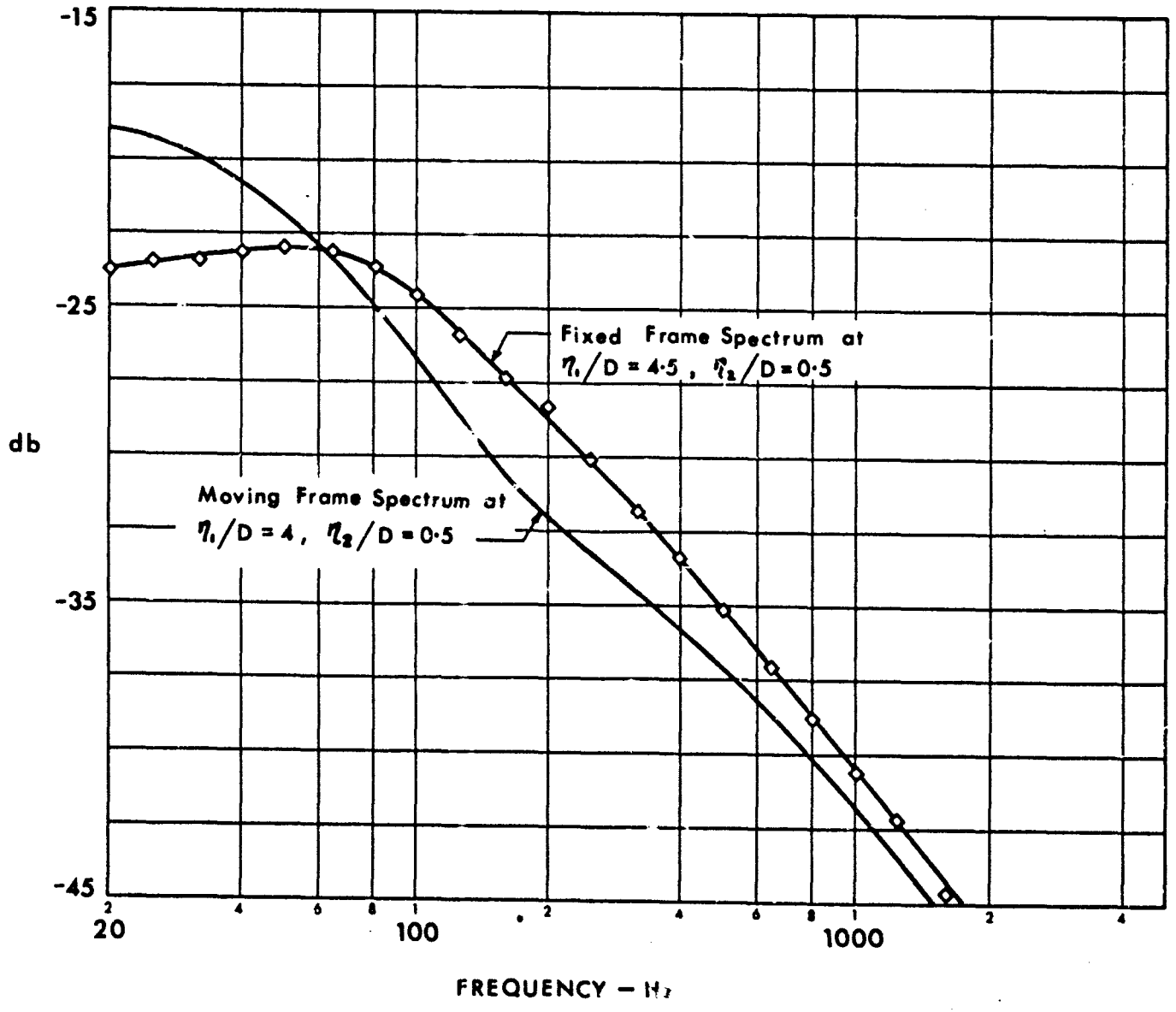


FIG. 20 FIXED AND MOVING FRAME SPECTRA; $U_j/a_o = 0.13$

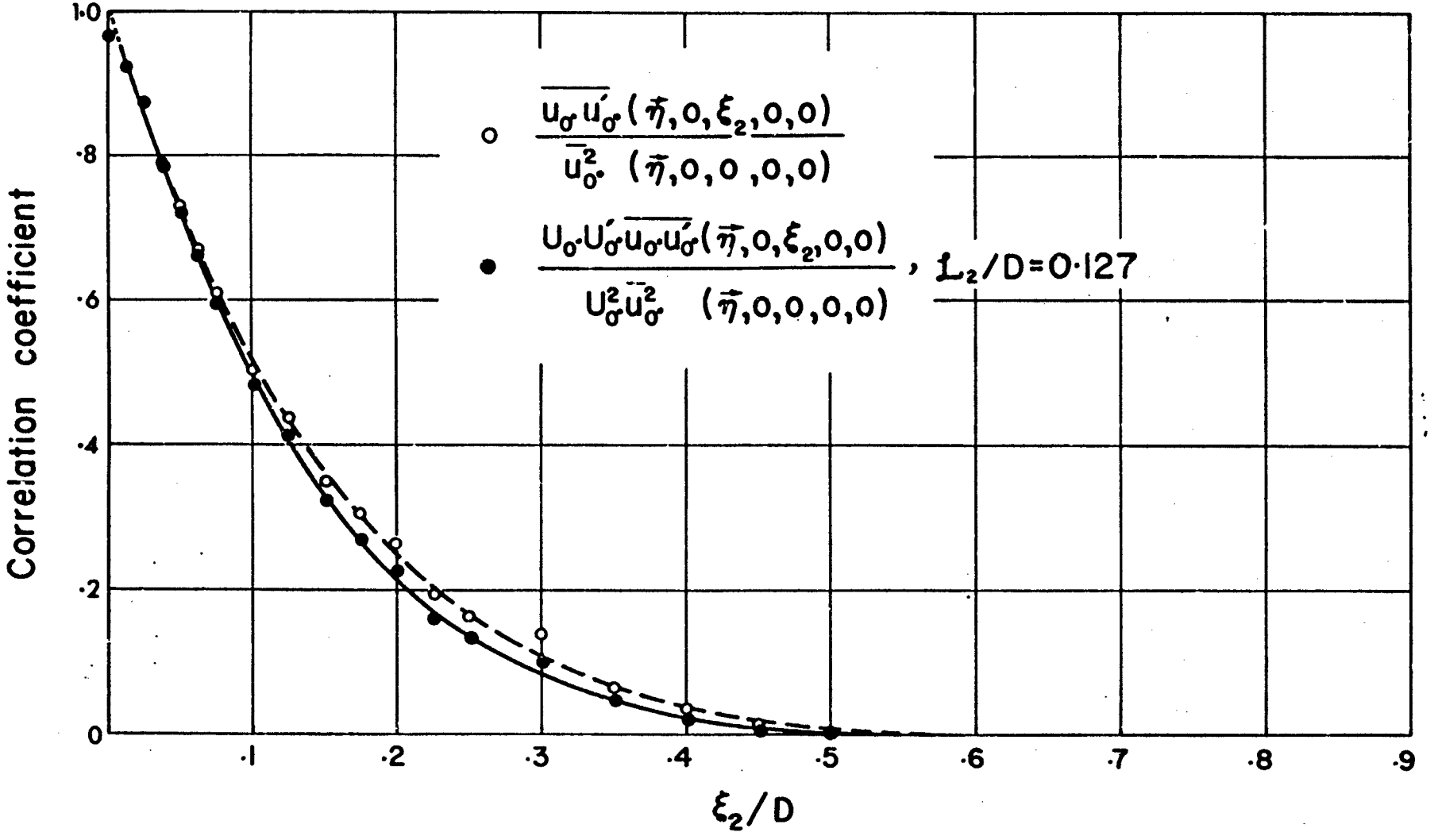


FIG. 21 TRANSVERSE SPACE CORRELATIONS OF $u_o$ IN 2-AXIS;
$\eta_1/D=4$, $\eta_2/D=0.5$, $U_j/a_o=0.13$

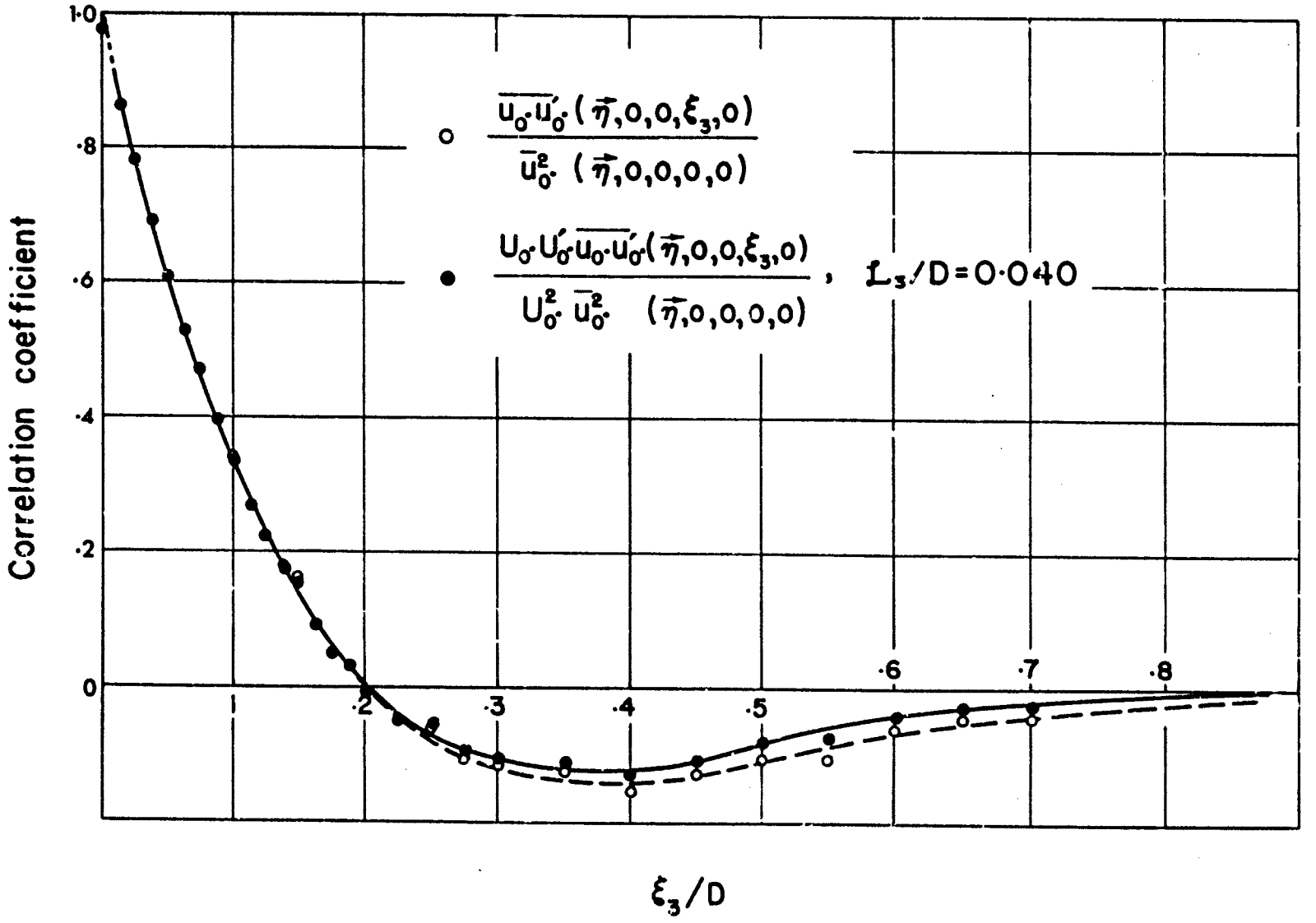


FIG. 22 TRANSVERSE SPACE CORRELATIONS OF $u_0$ IN 3-AXIS;
$\eta_1/D=4$, $\eta_2/D=0.5$, $U_j/a_o=0.13$

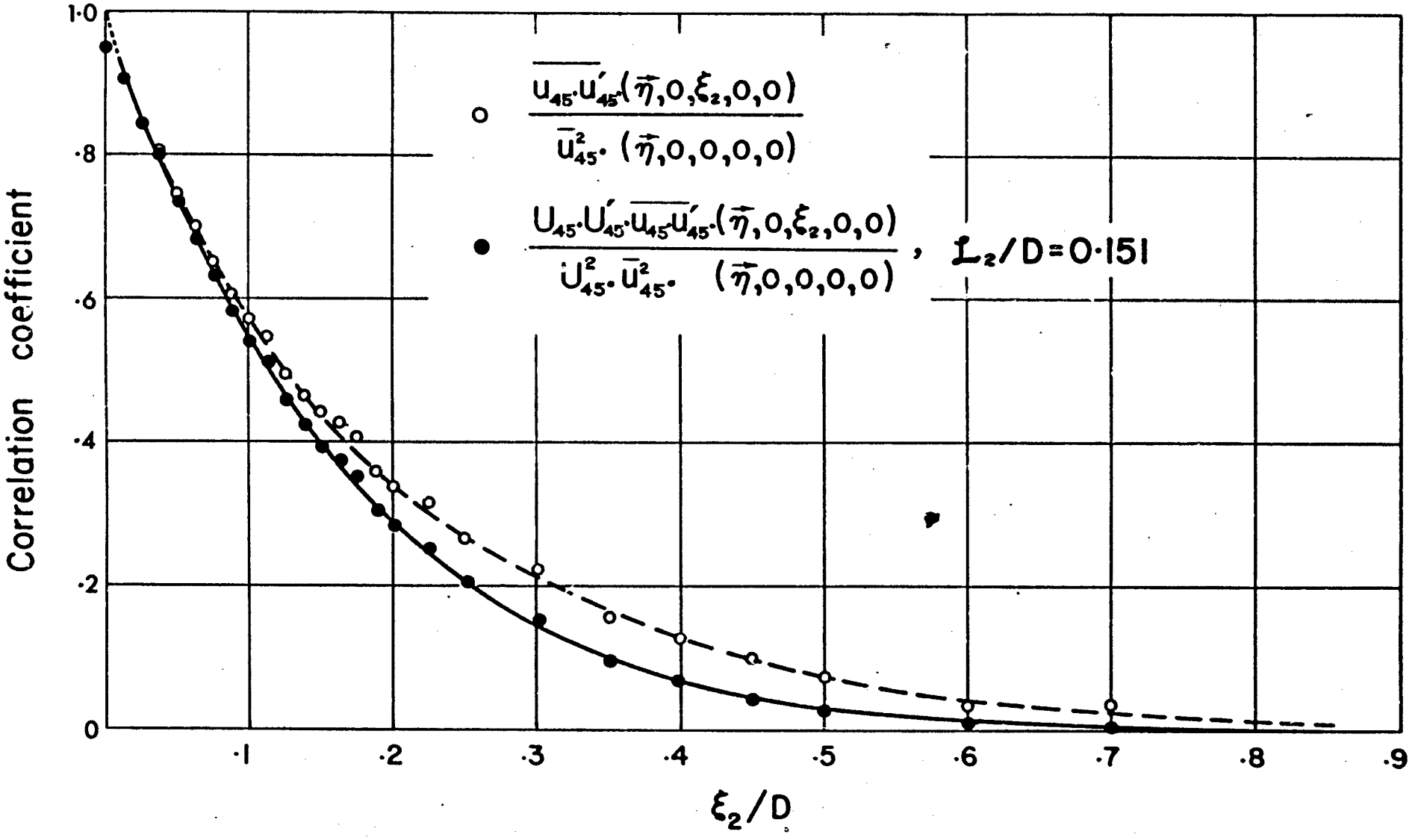


FIG. 23 TRANSVERSE SPACE CORRELATIONS OF $u_{45}$ IN 2-AXIS; $\eta_1/D=4$, $\eta_2/D=0.5$, $U_j/a_o=0.13$

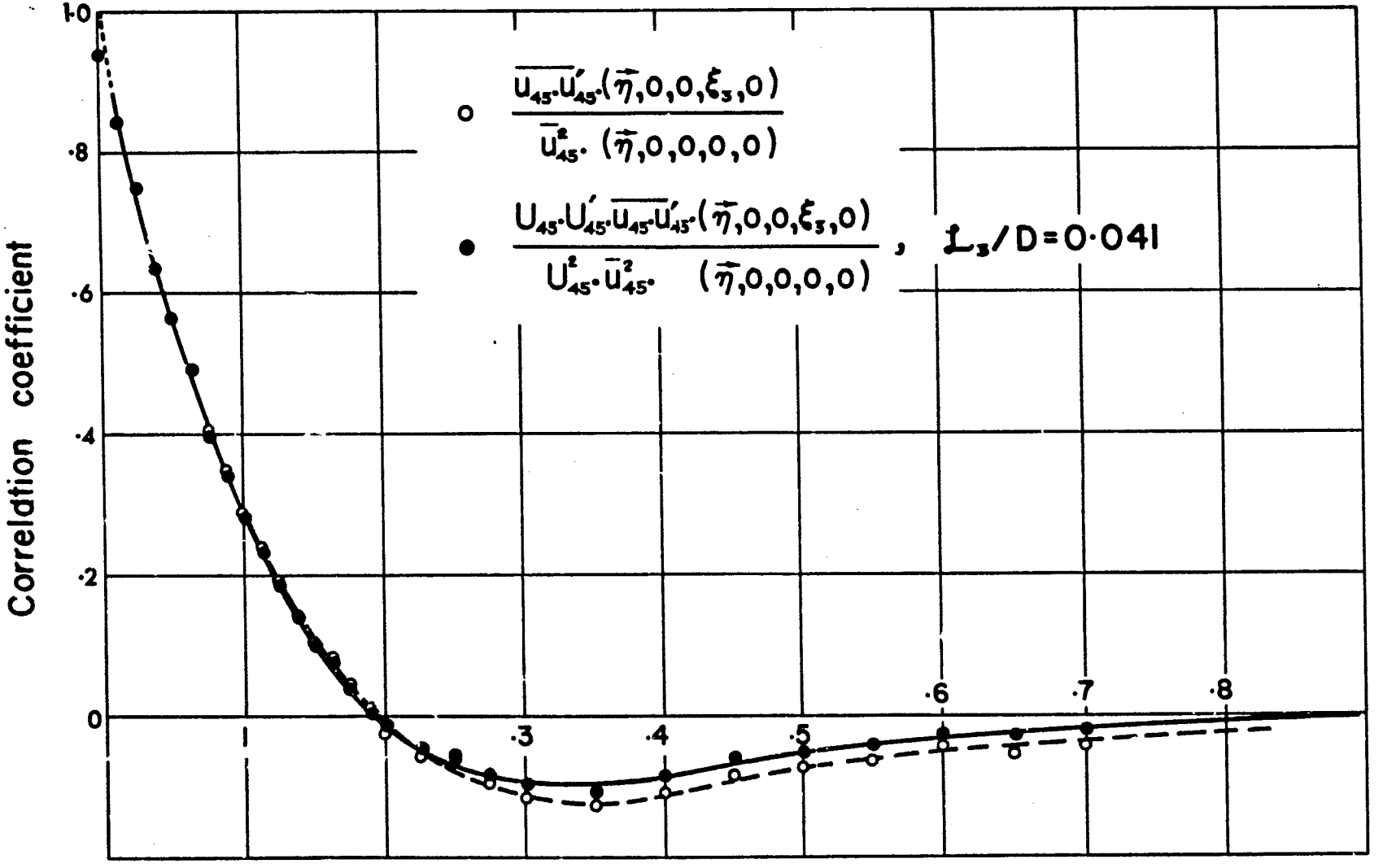


FIG. 24 TRANSVERSE SPACE CORRELATIONS OF $u_{45}$ IN 3-AXIS;
$\eta/D=4$, $\eta_2/D=0.5$, $U_j/a_o=0.13$

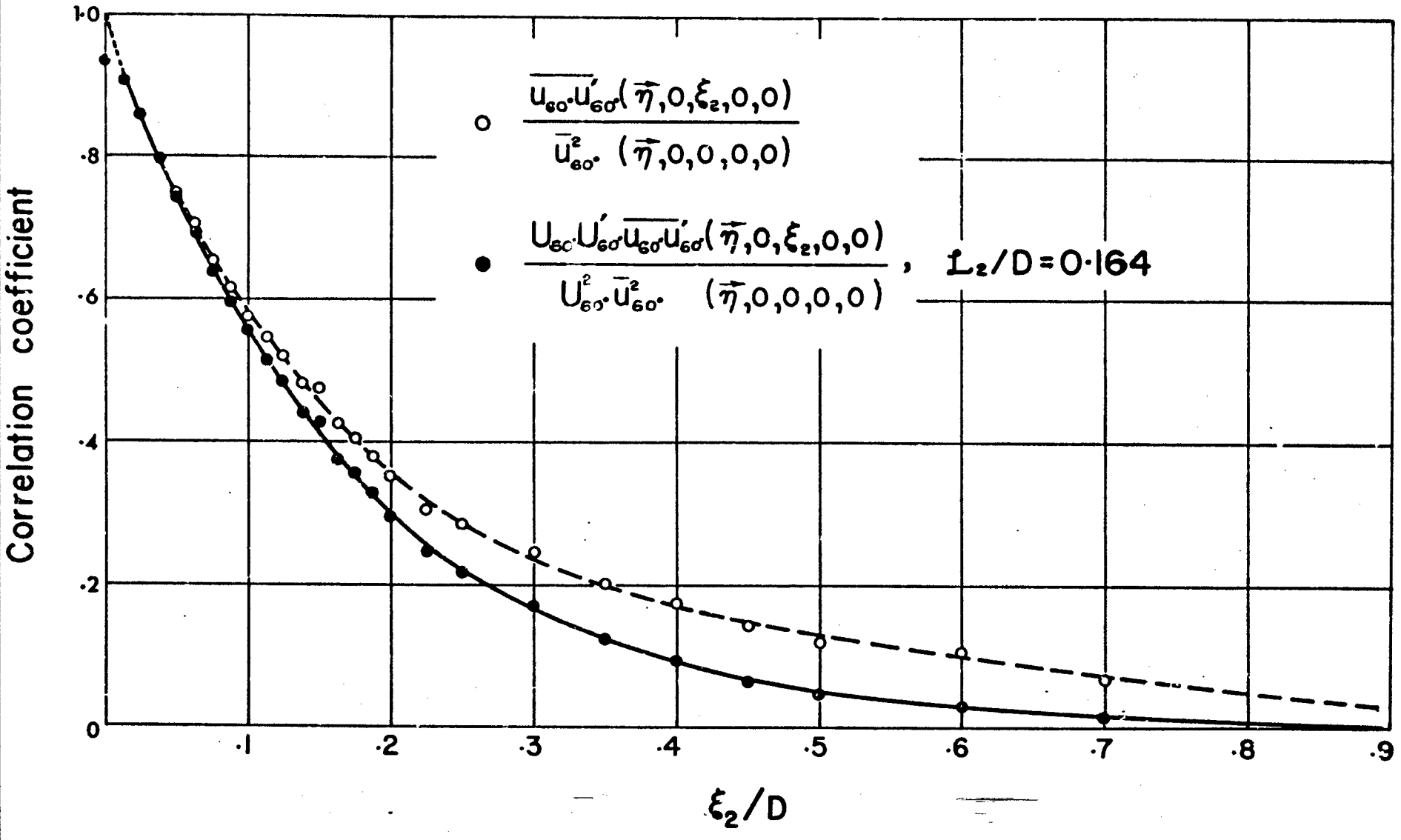


FIG. 25 TRANSVERSE SPACE CORRELATIONS OF $u_{60}$ IN 2-AXIS;
$\eta_1/D=4$, $\eta_2/D=0.5$, $U_j/a_o=0.13$

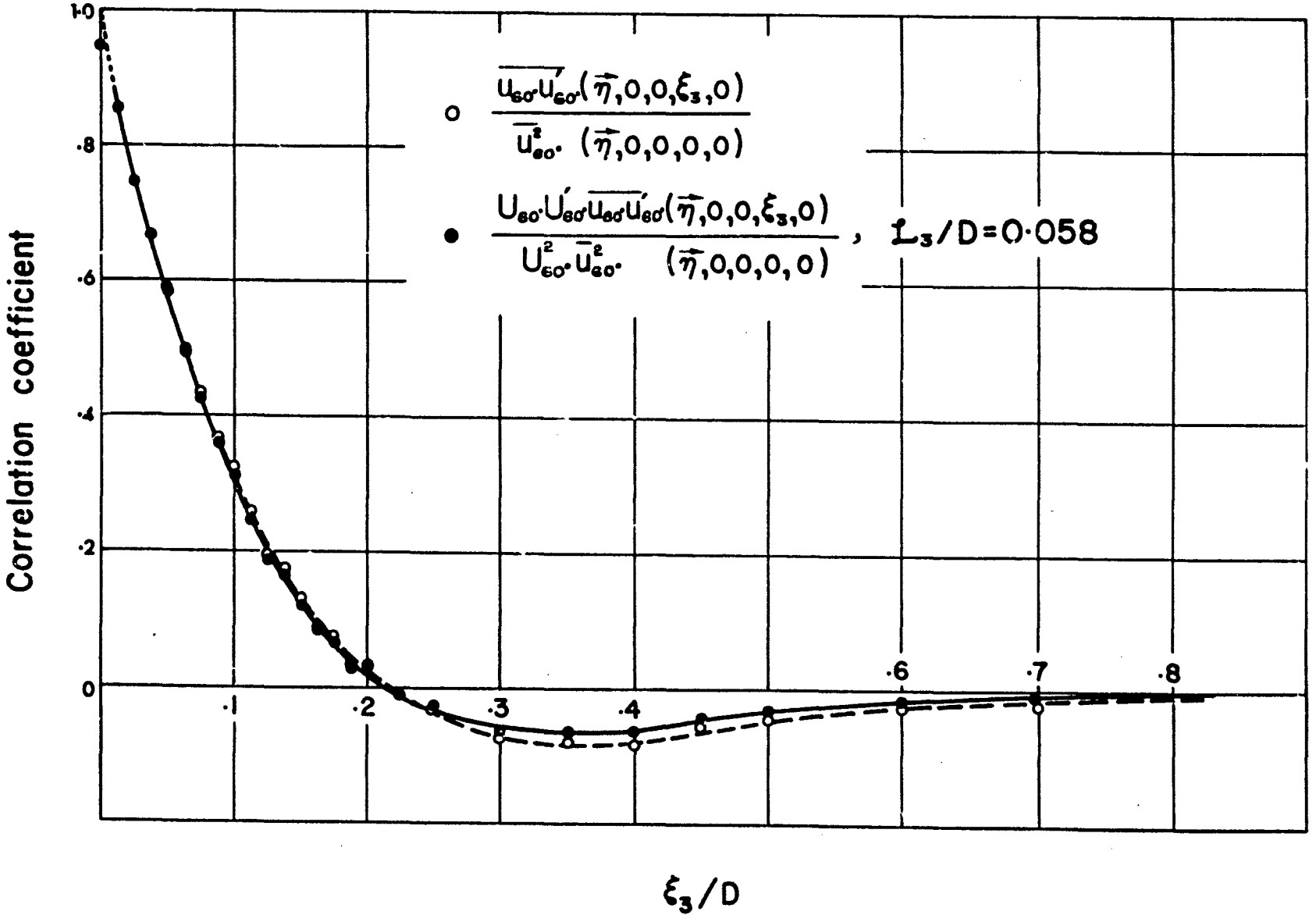


FIG. 26 TRANSVERSE SPACE CORRELATIONS OF $u_{60}$ IN 3-AXIS;
$\eta_1/D=4$, $\eta_2/D=0.5$, $U_j/a_o=0.13$

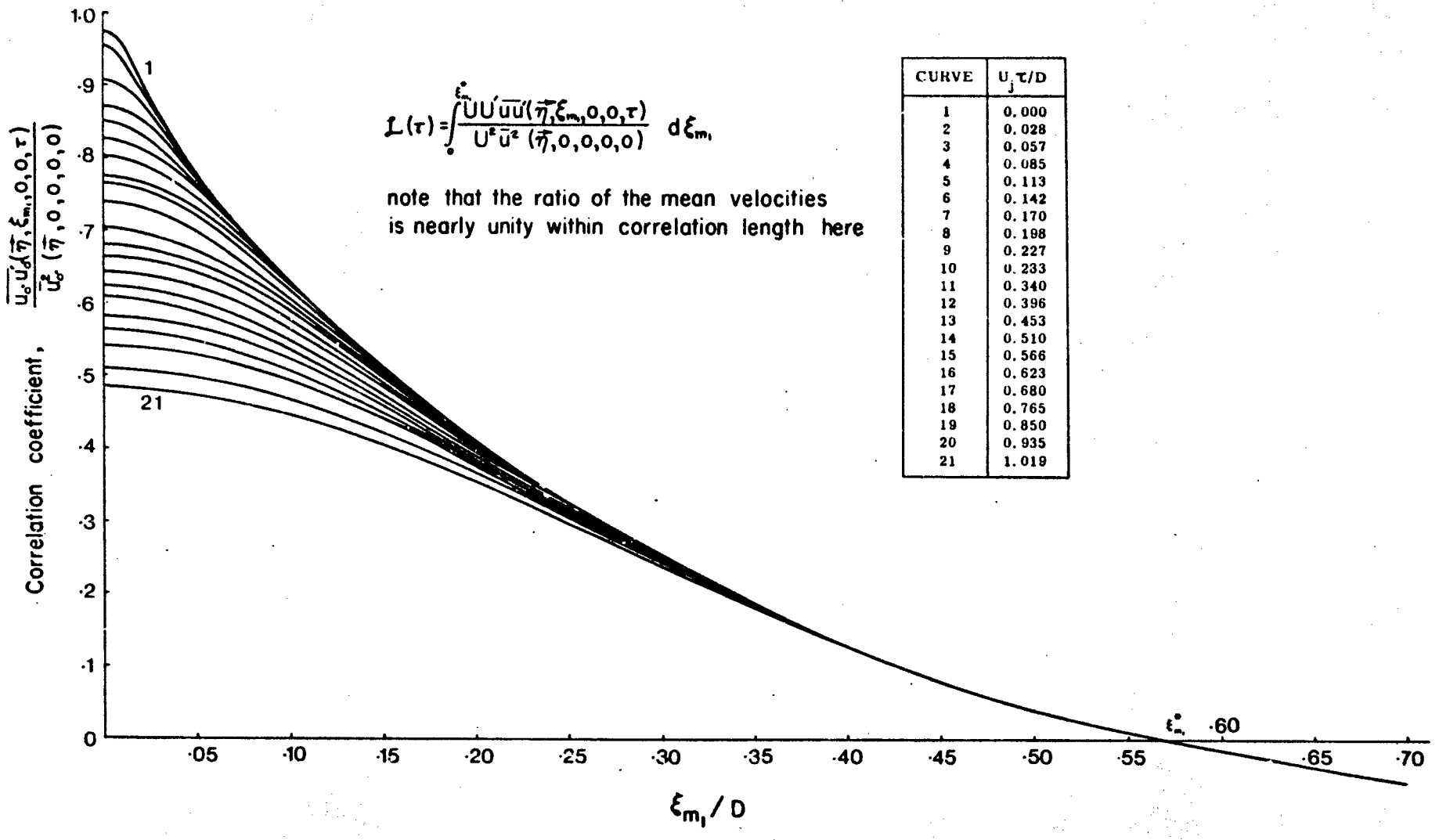


| CURVE | $U_j \tau / D$ |
|---|---|
| 1 | 0.000 |
| 2 | 0.028 |
| 3 | 0.057 |
| 4 | 0.085 |
| 5 | 0.113 |
| 6 | 0.142 |
| 7 | 0.170 |
| 8 | 0.198 |
| 9 | 0.227 |
| 10 | 0.233 |
| 11 | 0.340 |
| 12 | 0.396 |
| 13 | 0.453 |
| 14 | 0.510 |
| 15 | 0.566 |
| 16 | 0.623 |
| 17 | 0.680 |
| 18 | 0.765 |
| 19 | 0.850 |
| 20 | 0.935 |
| 21 | 1.019 |

FIG. 27 TYPICAL LONGITUDINAL SPACE-TIME CORRELATION OF TURBULENT VELOCITY AFTER MOVING-FRAME TRANSFORMATION USING DATA OF FIG. 13

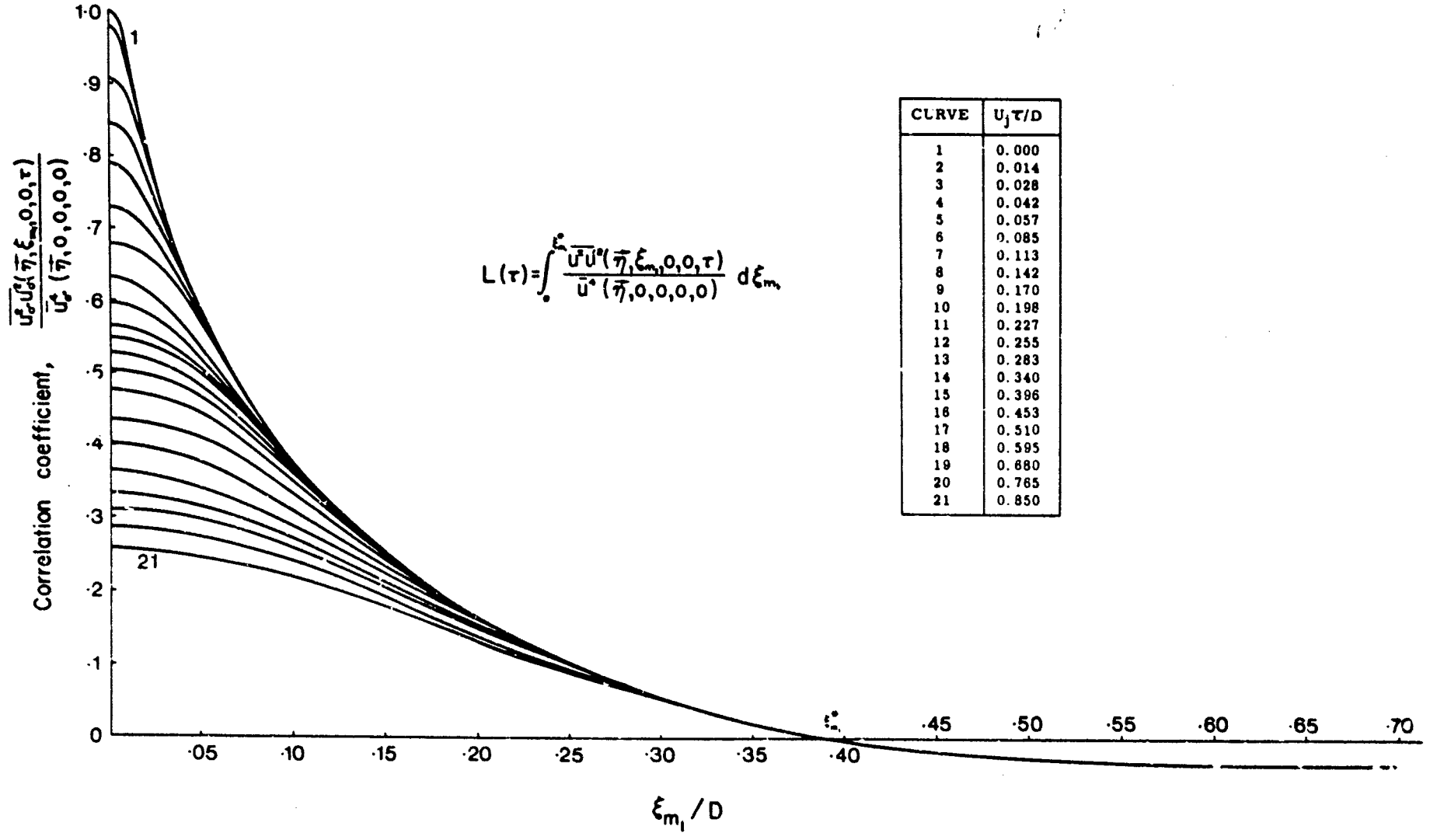


| CURVE | $U_j\tau/D$ |
|---|---|
| 1 | 0.000 |
| 2 | 0.014 |
| 3 | 0.028 |
| 4 | 0.042 |
| 5 | 0.057 |
| 6 | 0.085 |
| 7 | 0.113 |
| 8 | 0.142 |
| 9 | 0.170 |
| 10 | 0.198 |
| 11 | 0.227 |
| 12 | 0.255 |
| 13 | 0.283 |
| 14 | 0.340 |
| 15 | 0.396 |
| 16 | 0.453 |
| 17 | 0.510 |
| 18 | 0.595 |
| 19 | 0.680 |
| 20 | 0.765 |
| 21 | 0.850 |

FIG. 28 TYPICAL LONGITUDINAL SPACE-TIME CORRELATION OF TURNULENT VELOCITY SQUARED AFTER MOVING-FRAME TRANSFORMATION USING DATA OF FIG. 16

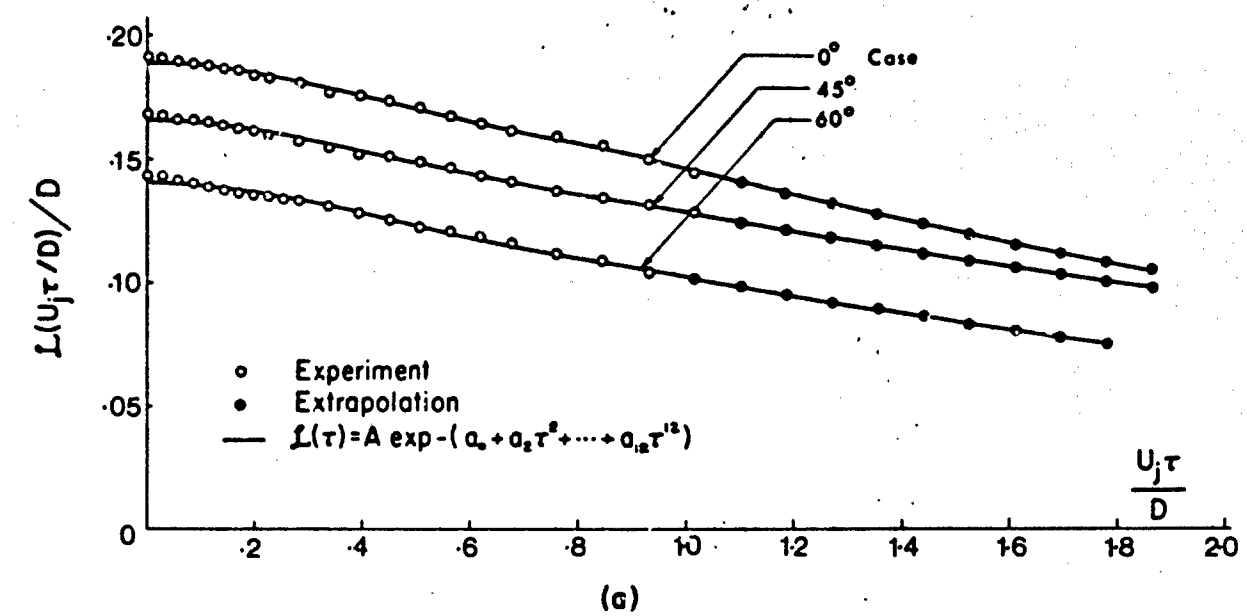


(a)

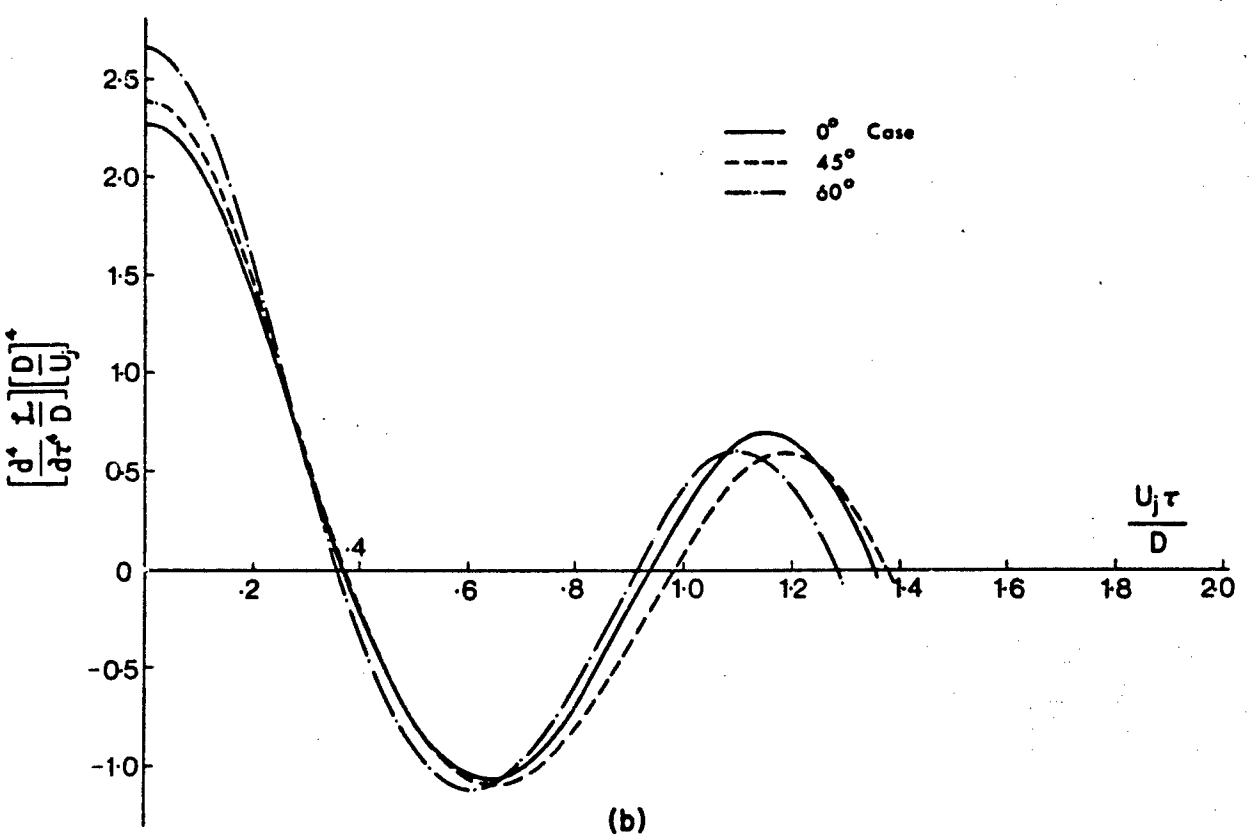


(b)

FIG. 29 FOR THE SHEAR NOISE CASES
(a) LEAST SQUARE CURVE FITTING TO THE INTEGRATED MOVING-FRAME CORRELATION FUNCTIONS
(b) THE CORRESPONDING FOURTH DERIVATIVES

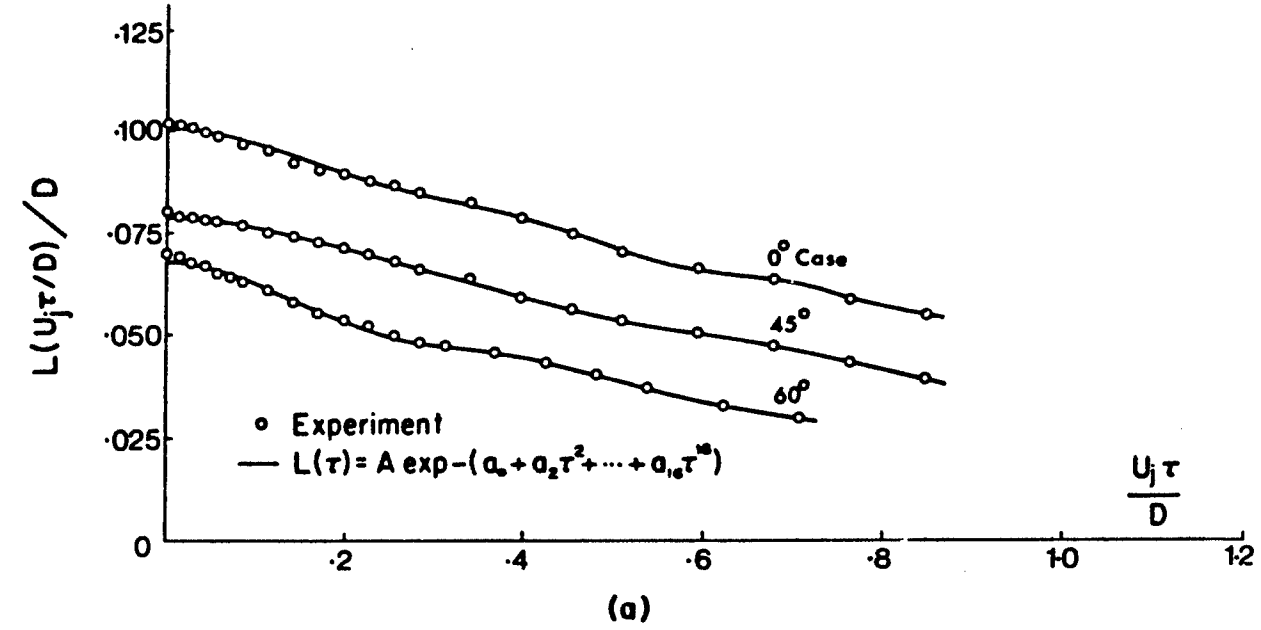


(a)

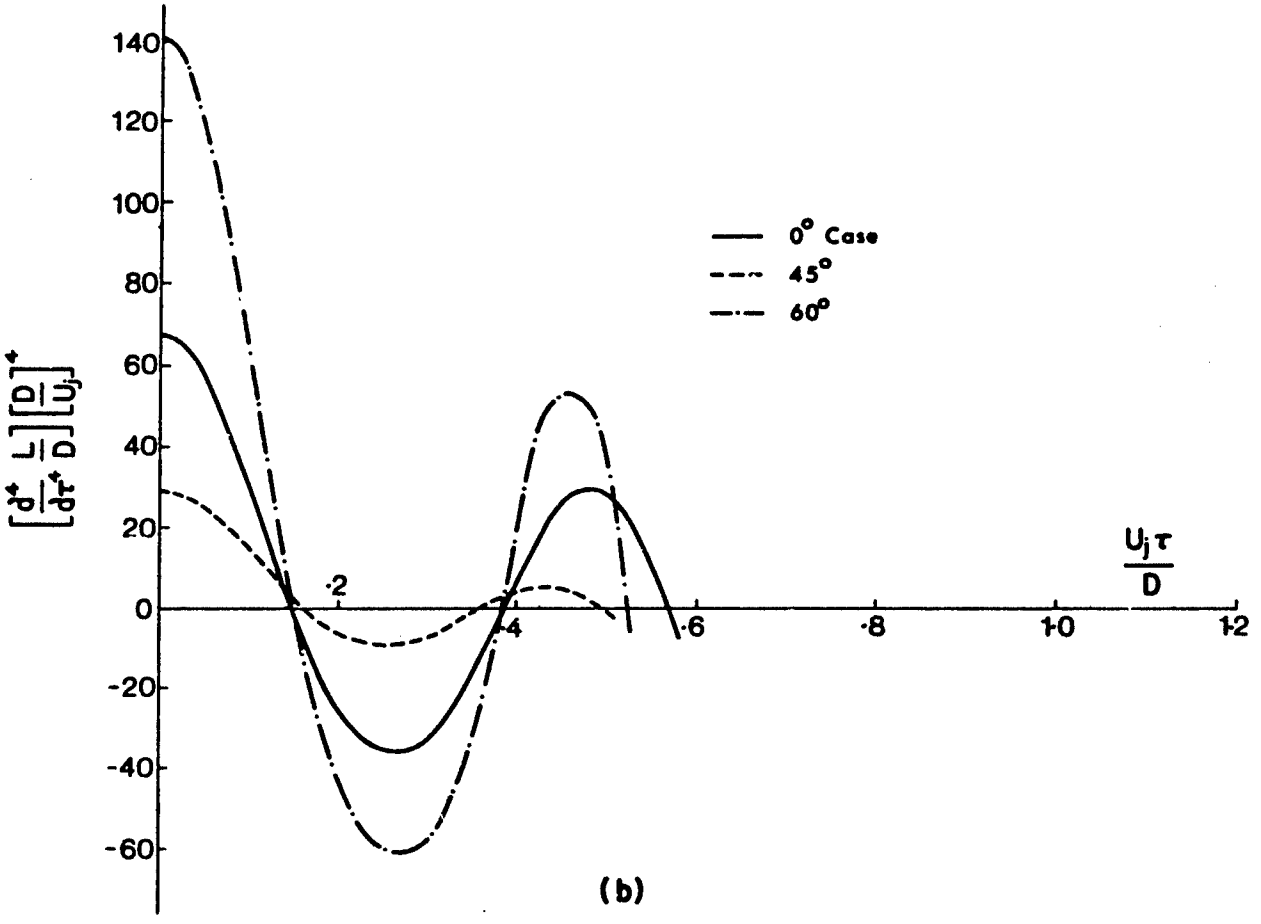


(b)

FIG. 30 FOR THE SELF NOISE CASES
(a) LEAST SQUARE CURVE FITTING TO THE INTEGRATED MOVING-FRAME CORRELATION FUNCTIONS
(b) THE CORRESPONDING FOURTH DERIVATIVES

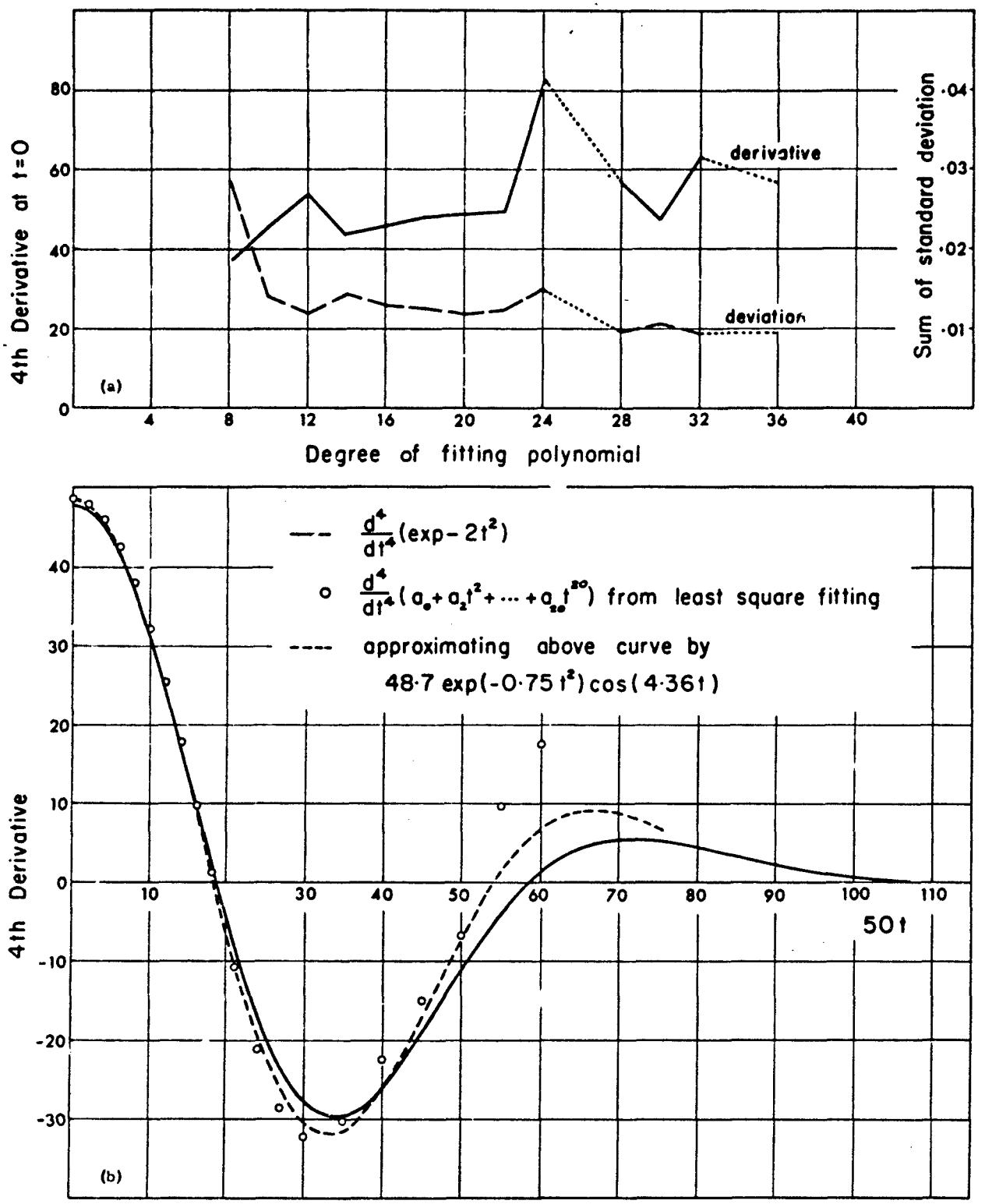


FIG. 31 (a) VARIATION OF FOURTH DERIVATIVE AT t=0 OF THE FITTING POLYNOMIAL (BY LEAST SQUARE) TO A GAUSSIAN FUNCTION WITH THE NUMBER OF DEGREE OF THE POLYNOMIAL
(b) COMPARISON BETWEEN THEORETICAL AND COMPUTED FOURTH DERIVATIVES

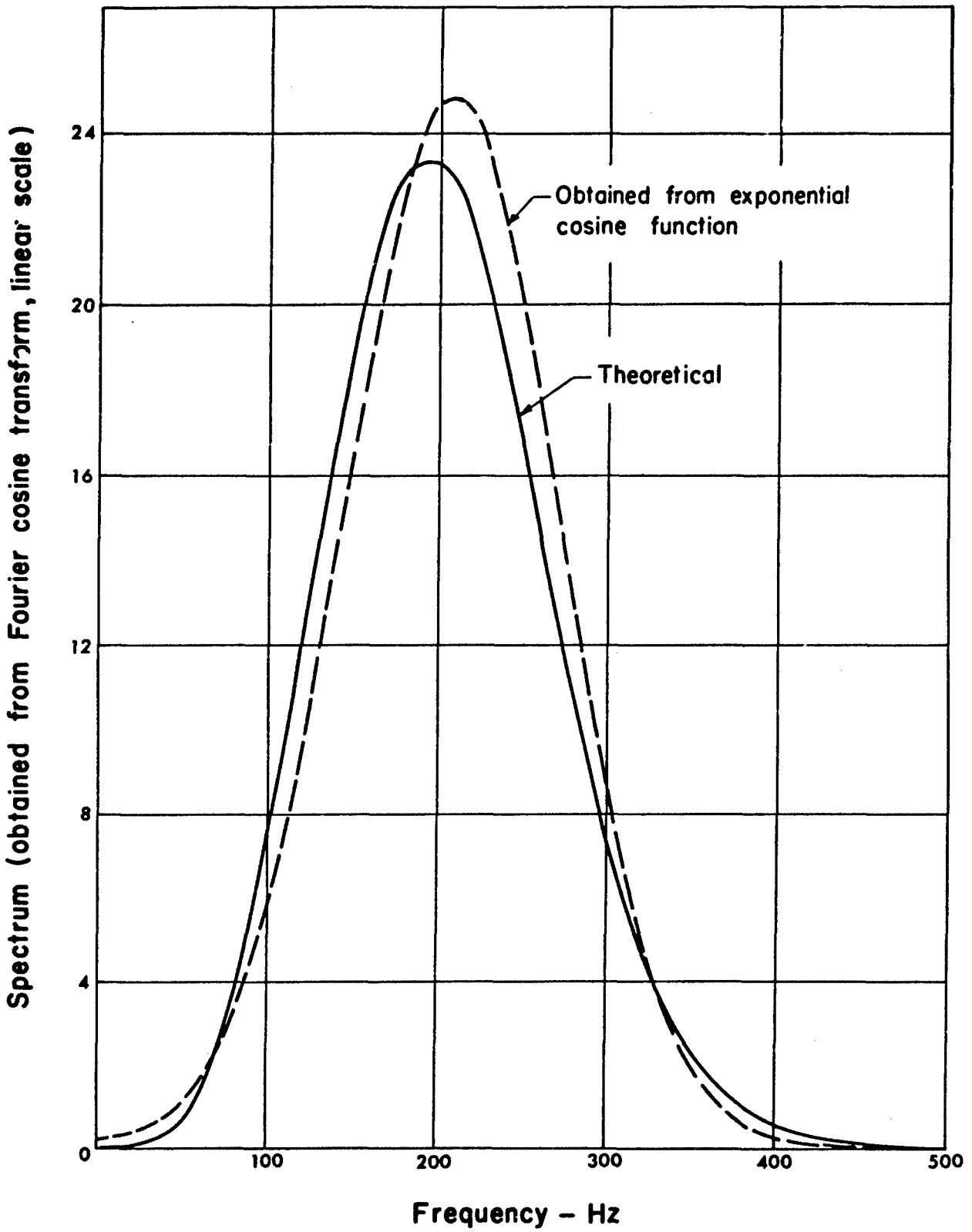


FIG. 32 COMPARISON BETWEEN THE FOURIER COSINE TRANSFORM OF THE FOURTH DERIVATIVES OF A GAUSSIAN FUNCTION AND THE APPROXIMATING FUNCTION

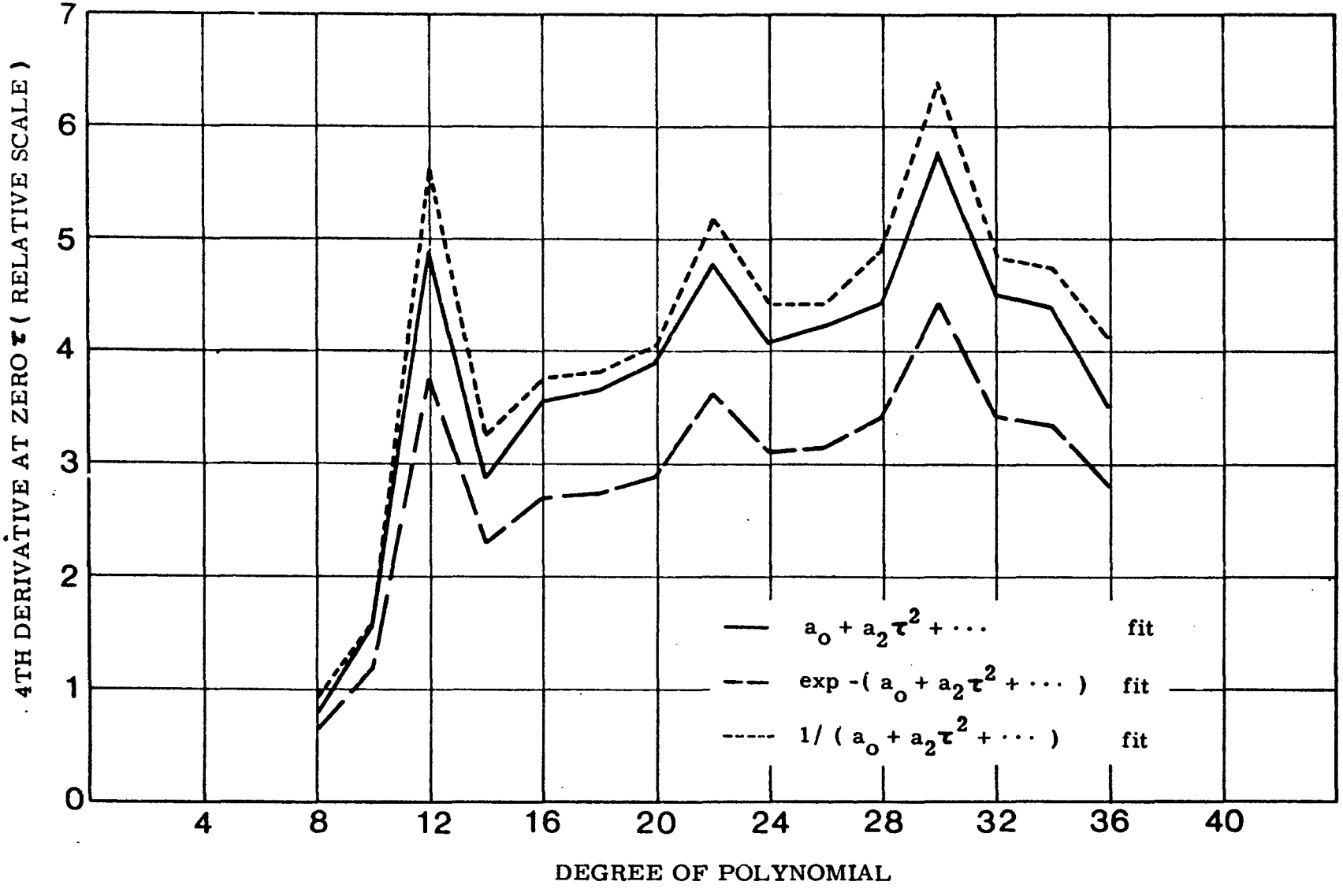


FIG. 33 TYPICAL COMPARISON OF THE VARIATION OF THE FOURTH DERIVATIVE AT ZERO $\tau$ WITH THE DEGREE OF THE LEAST SQUARE FITTING FUNCTIONS

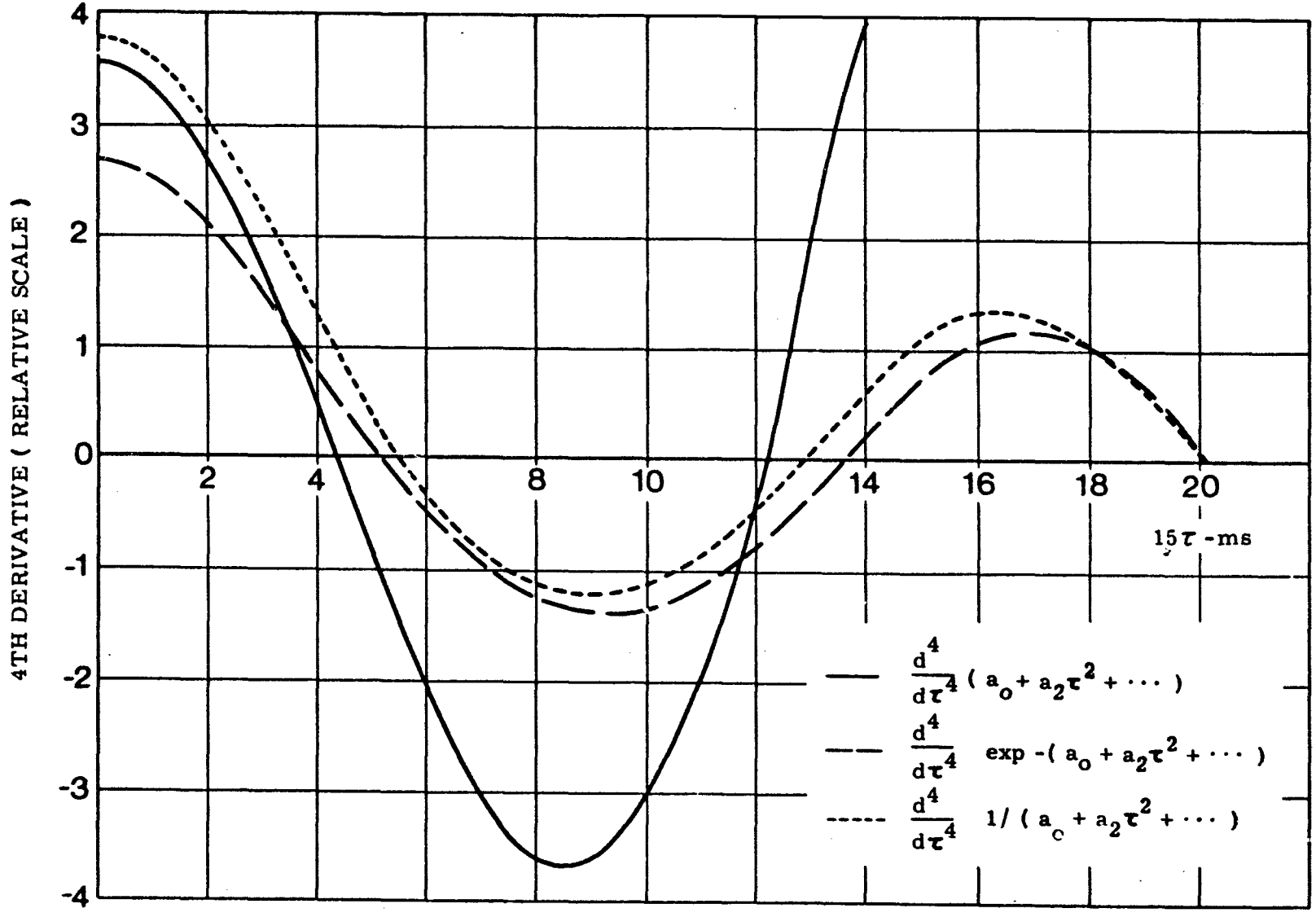


FIG. 34 TYPICAL COMPARISON OF THE FOURTH DERIVATIVES FROM THE THREE TYPES OF CURVE FITTING

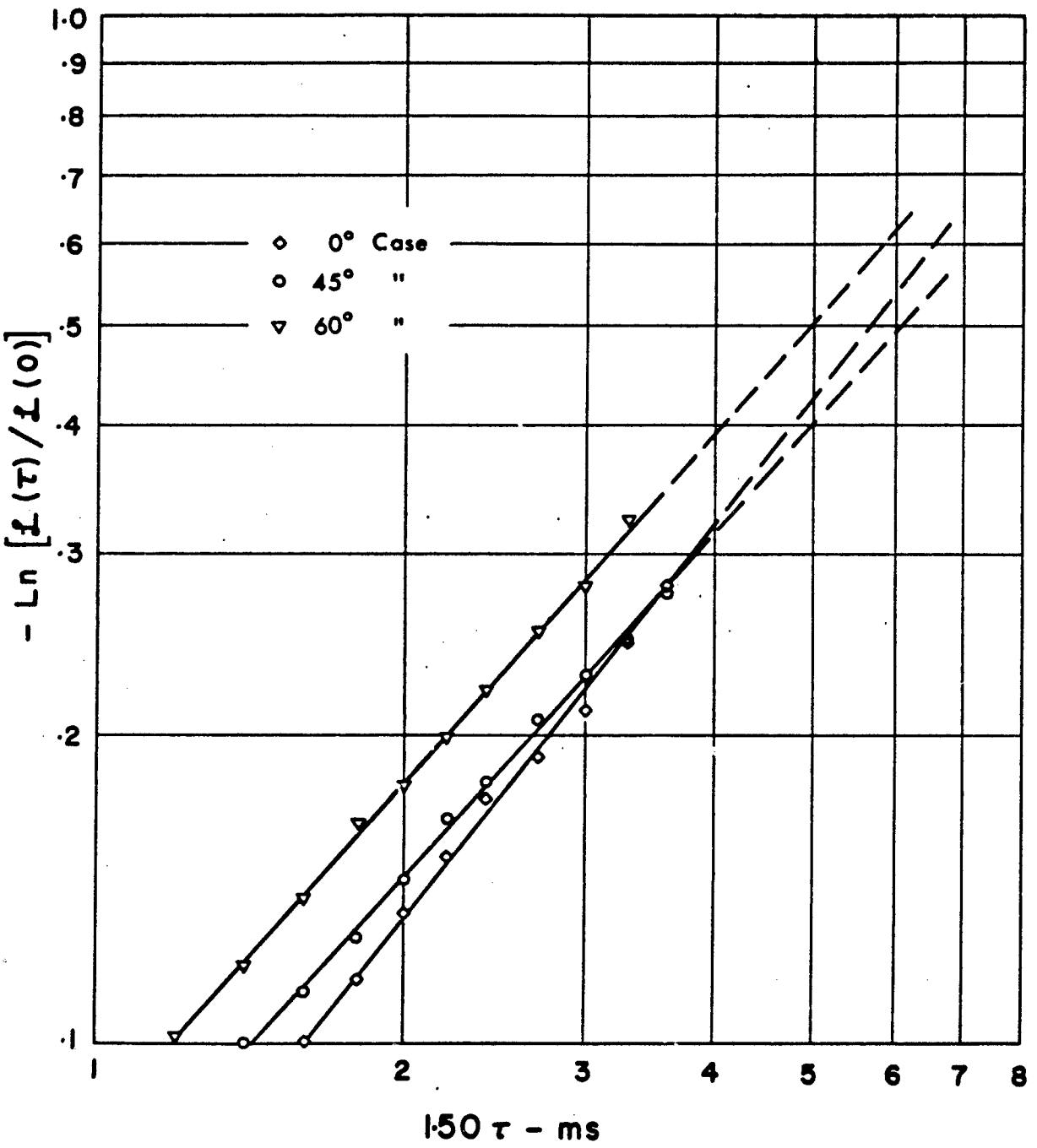


FIG. 35 REPLOT ON A LOG LOG SCALE OF THE TAIL-END DATA OF FIG. 29(a) (NORMALIZED BY VALUE AT $\tau = 0$ )

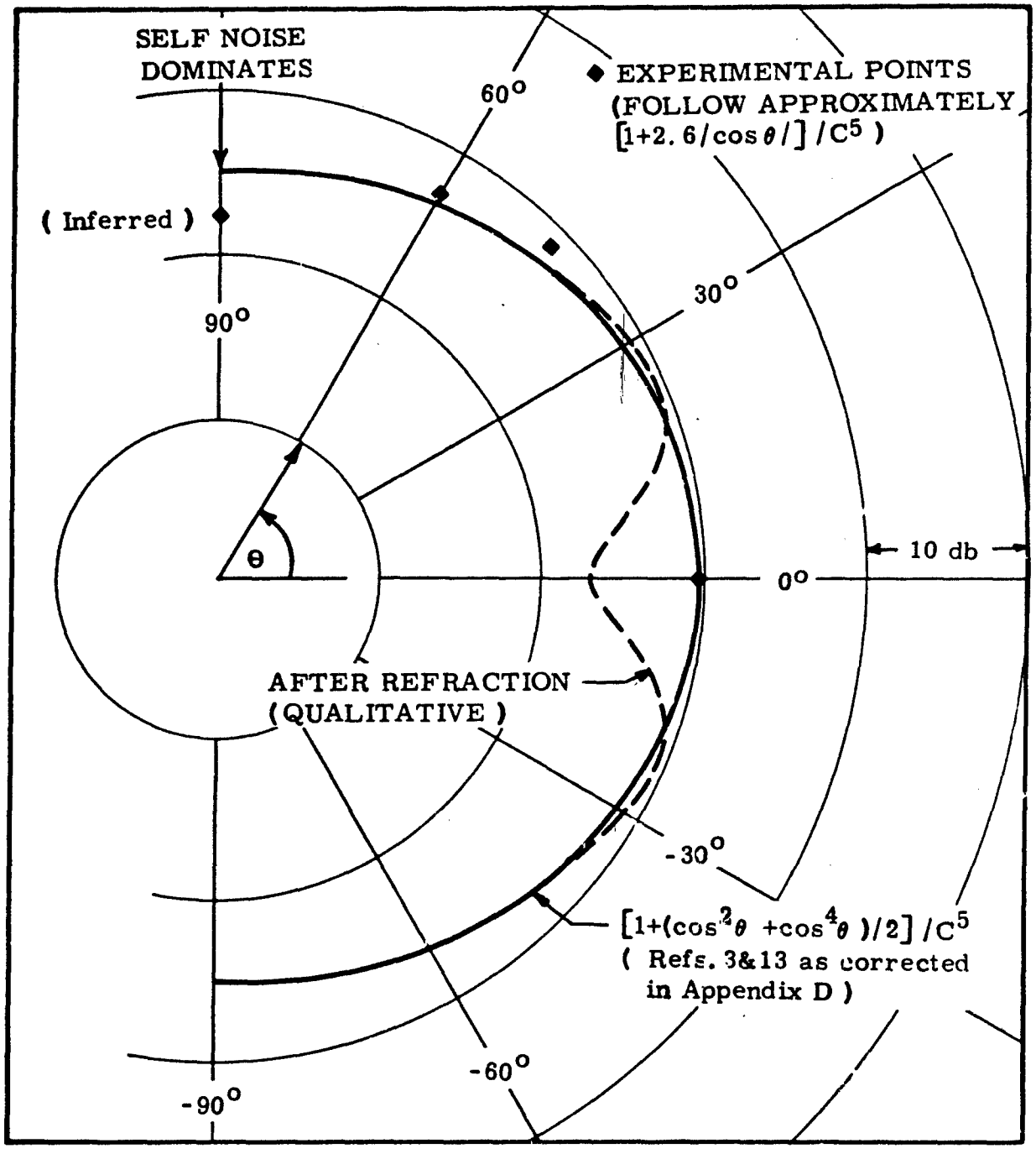


FIG. 36 BASIC DIRECTIVITY OF JET NOISE FROM TURBULENCE MEASUREMENTS

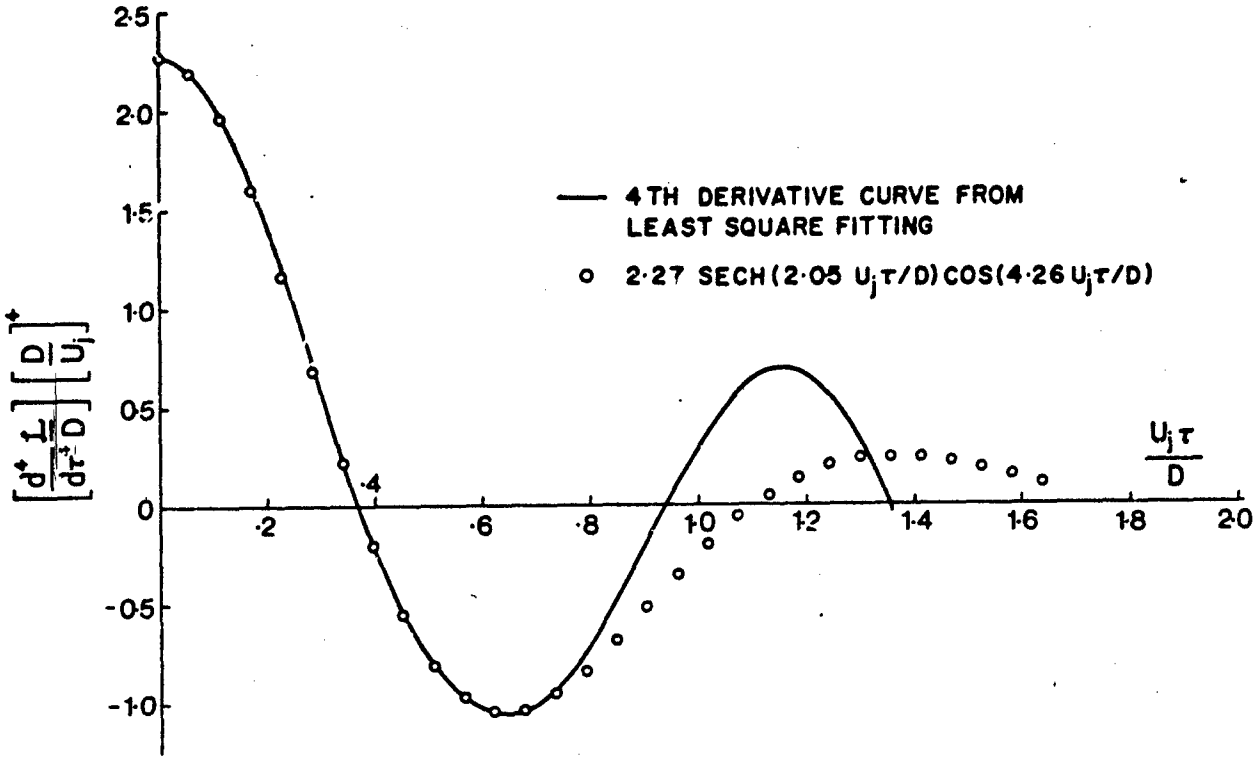


(a) 0° CASE, SHEAR NOISE

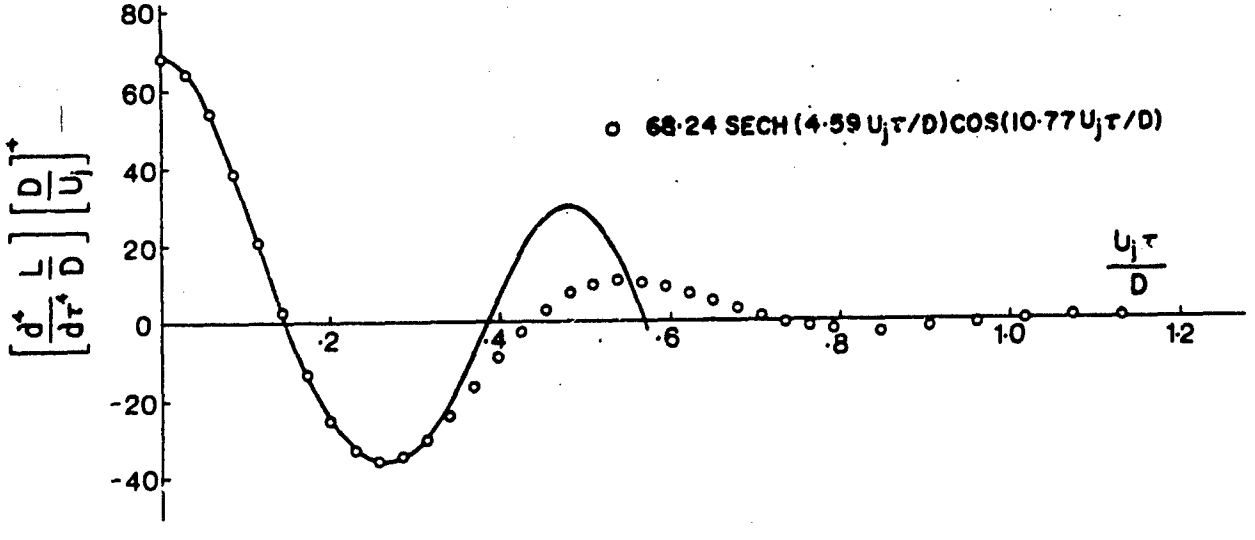


(b) 0° CASE, SELF NOISE

FIG. 37 APPROXIMATING THE FOURTH DERIVATIVE CURVES BY ANALYTICAL FUNCTIONS

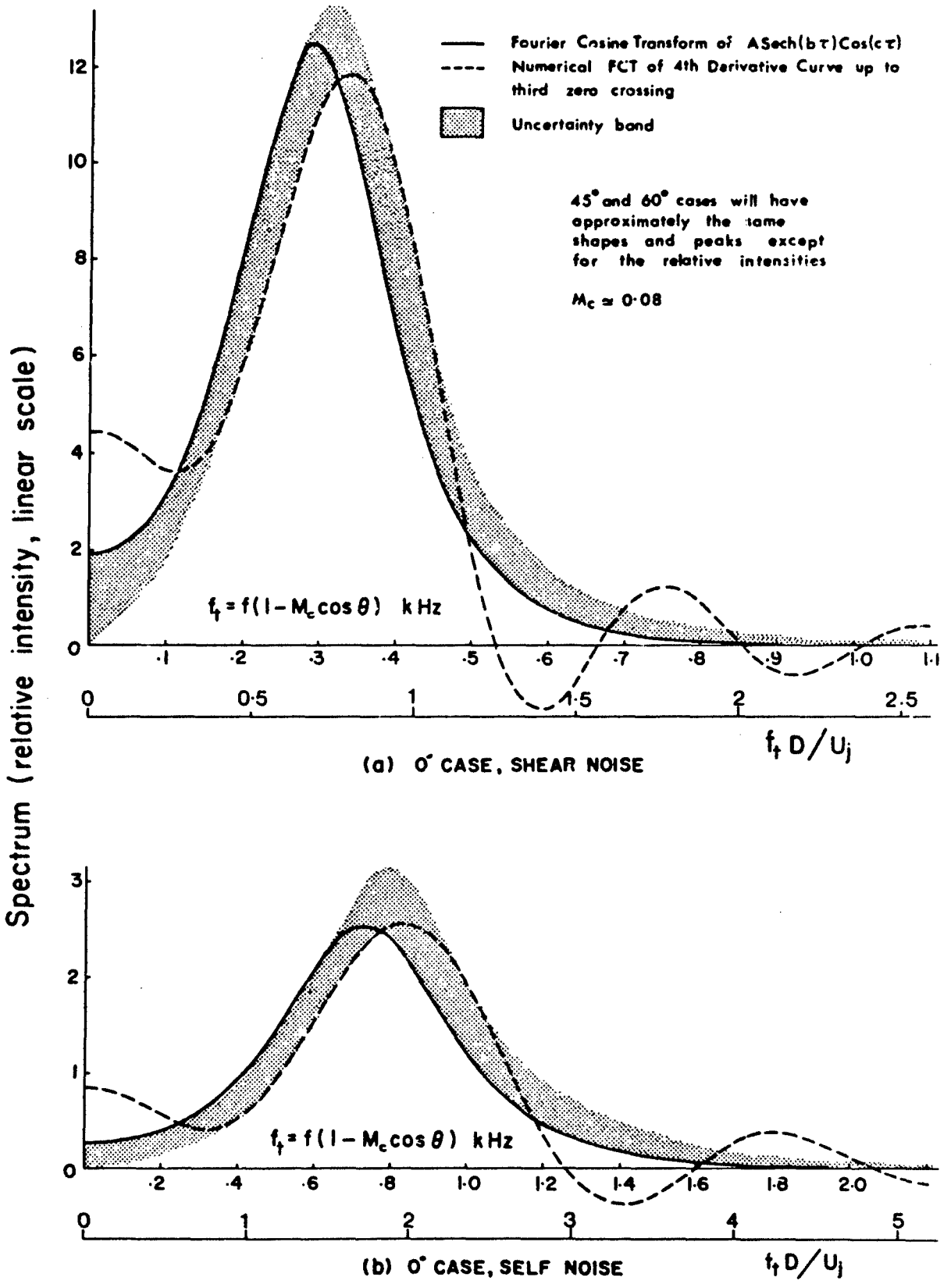


FIG. 38 ESTIMATED SPECTRA OF SHEAR AND SELF NOISE RADIATED FROM A'SLICE'OF JET AT $\bar{r}/D=4$, 0° CASE

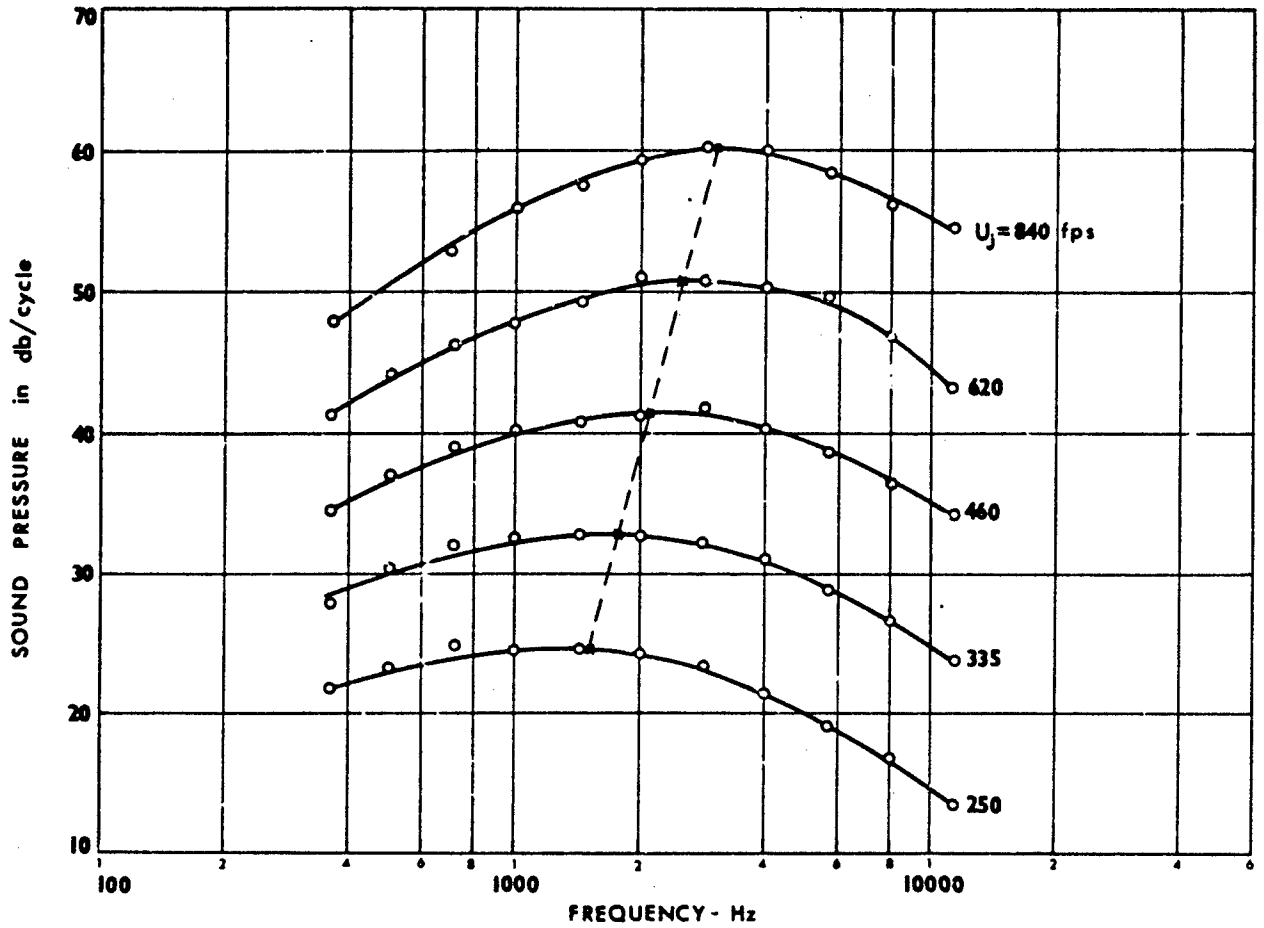


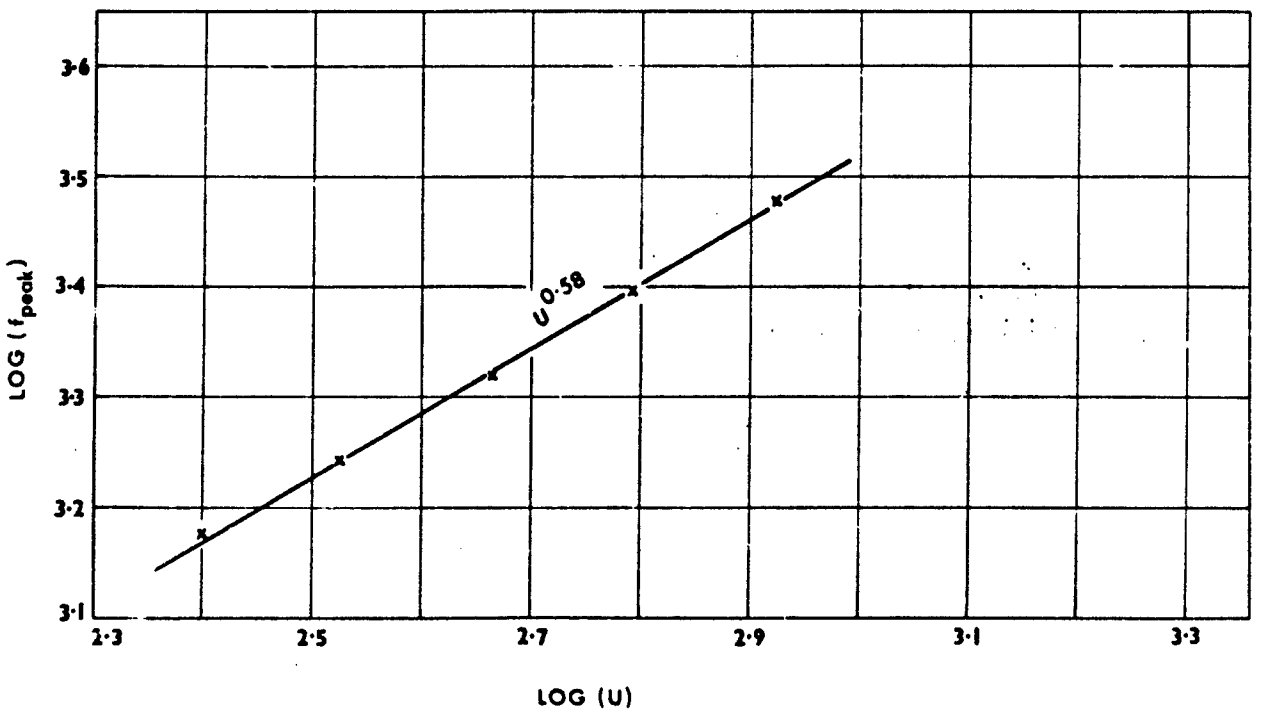


FIG. 39 REPLOT OF LEE'S RESULTS ( REF. 43 ) TAKEN AT 25° FROM JET AXIS

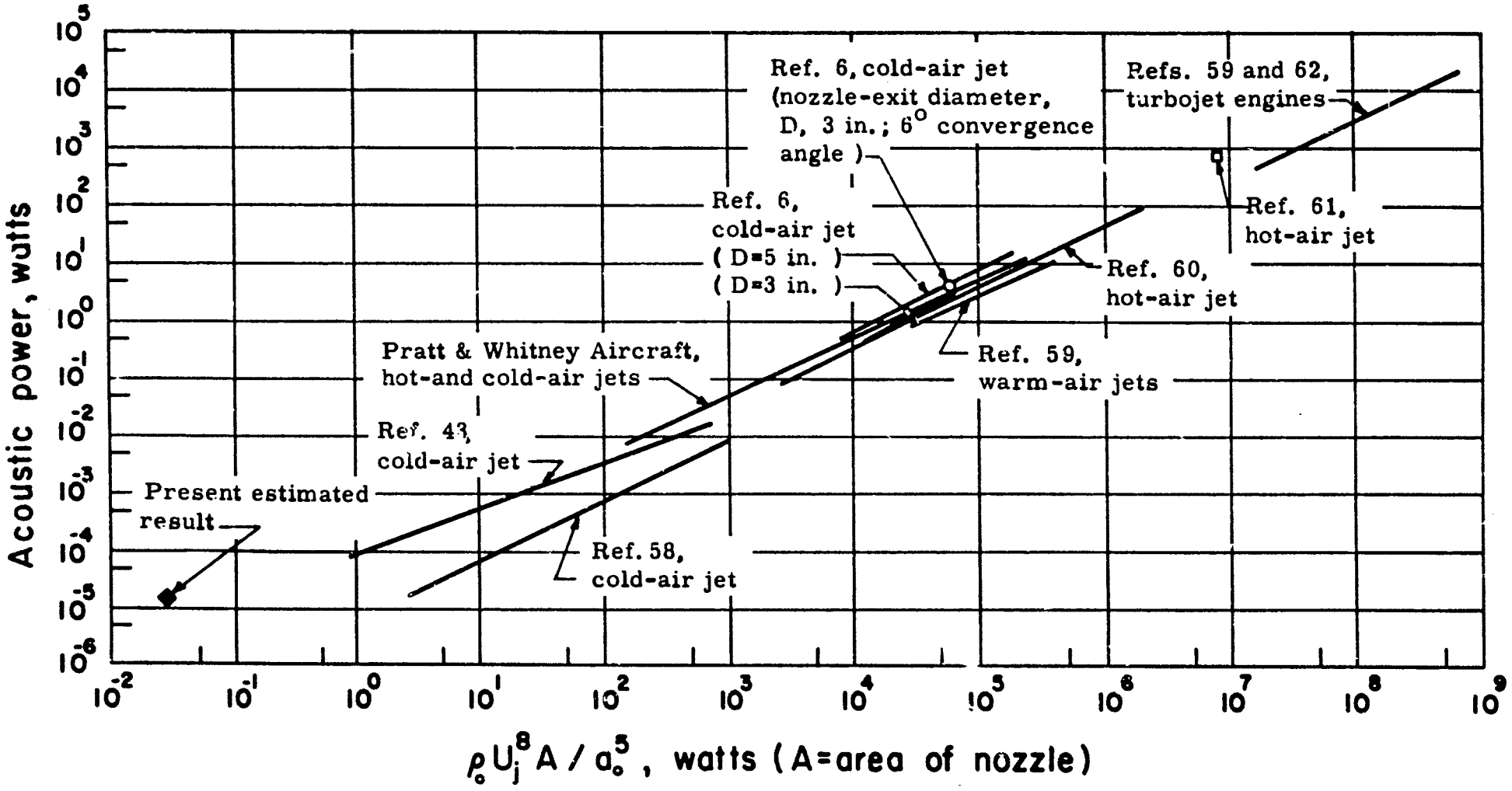


FIG. 40 COMPARISON OF THE PRESENT ESTIMATED TOTAL ACOUSTIC POWER FROM TURBULENCE MEASUREMENTS WITH EXISTING ACOUSTIC MEASUREMENTS ( REPLOT OF FIG. 7, REF. 6 )

## APPENDIX A

### Sensitivity of Inclined Hot-Wire

There is considerable disagreement as to the directional sensitivity of a hot-wire (Refs. 48, 49, 50, 51, 52, and 53 to quote a few). Of these, the first two reported the usual sine-law response for angles greater than $20^{\circ}$, whereas the rest reported some effects of the tangential component. A complete systematic investigation will be beyond the scope of the present experiment. Only one test has been performed with parameters nearly identical to those that would be used in subsequent experiment, i.e., linear operation mode with tungsten wire having length-to-diameter ratio of 230 and overheating ratio of 0.3.

The test was performed in the laminar core of the 4 inch jet. The hot-wire probe was mounted in a rotatable disk assembly as shown in Fig. A1. A telescope was used to assure that the hot-wire was at the center of rotation. The inclination of the wire was then determined from the angle of rotation of the disk. The initial zero position was determined by obtaining the same bridge current with the wire inclined at a positive and a negative angle to an arbitrary fixed datum. The mid point between these two angles would be the zero datum.

For each angle of inclination, the speed (measured with a pitot static probe) of the jet was changed and the bridge current versus speed was plotted. Since the linear operation mode was used, a least square fit was used to obtain the best possible straight line. Before changing to a different inclination, the wire was first brought back to the zero position and the bridge current was checked for the same maximum speed. From these bridge current versus speed plots for different inclination angles, the sensitivity of the inclined wire for three representative speed ranges was obtained and is shown in Fig. A2. Results indicated that there was no systematic deviation from the sine law for our particular case.

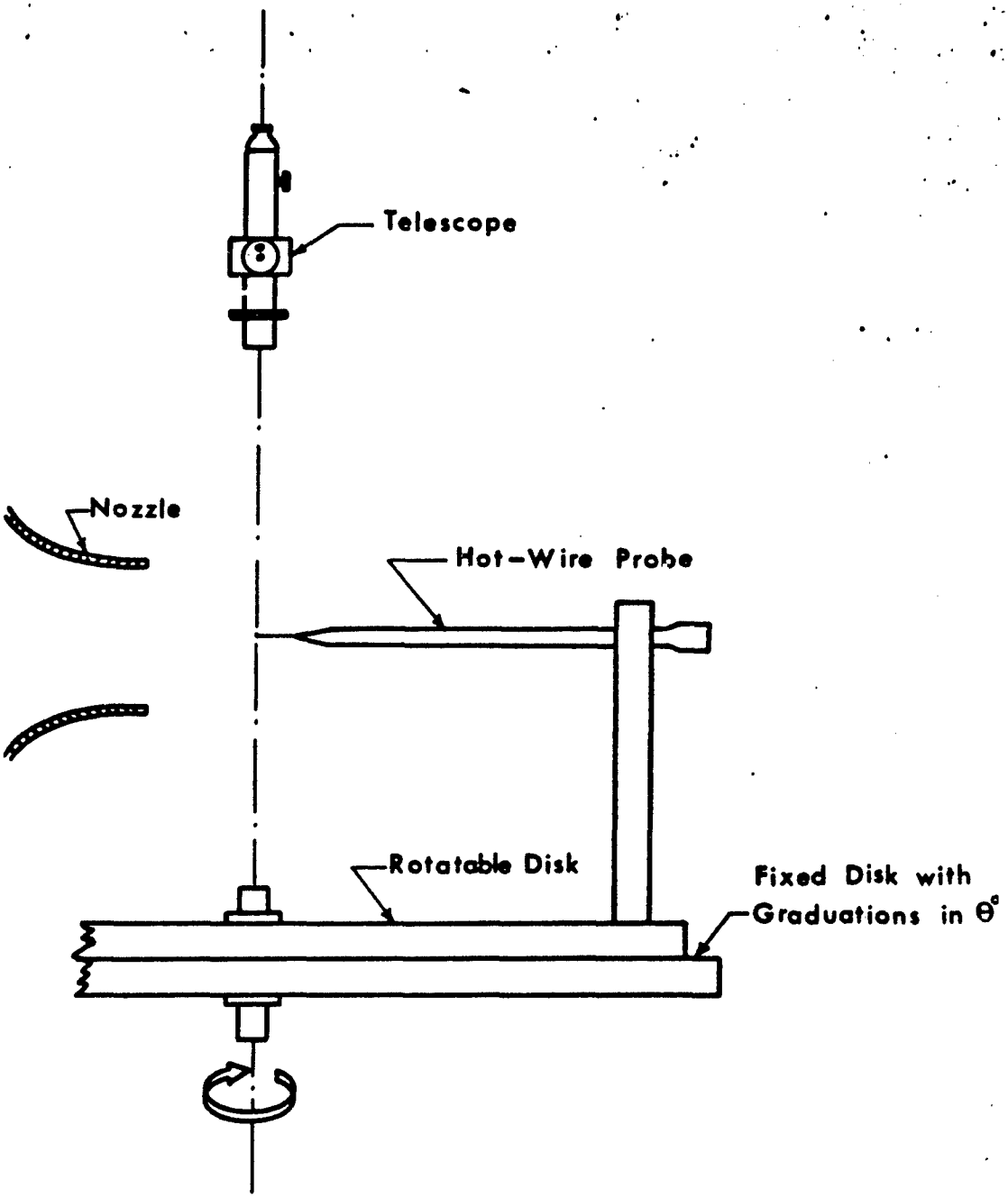


FIG. A1 SCHEMATIC OF SET-UP FOR YAWED-WIRE SENSITIVITY EXPERIMENT

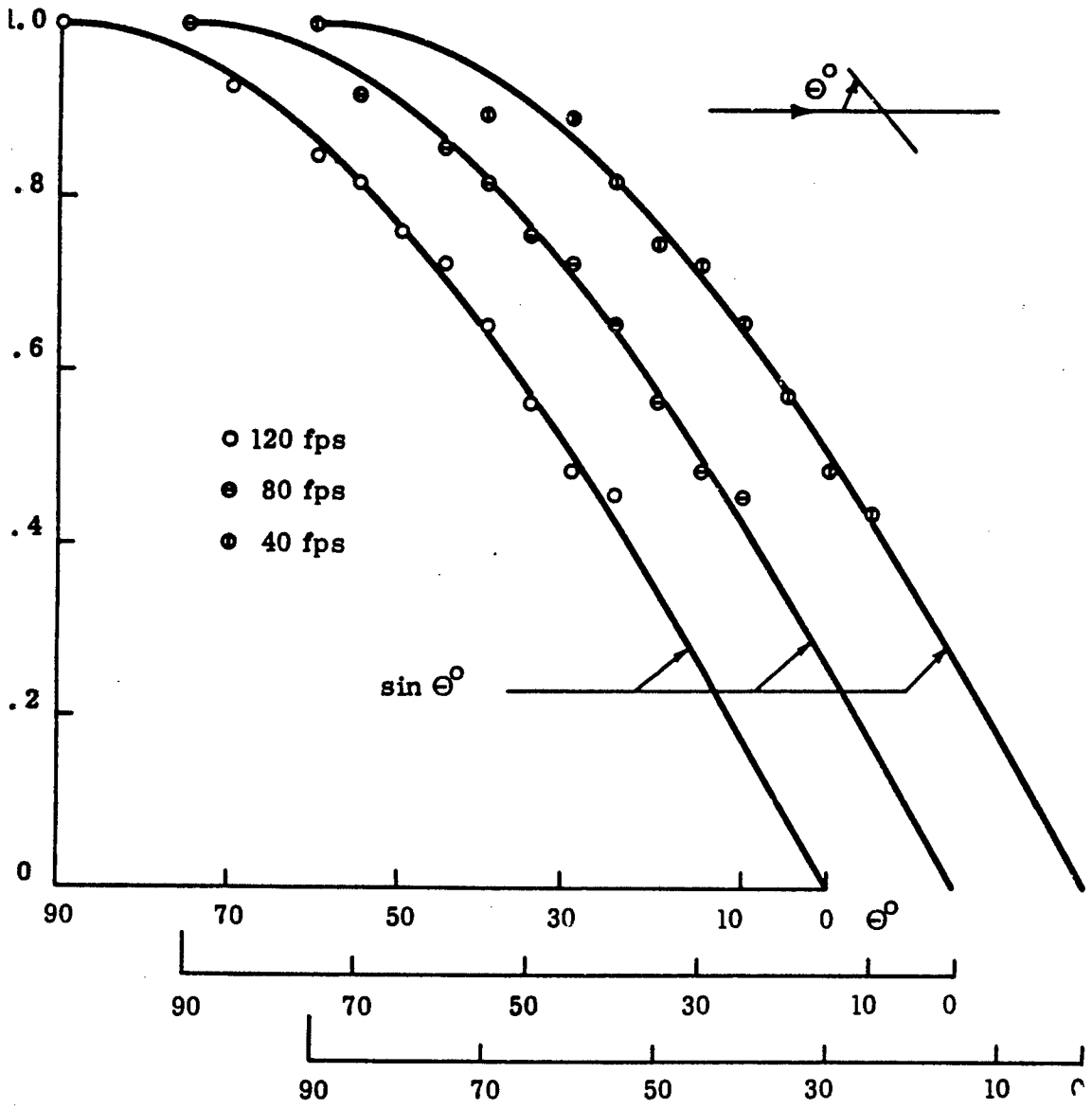


A2 SINE LAW RESPONSE OF INCLINED CONSTANT-TEMPERATURE HOT-WIRE

## APPENDIX B

### Effect of Low-Frequency Cut-Off on Correlation Functions

At tne time when the present author was looking into this p blem he was unaware of similar work done by Wooldridge and Willmarth (Ref. and Bull et al (Ref. 55). However the present approach takes a different form and is based on a relationship between a filtered and a non-filtered space-time correlation derived by Favre et al (Ref. 56). Moreover the eff on the shapes of the space-time correlations are considered in greater det

Suppose the turbulent field is stationary in time, the spac time correlation between the fluctuating velocities at two points separate by a distance $\underline{\xi}$ can be written as

$$R(\underline{\xi},\tau) = \overline{uu'}\,(\underline{\xi},\tau) = \frac{1}{4}\left\{\overline{[u + u'(\underline{\xi},\tau)]^2} - \overline{[u - u'(\underline{\xi},\tau)]^2}\right\} \tag{B.1}$$

The filtered space-time correlation is

$$R_f(\underline{\xi},\tau) = \overline{u_f u_f'}(\underline{\xi},\tau) = \frac{1}{4}\left\{\overline{[u_f + u_f'(\underline{\xi},\tau)]^2} - \overline{[u_f - u_f'(\underline{\xi},\tau)]^2}\right\} \tag{B.2}$$

Now if the frequency response (or energy response to be more exact) of the band-pass filter is A(f), then by definition

$$\overline{[u_f \pm u_f'\,(\underline{\xi},\tau)]^2} = \int_0^\infty A(f)\quad \Phi_\pm(f)\ df \tag{B.3}$$

and

$$\overline{[u \pm u'(\underline{\xi},\tau)]^2} = \int_0^\infty \Phi_\pm(f)\ df \tag{B.4}$$

where $\Phi_\pm(f)$ is the respective power spectral density function. Let us de fine the following autocorrelation functions,

$$R_\pm\,(\tau') = \overline{[u \pm u'(\underline{\xi},\tau)]\ \ [u(\tau') \pm u'\,(\underline{\xi},\tau + \tau')]} \tag{B.5}$$

Then using the Wiener-Khinchin relationship

$$\Phi_\pm(f) = 4\int_0^\infty R_\pm\,(\tau')\cos 2\pi f\tau'\ d\tau' \tag{B.6}$$

Now expanding the autocorrelation functions, we have

$$R_\pm\,(\tau') = R(0,\tau') + R'(0,\tau') \pm [R(\underline{\xi},\ \tau+\tau') + R(\underline{\xi},\tau - \tau')] \tag{B.7}$$

From Eqs. B.2 and B.3,

$$R_f(\underline{\xi},\tau) = \frac{1}{4}\left\{\int_0^\infty A(f)\,\Phi_+(f)df - \int_0^\infty A(f)\Phi_-(f)df\right\}$$

$$= \int_0^\infty A(f)df \int_0^\infty R_+(\tau')\cos 2\pi f\tau' d\tau'$$

$$- \int_0^\infty A(f)df \int_0^\infty R_-(\tau')\cos 2\pi f\tau' d\tau' \qquad (B.8)$$

Inserting $R_{\pm}(\tau')$ we obtain

$$R_f(\underline{\xi},\tau) = 2\int_0^\infty A(f)df \int_0^\infty [R(\underline{\xi},\tau+\tau') + R(\underline{\xi},\tau-\tau')]\cos 2\pi f\tau' d\tau' \qquad (B.9)$$

The above equation is the result of Favre et al (Ref. 56).

Since we are interested in the effect of low-frequency cut-off, we assume a hypothetical energy response of the system to be

$$A(f) = (1 - e^{-f^2/f_c^2}) \qquad (B.10)$$

where $f_c$ is the cut-off frequency corresponding to a 2 db fall off. This assumed form is more realistic than a sharp vertical cut-off. Inserting (B.10) into (B.9),

$$R_f(\underline{\xi},\tau) = 2\iint_0^\infty [R(\underline{\xi},\tau+\tau') + R(\underline{\xi},\tau-\tau')]\cos 2\pi f\tau' df d\tau'$$

$$- 2\int_0^\infty [R(\underline{\xi},\tau+\tau') + R(\underline{\xi},\tau-\tau')]\int_0^\infty e^{-f^2/f_c^2}\cos 2\pi f\tau' df d\tau' \qquad (B.11)$$

The first term is just the unfiltered space-time correlation, as can be seen from (B.9) with $A(f) = 1$. Therefore,

$$R_f(\underline{\xi},\tau) = R(\underline{\xi},\tau) - 2\int_0^\infty e^{-f^2/f_c^2}\,df \int_0^\infty [R(\underline{\xi},\tau+\tau') + R(\underline{\xi},\tau-\tau')]\cos 2\pi f\tau' d\tau' \qquad (B.12)$$

Note that even when $\tau = 0$ the space correlation will also be affected by the low-frequency cut-off. The above equation is useful in estimating the filtered correlation from the non-filtered one, but the reverse procedure would involve solving an integral equation. By a change of variables, one can show that

$$\int_0^\infty [R(\underline{\xi},\tau+\tau') + R(\underline{\xi},\tau-\tau')]\cos 2\pi f\tau' d\tau'$$

$$= \int_{-\infty}^{\infty} R(\underline{\xi},T)\,[\cos 2\pi fT\cos 2\pi f\tau + \sin 2\pi fT\sin 2\pi f\tau]\,dT \qquad (B.13)$$

Therefore

$$R_f(\underline{\xi},\tau) = R(\underline{\xi},\tau) - 2\int_0^\infty e^{-f^2/f_c^2} df \int_{-\infty}^{\infty} R(\underline{\xi},T)\,[\cos 2\pi fT \cos 2\pi f\tau + \sin 2\pi fT \times \sin 2\pi f\tau\,]dT \qquad (B.14)$$

Now one can identify the two terms in the last integral as the real and imaginary parts of the cross-spectral density associated with $R(\underline{\xi},\tau)$, i.e.

$$R_f(\underline{\xi},\tau) = R(\underline{\xi},\tau) - 2\int_0^\infty e^{-f^2/f_c^2}\, df(2\pi\,\Phi_R(\underline{\xi},\omega)\cos\omega\tau - 2\pi\Phi_I(\underline{\xi},\omega) \quad \sin\omega\tau)$$

$$= R(\underline{\xi},\tau) - 2\int_0^\infty e^{-\omega^2/\omega_c^2}\, d\omega \;\; [\,|\Phi(\underline{\xi},\omega)|\cos\alpha\cos\omega\tau$$

$$- \quad |\Phi(\underline{\xi},\omega)|\sin\alpha\sin\omega\tau\,]$$

$$= R(\underline{\xi},\tau) - 2\int_0^\infty e^{-\omega^2/\omega_c^2} \quad |\Phi(\underline{\xi},\omega)|\cos(\omega\tau + \alpha)\, d\omega$$

where

$$|\Phi(\underline{\xi},\omega)|^2 = \Phi_R^{\,2}(\underline{\xi},\omega) + \Phi_I^2(\underline{\xi},\omega)$$

$$\alpha = \tan^{-1} \frac{\Phi_I}{\Phi_R} \qquad (B.15)$$

If we follow Bull et al's assumption that the cut-off is sharp and $|\Phi(\underline{\xi},\omega)|$ is constant from the cut-off frequency down to zero frequency, we obtain instead

$$R_f(\underline{\xi},\tau) = R(\underline{\xi},\tau) - 2\,|\Phi(\underline{\xi},\omega)|_0 \int_0^{\omega_c} \cos(\omega\tau + \alpha)d\omega \qquad (B.16)$$

Defining a convection velocity $U_c$ by $\alpha = -\xi_1\omega/U_c$ and assuming it to be independent of frequency, the result becomes

$$R_f(\underline{\xi},\tau) = R(\underline{\xi},\tau) - 2\,|\Phi(\underline{\xi},\omega)|_0 \quad \frac{\sin\omega_c\,(\tau - \frac{\xi_1}{U_c})}{(\tau - \frac{\xi_1}{U_c})} \qquad (B.17)$$

which is identical to that obtained by Bull et al. Although the convection velocity defined here is slightly different from that defined in the text, they can be considered as equivalent to a first approximation. If this is the case, then on transforming to the moving frame the error term in (B.17) will be independent of $\tau$ as $U_c\tau - \xi_1$ becomes $-\xi_{m_1}$. It follows that the low-frequency cut-off will not affect the fourth time-derivative of the moving-frame space-time correlation. However, it will affect our length scales especially the longitudinal one.

From Eq. B.14, when $\tau = 0$ we obtain

$$R_f(\underline{\xi},0) = R(\underline{\xi},0) - 2 \int_0^\infty e^{-f^2/f_c^2}\, df \int_{-\infty}^{\infty} R(\underline{\xi},T) \cos 2\pi f T\, dT \qquad (B.18)$$

Let us first consider the transverse correlations. A plausible form for the space-time correlation will be

$$R(\xi_i,T) = R(\xi_i,0)\, e^{-aT^2} \quad ; \; i = 2,3 \qquad (B.19)$$

Then it can be shown fairly easily that

$$R_f(\xi_i,0) = R(\xi_i,0) \left(1 - \frac{\pi}{\sqrt{\pi^2 + \frac{a}{f_c^2}}}\right) \qquad (B.20)$$

The above equation indicates that the low-frequency cut-off will affect the magnitudes of the transverse space correlations but not their characteristics. In other words, if the transverse space correlation is non-negative, it will remain non-negative. The situation is quite different for the longitudinal space correlation as seen in the next paragraph.

In order to simplify the mathematics, we have chosen a 'frozen' convective form of the space-time correlation for the longitudinal case, i.e.,

$$R(\xi_1,T) = e^{-A(\xi_1 - U_c T)^2} \qquad (B.21)$$

and

$$R(\xi_1,0) = e^{-A\xi_1^2}$$

With this assumed form, Eq. B.18 can be integrated to give

$$R_f(\xi_1,0) = R(\xi_1,0) \left[ 1 - \frac{\pi}{\sqrt{\pi^2 + \frac{U_c^2 a}{f_c^2}}}\; e^{a\xi_1^2 \left(1 - \frac{\pi^2}{\pi^2 + \frac{U_c^2 a}{f_c^2}}\right)} \right] \qquad (B.22)$$

One can see that for large enough $\xi_1$, the bracketed term can become negative. In other words, even if $R(\xi_1,0)$ is non-negative as in the assumed form here, the low-frequency cut-off will render it negative at large $\xi_1$. In fact the resultant space correlation $R_f(\xi_1,0)$ will have equal positive and negative areas This can be shown by integrating Eq. B.22 to infinity with respect to $\xi_1$. Thus the ordinary definition of length scale defined by this integral will no longer be meaningful because it will be zero. Thus one must be careful in interpreting the length scales obtained by different workers: the truncation of the integral in conjunction with low-frequency cut-off effect will lead to a variety of "scales".

Since we have used the 'frozen' convected pattern, the remarks of the last paragraph can also be applied to autocorrelations and time scales. This is possible because there is interchangibility between autocorrelation

and longitudinal space correlation in a 'frozen' convected turbulence field.

Except for the case of autocorrelation, it is fairly difficult to correct for the low-frequency cut-off effect because it will involve measurements of the cross-spectral density function as indicated by Eq. B.15. In the forthcoming Reference 57, an actual case is presented in which an autocorrelation function has been corrected for the low-frequency cut-off from a knowledge of the spectral density function. Here the best we can do is to obtain an estimate of its effect on the length scales.

By approximating our data by the assumed forms of the space-time correlations, it was estimated that our two transverse length scales might be off by about 10% and that the longitudinal length scale might be lower by as much as 20% if we limited the scale integral to the positive area only.

## APPENDIX C

### Functions Used in Least Square Curve Fitting

The functions used are of the form

$$A\, e^{-(a_o + a_2 T^2 + a_4 T^4 + \ldots)}$$

where

$$T = 300.0 x_T \text{ second}$$

'shear' noise cases

| | 0° Case | 45° Case | 60° Case |
|---|---|---|---|
| A | 0.766 | 0.674 | 0.576 |
| $a_o$ | 0.130350E-01* | 0.157922E-01 | 0.238837E-01 |
| $a_2$ | 0.110723E+01 | 0.123883E+01 | 0.148080E+01 |
| $a_4$ | -0.279533E+01 | -0.327688E+01 | -0.412232E+01 |
| $a_6$ | 0.511338E+01 | 0.566124E+01 | 0.800265E+01 |
| $a_8$ | -0.483750E+01 | -0.510798E+01 | -0.820410E+01 |
| $a_{10}$ | 0.222496E+01 | 0.226621E+01 | 0.413337E+01 |
| $a_{12}$ | -0.394520E+00 | -0.390888E+00 | -0.806750E+00 |

'self' noise cases

| | 0° Case | 45° Case | 60° Case |
|---|---|---|---|
| A | 0.408 | 0.320 | 0.279 |
| $a_o$ | 0.159178E-01 | 0.188755E-01 | 0.304724E-01 |
| $a_2$ | 0.848186E+01 | 0.664074E+01 | 0.185413E+02 |
| $a_4$ | -0.155508E+03 | -0.800311E+02 | -0.353693E+03 |
| $a_6$ | 0.164690E+04 | 0.859596E+03 | 0.277588E+04 |
| $a_8$ | -0.762908E+04 | -0.497161E+04 | 0.111248E+03 |
| $a_{10}$ | 0.770442E+04 | 0.957882E+04 | -0.836756E+05 |
| $a_{12}$ | 0.516812E+05 | 0.276362E+05 | 0.125948E+06 |
| $a_{14}$ | -0.167787E+06 | -0.142374E+06 | 0.127532E+07 |
| $a_{16}$ | 0.146786E+06 | 0.161550E+06 | -0.343257E+07 |

* $0.130350E\text{-}01 = 0.130350 \times 10^{-1}$

## APPENDIX D

### Differences in Emission from Unit Volumes Around the Jet at Same Radial Distance from Jet Axis

Although there is axis-symmetry in the overall jet noise pattern, the noise radiated in a certain direction from volume elements around the jet at a given downstream position will not be the same. In an unpublished work, Ribner has taken into account the dependence of radiation from volume elements on this azimuth angle $\phi$ (see figure below)

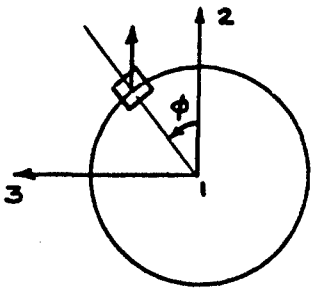


Looking down on the jet exit. Observer on 1-2 plane making $\theta$ with 1-axis.

and obtained the following corrected theoretical directivity

$$\frac{\partial^3 I(\underline{x},\phi)}{\partial^3 \underline{\eta}} \sim 1 + \cos^4\theta + \cos^2\theta \sin^2\theta \sin^2\phi$$

As $\phi$ varies from 0 to $2\pi$ , this varies sinusoidally between

$$1 + \cos^4\theta \qquad \text{and } 1 + \cos^2\theta$$

so that the $\phi$-average is

$$\left\langle \frac{\partial^3 I(\underline{x},\phi)}{\partial^3 \underline{\eta}} \right\rangle_{AV.\phi} \sim 1 + \frac{\cos^2\theta + \cos^4\theta}{2}$$

Thus it is seen that for the theoretical model the overall directivity does not differ markedly from his original $(1 + \cos^4)$ pattern taken at $\phi = 0$ (Refs. 3 and 13). In the absence of other information we shall assume a similar relationship for the experimental results herein; that is, (with other assumptions), the directional pattern emitted from a volume element at $\underline{\eta}$ , as inferred for the plane containing $\underline{\eta}$ and the jet axis, is essentially the directional pattern inferred for the jet as a whole.

## APPENDIX E

### Spectrum Functions Obtained from Truncated Autocorrelation Functions

One of the difficulties in experimental work with random fluctuations is that it is impossible to obtain a complete form of the autocorrelation function up to infinite time delay; the function is always 'truncated' at a finite time delay. If one is interested in the spectrum function obtained from the autocorrelation by the Fourier cosine transform, some idea of how this truncation of the autocorrelation function affects the final spectrum function should be known.

A hypothetical case is a pure cosine function. The corresponding spectrum function will be a delta function centered at the same frequency. If this cosine function terminates at a finite time $\tau$ , the corresponding spectrum function will be of the form $\sin(\omega-\omega_o)\tau/2(\omega-\omega_o)$ which resembles a damped oscillation centered at $\omega_o$. This function has negative values and approaches the delta function for large $\tau$.

A more realistic autocorrelation function is the exponential cosine function which has both the infinite and finite Fourier cosine transforms. Figure B1 again shows the occurance of negative values and a general broading of the spectrum function for the truncated autocorrelation function. However, the position of the peak frequency is not affected.

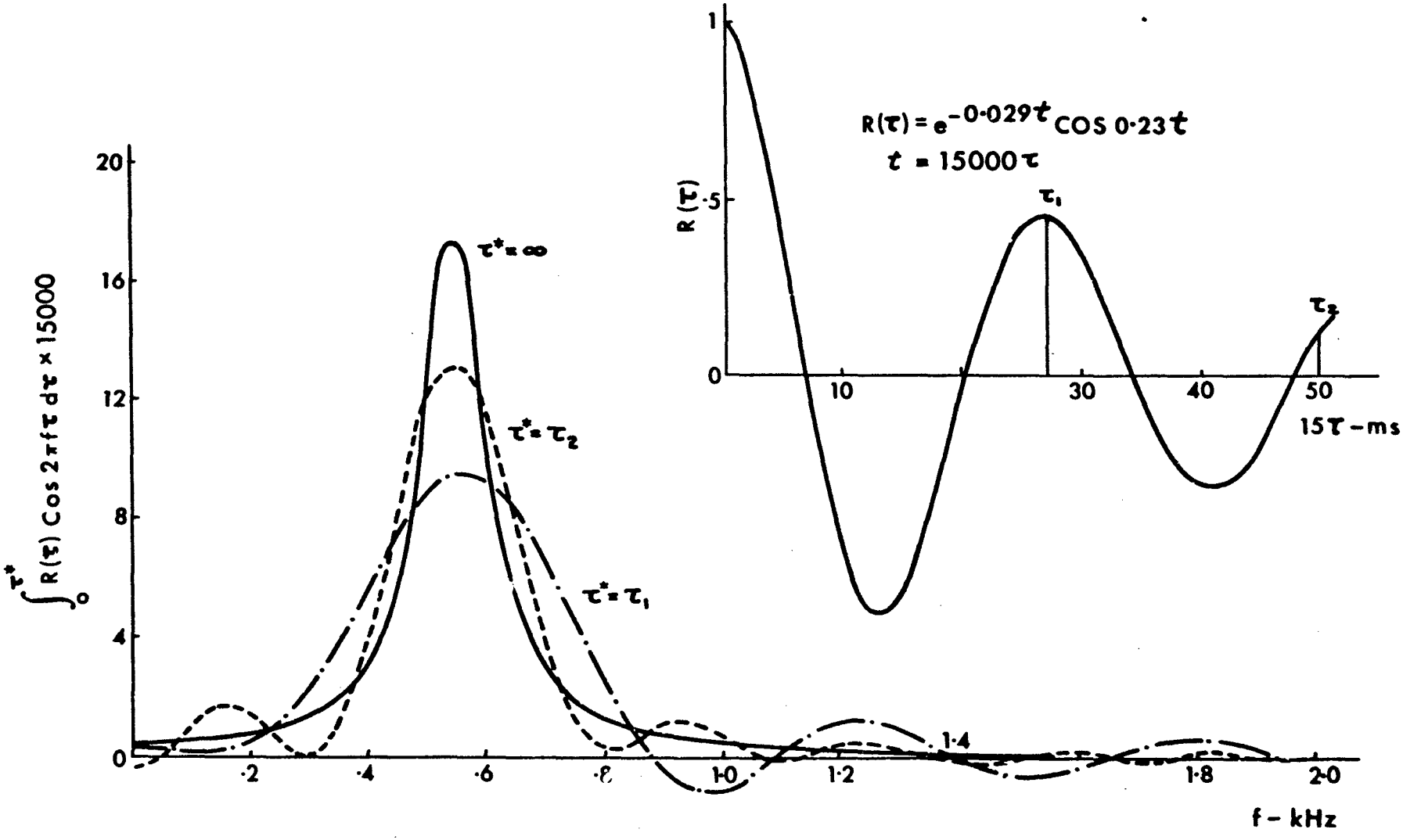


FIG. E1 EFFECT OF TRUNCATED AUTOCORRELATION FUNCTION ON SPECTRUM

## APPENDIX F

### Estimation of Acoustic Power

Based on a theoretical model, Ribner (Ref.3) has shown that the acoustic intensity emitted in direction $\theta$ from a volume element is (as corrected in Appendix D)

$$\frac{\partial^3 I(\underline{X})}{\partial^3 \underline{\eta}} \sim \frac{\bar{\rho}^2 \bar{u}_1^{-2} \omega_f^{\,4} L^3}{|\underline{X}|^2 \rho_o a_o^5 c^5} \left(1 + \frac{\cos^2\theta + \cos^4\theta}{2}\right) \qquad (F.1)$$

which can be re-written as

$$\left(\frac{\partial^3 I(\underline{X})}{\partial^3 \underline{\eta}}\right) \frac{1}{1+\frac{\cos^2\theta + \cos^4\theta}{2}} \sim \underbrace{\frac{\bar{\rho}^2 U^8}{|\underline{X}|^2 \rho_o a_o^5 c^5 L} \left(\frac{\bar{u}_1^2}{U^2}\right)^2 \left(\frac{\omega_f L}{U}\right)^4}_{f}$$

$$\times \underbrace{\left\{\left(\frac{\hat{\bar{\rho}}}{\bar{\rho}}\right)^2 \left(\frac{\hat{\bar{u}}_1^2}{\bar{u}_1^2}\right)^2 \left(\frac{\hat{\omega}_f}{\omega_f}\right)^4 \left(\frac{\hat{L}}{L}\right)^3 \left(\frac{c}{\hat{c}}\right)^5\right\}}_{g} \qquad (F.2)$$

Values with $\wedge$ designate values at arbitrary radial position $\eta_2$ whereas values without $\wedge$ refer to that value of $\eta_2$ where $\partial^3 I(\underline{X})/\partial^3 \underline{\eta}$ peaks for given $\eta_1$. The frequency $\omega_f$ is a typical radian frequency in the turbulence; it is defined by approximately matching a function $\exp(-\omega_f/\tau/)$ to the experimental autocorrelation of $u_1$ in the convected reference frame.

For a given jet at a given operating condition, f and g are functions of position only: $f = f(\eta_1)$, $g = g(\eta_2,\eta_1)$. The function $g(\eta_2,\eta_1)$ is a measure of the radial distribution of the effective sound sources. The integral of $g(\eta_2,\eta_1)dS$ measures the effective area $S(\eta_1)$ occupied by the sound emitters in a 'slice' of jet $d\eta_1$ at $\eta_1$, considered as replaced by emitters of the (radially) uniform strength $f(\eta_1)$. Thus we can write

$$\frac{\partial I(\underline{X})}{\partial \eta_1} \frac{1}{1+\frac{\cos^2\theta + \cos^4\theta}{2}} \sim \left[\frac{\bar{\rho}^2 U^8}{|\underline{X}|^2 \rho_o a_o^5 c^5 L} \left(\frac{\bar{u}_1^2}{U^2}\right)^2 \left(\frac{\omega_f L}{U}\right)^4\right] S(\eta_1) \qquad (F.3)$$

(peak value at $\eta_1$)

Four our case, we have measured experimentally the value on the right-hand side in the more exact form at $\eta_1 = 4D$. It is only necessary to estimate $S(\eta_1)$ from the g function at the same location. The effective area will be an annular one as shown:

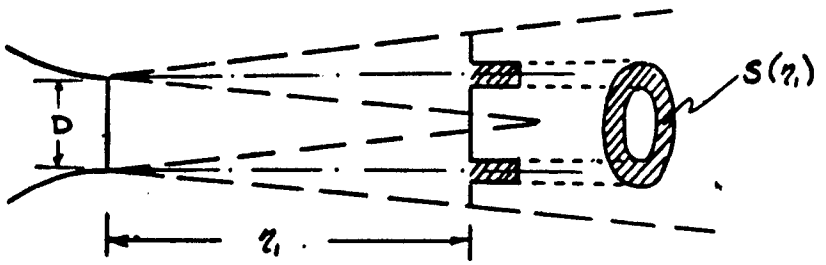


Now across the mixing region only $\overline{u_1^2}$ and $\omega_f$ will vary appreciably. The variation of $\overline{u_1}^2$ was obtained from the present experiment whereas the variation of $\omega_f$ had to be inferred from Ref. 8, assuming similarity between the two jets. The effective area was estimated to be

$$S(\eta_1) = 0.12\ \eta_1\ D \qquad (F.4)$$

$$( = 0.48\ D^2 \text{ for our case})$$

which agreed with the result of Ref. 12 using a slightly different function.

The power generated by a slice of jet was then obtained by integrating the intensities at different directions over the surface of a sphere. The experimental basic directivity of $(1 + 2.6/\cos\theta/)$ was used and the correction factor $C^{-5}$ was replaced by $\theta^{-5}$ for convenience in integration.

Since 'slices' of jet in the mixing region emit the same noise power and the emission falls off very abruptly (about like $\eta_1^{-7}$) beyond six diameters or so (Refs. 12, 14, and 15), the total acoustic power was roughly obtained by multiplying the result for our unit length 'slice' by a length of six diameters. The estimated power generated by our jet was about $1.46 \times 10^{-5}$ watts according to this estimation.

Security Classification

**DOCUMENT CONTROL DATA - R&D**

*(Security classification of title, body of abstract and indexing annotation must be entered when the overall report is classified)*

| | |
|---|---|
| 1. ORIGINATING ACTIVITY (Corporate author)<br>Institute for Aerospace Studies,<br>University of Toronto, Toronto 5, Ont. | 2a. REPORT SECURITY CLASSIFICATION<br>Unclassified<br>2b. GROUP |

3. REPORT TITLE

TURBULENCE MEASUREMENTS RELEVANT TO JET NOISE

4. DESCRIPTIVE NOTES (Type of report and inclusive dates)
UTIAS Technical Report

5. AUTHOR(S) (Last name, first name, initial)

Chu, Wing, T.

| 6. REPORT DATE | 7a. TOTAL NO. OF PAGES | 7b. NO. OF REFS |
|---|---|---|
| November 1966 | 83 | 62 |

| | |
|---|---|
| 8a. CONTRACT OR GRANT NO.<br>AFOSR 672-66<br>b. PROJECT NO.<br>c.<br>d. | 9a. ORIGINATOR'S REPORT NUMBER(S)<br>UTIAS Report No. 119<br>9b. OTHER REPORT NO(S) (Any other numbers that may be assigned this report) |

10. AVAILABILITY/LIMITATION NOTICES
Institute for Aerospace Studies,
University of Toronto,
Toronto 5, Ont. Canada

| 11. SUPPLEMENTARY NOTES | 12. SPONSORING MILITARY ACTIVITY |
|---|---|
| | Air Force Office of Scientific Research SREM |

13. ABSTRACT

Lighthill's equation for aerodynamic noise has been reformulated in terms of its spectral characteristics using the one-dimensional Fourier cosine transform. The final formalism is more revealing in that both the Doppler effect of moving eddies and the extent to which retarded time differences can be neglected are explicit in the final equation. Also the convection effect can be distinguished as a combined effect of Doppler shift and amplification. Experimentally, two-point space-time correlations of both the turbulent velocities and the square of these velocities have been measured in the mixing region ($\xi_1/D = 4, \xi_2/D = 0.5$) of a 4 inch model jet (about 142 fps) with constant temperature hot-wire anemometers. These measurements included the orindary u-component and also the components at $45^o$ and $60^o$ to the jet axis. Results for the u-component agree well with those of previous investigators. Using the moving axis transformation of these space-time correlation functions together with the mean velocity measurements, an estimate of the basic directivity, the intensity, and the spectrum of both the 'shear' and the 'self' noise generated by a unit volume of jet turbulence was obtained. The calculations were based on the Proudman form of Lighthill's equation and Ribner's notion of 'shear' and 'self' noise. These results show reasonable quantitative comparison with actual acoustic measurements of other investigators and they are also in qualitative agreement with some of the theoretical predictions made by Ribner.

DD FORM 1 JAN 64 1473

Security Classification

| 14. KEY WORDS | LINK A | | LINK B | | LINK C | |
|---|---|---|---|---|---|---|
| | ROLE | WT | ROLE | WT | ROLE | WT |
| Jet Noise<br>Turbulence<br>Free Jet<br>Aerodynamic Noise<br>Acoustics | | | | | | |

## INSTRUCTIONS

1. ORIGINATING ACTIVITY: Enter the name and address of the contractor, subcontractor, grantee, Department of Defense activity or other organization *(corporate author)* issuing the report.

2a. REPORT SECURITY CLASSIFICATION: Enter the overall security classification of the report. Indicate whether "Restricted Data" is included. Marking is to be in accordance with appropriate security regulations.

2b. GROUP: Automatic downgrading is specified in DoD Directive 5200.10 and Armed Forces Industrial Manual. Enter the group number. Also, when applicable, show that optional markings have been used for Group 3 and Group 4 as authorized.

3. REPORT TITLE: Enter the complete report title in all capital letters. Titles in all cases should be unclassified. If a meaningful title cannot be selected without classification, show title classification in all capitals in parenthesis immediately following the title.

4. DESCRIPTIVE NOTES: If appropriate, enter the type of report, e.g., interim, progress, summary, annual, or final. Give the inclusive dates when a specific reporting period is covered.

5. AUTHOR(S): Enter the name(s) of author(s) as shown on or in the report. Enter last name, first name, middle initial. If military, show rank and branch of service. The name of the principal author is an absolute minimum requirement.

6. REPORT DATE: Enter the date of the report as day, month, year; or month, year. If more than one date appears on the report, use date of publication.

7a. TOTAL NUMBER OF PAGES: The total page count should follow normal pagination procedures, i.e., enter the number of pages containing information.

7b. NUMBER OF REFERENCES: Enter the total number of references cited in the report.

8a. CONTRACT OR GRANT NUMBER: If appropriate, enter the applicable number of the contract or grant under which the report was written.

8b, 8c, & 8d. PROJECT NUMBER: Enter the appropriate military department identification, such as project number, subproject number, system numbers, task number, etc.

9a. ORIGINATOR'S REPORT NUMBER(S): Enter the official report number by which the document will be identified and controlled by the originating activity. This number must be unique to this report.

9b. OTHER REPORT NUMBER(S): If the report has been assigned any other report numbers *(either by the originator or by the sponsor)*, also enter this number(s).

10. AVAILABILITY/LIMITATION NOTICES: Enter any limitations on further dissemination of the report, other than those imposed by security classification, using standard statements such as:

(1) "Qualified requesters may obtain copies of this report from DDC."

(2) "Foreign announcement and dissemination of this report by DDC is not authorized."

(3) "U. S. Government agencies may obtain copies of this report directly from DDC. Other qualified DDC users shall request through _____."

(4) "U. S. military agencies may obtain copies of this report directly from DDC. Other qualified users shall request through _____."

(5) "All distribution of this report is controlled. Qualified DDC users shall request through _____."

If the report has been furnished to the Office of Technical Services, Department of Commerce, for sale to the public, indicate this fact and enter the price, if known.

11. SUPPLEMENTARY NOTES: Use for additional explanatory notes.

12. SPONSORING MILITARY ACTIVITY: Enter the name of the departmental project office or laboratory sponsoring *(paying for)* the research and development. Include address.

13. ABSTRACT: Enter an abstract giving a brief and factual summary of the document indicative of the report, even though it may also appear elsewhere in the body of the technical report. If additional space is required, a continuation sheet shall be attached.

It is highly desirable that the abstract of classified reports be unclassified. Each paragraph of the abstract shall end with an indication of the military security classification of the information in the paragraph, represented as *(TS), (S), (C), or (U)*.

There is no limitation on the length of the abstract. However, the suggested length is from 150 to 225 words.

14. KEY WORDS: Key words are technically meaningful terms or short phrases that characterize a report and may be used as index entries for cataloging the report. Key words must be selected so that no security classification is required. Identifiers, such as equipment model designation, trade name, military project code name, geographic location, may be used as key words but will be followed by an indication of technical context. The assignment of links, rules, and weights is optional.

GPO 886-551